HISTOLOGICAL ANALYSIS OF BETA-AMYLOID (Aβ) AND METAL ION AGGREGATION INTO NEURITIC PLAQUES IN TG2576 TRANSGENIC MICE

by

Everett-Teejay Brown

A Thesis
Submitted to the
Graduate Faculty
of
George Mason University
in Partial Fulfillment of
The Requirements for the Degree
of
Master of Arts
Psychology

Committee:

Jane M Flinn — Director

Jan B. Butler

Maria K. Butler — Department Chairperson

Dean, College of Humanities and Social Sciences

Date: May 4, 2011

Spring Semester 2011
George Mason University
Fairfax, VA

Histological Analysis of Beta-Amyloid (Aβ) and Metal Ion Aggregation into Neuritic Plaques in Tg2576 Transgenic Mice

A thesis submitted in partial fulfillment of the requirement for the degree of Master of Arts at George Mason University

By

Everett-Teejay Brown
Bachelor of Science
George Mason University, 2005

Director: Jane Flinn, Associate Professor
Department of Psychology

Spring 2011
George Mason University
Fairfax, VA

ACKNOWLEDGEMENTS

I would like to thank my committee members, Dr. Jane Flinn, Dr. Ann Butler, and Dr. Patrick McKnight, for their guidance and knowledge. I would like to thank Lloyd Kinzer and Devin McCorry for their help in calibrating and establishing protocol for the BioQuant system and Jumana Kamal for her help with image design. I would like to also thank Dean Marcelle Heerschap and Dr. Joya A. Crear, my former and current supervisors, for their support in my academic pursuits. Lastly, I give special thanks to my family and friends for their love, tireless support, positive reinforcement and understanding throughout my graduate experience.

TABLE OF CONTENTS

LIST OF TABLES

LIST OF FIGURES

LIST OF ABBREVIATIONS

Aβ	amyloid-beta	GPe/GPi	globus pallidus external segment/internal segment
Aβ40	amyloid-beta ending at residue 40	HC	hippocampus
Aβ42	amyloid-beta ending at residue 42	IL-1B	interleukin-1B
ACh	acetylcholine	Irt	iron-regulated transporter protein
AChE	acetylcholinesterase	LH_2O	lab water
AChEI	acetylcholinesterase inhibitor	LTP	long-term potentiation
AD	Alzheimer's disease	MRI	magnetic resonance imaging
AMG	amygdala	MT	metallothionein
ANOVA	analysis of variance	MWM	Morris water maze
APLP2	amyloid precursor like protein 2	NC	neocortex
ApoE	apolipoprotein E	NFT	neurofibrillary tangle
APP	amyloid-beta precursor protein	PHF*t*	hyperphosphorylated tau

APPsα	α-secretase amyloid-beta precursor protein	PIB	Pittsburgh Compound-B
APPsβ	β-secretase amyloid-beta precursor protein	PPN	pedunculopontine nucleus
BBB	blood brain barrier	PrPsc	scrapie prion protein
BCB	blood cerebrospinal fluid barrier	PS1	presenilin 1, chromosome 14
BG	basal ganglia	PS2	presenilin 2, chromosome 1
BPSD	behavioral and psychological symptoms of dementia	RGB	red-green-blue threshold
CA	cornu ammonis fields of the hippocampus	ROS	reactive oxygen species
CNS	central nervous system	SAD	sporadic Alzheimer's disease
CR	conditioned response	S1	primary somatosensory cortex
CRF	corticotropin releasing factor	SDS	sodium dodesyl sulphate
CS	conditioned stimulus	SNc	substantia nigra pars compacta
CSF	cerebrospinal fluid	SNr	substantia nigra reticulata
CTFα	α-carboxyl terminal fragment	S-R	stimulus-response associations
CTFβ t	β-carboxyl terminal fragment	SRIF	somatostatin

CTFβ’	β’-carboxyl terminal fragment	STN	subthalamic nucleus
CTFγ	γ-carboxyl terminal fragment	TBI	traumatic brain injury
Ctr1	copper transporter protein 1	Tg	transgenic
CuBD	copper binding domain	TfR1	transferrin receptor 1
$CuCO_3$	copper carbonate	US	unconditioned stimulus
DG	dentate gyrus	V1	primary visual cortex
DMT1	divalent metal transporter 1	V2	secondary visual cortex
DNA	deoxyribonucleic acid	Wt	wild type
FAD	familial Alzheimer’s disease	ZIP	Zrt-Irt like proteins
$Fe(NO_3)_2$	iron nitrate	$Zn(CO_3)$	zinc carbonate
fMRI	func. magnetic resonance imaging	ZnT	zinc transporter protein
GABA	gamma-aminobutyric acid	Zrt	zinc-regulated transporter protein

ABSTRACT

HISTOLOGICAL ANALYSIS OF BETA AMYLOID (Aβ) AND METAL ION AGGREGATION INTO NEURITIC PLAQUES IN TG2576 TRANSGENIC MICE

Everett-Teejay Brown, M.A.

George Mason University, 2011

Thesis Director: Dr. Jane Flinn

Alzheimer's disease (AD) is a neurodegenerative disease that affects cognition, behavior, and function. AD is considered a growing health concern because the number of patients with AD doubles every five years after age 65. AD is characterized by two types of lesions in the brain: intraneuronal neurofibrillary tangles and extracellular neuritic (senile) amyloid plaques--the plaques are an accumulation of β-amyloid (Aβ). There is considerable evidence suggesting that metals play a critical role in aggregating Aβ into neuritic plaques. Studies examining the role of metals in formulating Aβ plaque complexes have produced varying results. Further investigation into the role of metals in plaque formation might help uncover possible treatment interventions. The current study examines brain tissue from the Tg2576 transgenic mice model. The Tg2576 model is considered a staple in AD-related studies, and it is the most widely used model of AD in the world. In the current study, Tg2576 mice were split into groups and administered lab water, 10ppm zinc (Zn) water, 10ppm iron (Fe) water, or 10ppm zinc and copper (Cu)

water. In AD, amyloid plaque congregation has been studied throughout the brain, including in transition cortex, piriform cortex, hippocampus, neocortex, amygdala nuclei, and basal ganglia. These brain regions are most commonly associated with learning and memory. Plaque-containing brain tissue from each of these regions was analyzed in Tg2576 mice using BioQuant. Plaque burden was assessed using three measurement parameters: normalized area, average area, and plaque number. Results showed that overall plaque burden was highest in the brains of animals raised on Zn and Zn + Cu water and highest in the cortical areas (transition & piriform cortex followed by neocortex). Plaque burden was less in the brains of mice raised on Fe water and less in the basal ganglia. The effects of metal type and brain region appeared to be independent.

CHAPTER 1

INTRODUCTION

AD is a neurodegenerative disease that affects cognition, behavior, and function (Mehta, 2007). It is the leading cause of dementia in individuals age 65 and older, affecting approximately 24 million people around the world (Pierrot & Octave, 2008). AD is considered a growing health concern because the number of patients with AD doubles every five years after age 65 (Pierrot & Octave, 2008). The etiology of AD is complex with multiple factors contributing to its onset. However, its primary risk factors are aging and family genetics (Mehta, 2007). Examination of the neurodegeneration involved in Alzheimer's disease (AD) can lead to better understanding of the underlying anatomical mechanisms involved in memory and learning since AD involves the selective degeneration of key brain areas implicated in learning and memory (Dawbarn & Allen, 2007).

A small percentage of AD cases are the result of the mutations of known genes and are referred to as familial Alzheimer's disease (FAD). However, most AD cases are called sporadic (SAD), and they have unknown etiology (Inestrosa, Dinamarca, & Alvarez, 2008). These two forms of AD are also known as early-onset and late-onset respectively. Early-onset AD is caused by deficits in one of the three genes associated with AD; these genes include presenilin 1 (PS1) on chromosome 14, presenilin 2 (PS2)

on chromosome 1, and β-amyloid precursor protein (APP) on chromosome 21 (Hsiao et al., 1995; Mehta, 2007). Also, a polymorphism in the apolipoprotein E (Apo E) gene (the E4 allele) has been associated with an increased susceptibility to early onset and late onset AD (Mehta, 2007; Yan & Feng, 2004). Apo E is the primary apolipoprotein in the brain that is synthesized and secreted mainly by glial cells (Qi et al., 2007), and it is involved in transporting and redistributing lipids to various tissues (Mehta, 2007). Apo E is located on chromosome 16. It has three isoforms (E2, E3, E4), and it is encoded by three alleles (E2, E3, E4). The pathological features of FAD are indistinguishable from the sporadic form of AD (SAD), so studying the genetic component of FAD can reveal the underlying mechanisms of AD pathology in general (Y. Zhang & Xu, 2007).

Long-term memory is divided into two distinct types—the capacity for conscious recollection of facts and events (declarative memory) and a heterogeneous collection of nonconscious learning capacities (non-declarative memory) (Squire & Zola, 1996). The diagnostic criteria, according to the American Psychiatric Association for Alzhiemer's-Type Dementia, are shown in Appendix A (Storandt, 2008). Initial symptoms include working memory deficits, attentional issues, personality change, and a decrease in inhibitory control, but AD is most commonly associated with explicit (or declarative) memory impairment, specifically episodic memory (Storandt, 2008). However, the display of symptoms depends on the stage of AD.

For instance, many facets of implicit (or non-declarative) memory, like spatial cuing, repetition, semantic priming and perceptual priming—memory that draws on previous experience—remain intact until the latest stages of AD (Willems, Salmon, &

Van der Linden, 2008). These processes involve accessing information already present in the brain. For example, persons with AD can read and write in the later stages of AD. However, problems arise in difficulty inhibiting automatic activation of these systems. Because these patients are unable to inhibit "false memories," their selective attention may result in apparent memory deficits (Castel, Balota, & McCabe, 2009; Storandt, 2008).

Contrarily, poor performance on tasks involving explicit memory is common throughout the stages of AD (Willems et al., 2008). Difficulty with episodic memory, in particular, manifests itself in such a way that the afflicted will need words repeated to them, they do not recall events, or they forget where they are supposed to be and when (Storandt, 2008). However, episodic memory difficulties in AD patients may actually be a component of deficits in attentional mechanisms (Castel et al., 2009; Storandt, 2008). This implicit-explicit dissonance supports the hypothesis that these differing memory forms are parts of different memory systems in the brain.

Perceptual, cognitive, and behavioral symptoms also manifest in this disorder. These include difficulty with familiar tasks, such as preparing a meal, driving a car, or balancing a checkbook. These tasks involve procedural memory as well as executive functions, such as attention, working memory, and inhibitory control (Storandt, 2008). These impairments may even occur before any memory deficits manifest. In general, more widespread symptoms do not manifest until later in the disease (Storandt, 2008; Willems et al., 2008).

Diagnosis of AD cannot be made definitively without histopathological confirmation postmortem via autopsy (Mehta, 2007; Qi et al., 2007). Autopsies show characteristic lesions in specific regions of the brain, most notably the hippocampus (HC), amygdala, and association cortices of the frontal, temporal, and parietal lobes of the cortex (Qi et al., 2007). Therefore, diagnosis of living patients is often made with the use of various clinical evaluations and exclusion of other causes of dementia (Mehta, 2007). The neurological symptoms of AD are best understood through the underlying physiological characteristics of AD.

Pathogenesis of AD

Alzheimer's disease is characterized by two types of lesions in the brain: intraneuronal neurofibrillary tangles and extracellular senile amyloid plaques—the senile plaques are an accumulation of β-amyloid (Aβ) (Braak, Braak, Ohm & Bohl, 1989). AD is also characterized by neuroinflammation. Additionally, cumulative damage perpetrated by free radicals contributes to the etiology of AD (Becaria, Bondy, & Campbell, 2003; Dawbarn & Allen, 2007). This increased oxidative damage to proteins, DNA, and lipids occur in neurons during normal ageing, and the same types of damage are increased significantly in the progression of AD. This damage is apparent early on in the progression of AD, which suggests age-related oxidative stress is involved in the pathogenesis of AD (Dawbarn & Allen, 2007).

Aβ is the most prominent culprit in AD pathogenesis (Y. Zhang & Xu, 2007). Aβ is formed by the cleavage of APP. Soluble Aβ is produced in normal cell metabolism,

and it can be found in plasma, cerebrospinal fluid (CSF) and other various body fluids (Mehta, 2007). Aβ is produced continuously throughout life, but accumulation of Aβ does not occur until advanced ages. This suggests that Aβ is usually non-pathogenic and is not toxic until a specific concentration is reached (Dawbarn & Allen, 2007). The synaptic terminal is implicated in this domino effect of amyloid neurodegeneration. The loss of synaptic markers correlated with the extent of cognitive deterioration associated with AD (Dawbarn & Allen, 2007). Excess Aβ is implicated in the loss of these synaptic markers.

Overabundance of Aβ triggers a domino effect of neurodegenerative steps resulting in amyloid plaques, neurofibrillary tangles, and neuronal cell loss in the AD brain (Y. Zhang & Xu, 2007). The amyloid plaques consist of deposits of Aβ that derive from cleavage of APP by enzymes (Armstrong, Lantos, & Cairns, 2008; Y. Zhang & Xu, 2007). This extracellular insoluble Aβ forms into plaques in the synapses between neurons. This indirectly suggests that Aβ within synaptic vesicles is released when the cell is excited, therefore, depressing synaptic transmission (Dawbarn & Allen, 2007). Most of the mutations in the APP gene are found around the cleavage sites, which increases the rate of cleavage, thereby producing more Aβ (Yan & Feng, 2004). Furthermore, fibrillar Aβ enhances neurofibrillary tangle formation (Dawbarn & Allen, 2007). Neurofibrillary tangles (NFTs) are insoluble twisted filaments inside neurons that consist of tau (Y. Zhang & Xu, 2007). In NFTs, tau is an abnormal form of microtubule associated tau protein (Sergeant, David, Champain, Ghestem, Wattez, & Delacourte,

2002; Storandt, 2008). In a normal brain, tau is part of the structure of the microtubules that form part of the cells' transportation system (Storandt, 2008).

The enzymes that mediate the metabolism of APP are called secretases (Armstrong et al., 2008), and the cleavage occurs in the Aβ region. The activity of these enzymes is different depending on the region (α, β, γ) in which they are located (Sergeant et al., 2002). α-Secretase generates sAPPα and carboxly terminal fragment c83; β-Secretase generates sAPPβ and carboxly terminal fragment c99, and γ-Secretase generates AICD (APP intracellular domain) and Aβ peptides or the p3 peptide. APP cleaved by α-secretase follows the non-amyloidogenic pathway, and it excludes Aβ generation therefore it is non-toxic (Armstrong et al., 2008; Y. Zhang & Xu, 2007). APP cleavage by β–secretase and γ-secretase yields Aβ40 and Aβ42, the toxic forms of Aβ (Dawbarn & Allen, 2007; Hsiao et al., 1995; Sergeant et al., 2002). Figure 1.1 illustrates the cleavage carried out by the three secretases.

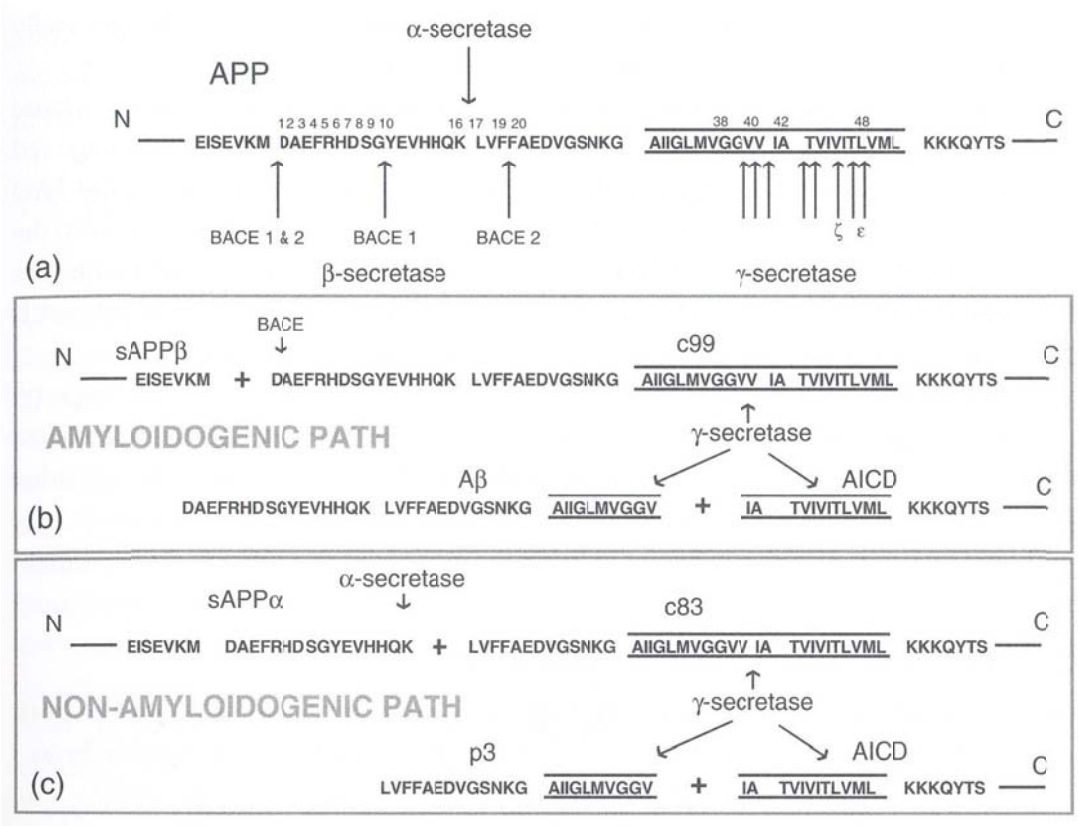

Figure 1.1: Cleavage of APP by secretases (Dawbarn & Allen, 2007).

Aβ42 is most toxic, and it has a propensity to assemble into oligomers and polymers making it dense (Yan & Feng, 2004). Aβ40 is more common (approximately 80%), but the small proportion of Aβ42 (approximately 10%) is more amyloidogenic (Y. Zhang & Xu, 2007), and it plays the central role in neuritic plaque formation (Mehta, 2007). Studies involving the presenilin mutations in FAD show that these mutations have a higher Aβ42/40 ratio implicating elevated levels of Aβ42 as compared with Aβ40 in AD onset (Gandy et al.,2007; Y. Zhang & Xu, 2007).

The process that results in Aβ production is complex and involves several different mechanisms that can affect the outcome. For instance, the cleavage and regulation of APP is important for understanding the production of Aβ. APP trafficking and processing are regulated by signal transduction compounds, steroid and peptide hormones, PS1, and other proteins. A change in any of these processes would have an impact on Aβ production (Gandy et al., 2007).

Another enzyme associated with amyloid plaque deposits is called acetylcholinesterase (AChE). Acetylcholinesterase is the enzyme that breaks down the neurotransmitter acetylcholine (ACh) (Boston, Gopalkaje, Manning, Middleton, & Loxley, 2008), and it is the primary cholinesterase in the central nervous system (Dawbarn & Allen, 2007). Losses of cholinergic neurons and reduced ACh and AChE in the hippocampus and neocortex occur in the brains of AD patients (Dawbarn & Allen, 2007). Additionally, AChE is specifically associated with senile plaques in vivo, Aβ fibril formation, pre-amyloid diffuse deposits, cerebral blood vessels, and it is a marker for observed selective cholinergic deficit (Cerpa, Dinamarca, & Inestrosa, 2008; Inestrosa et al., 2008).

In vivo studies have shown that Aβ aggregation and amyloid fibril formation are enhanced by the work of AChE (Inestrosa et al., 2008). AChE that combines with Aβ complexes differs enzymatically from AChE in normal tissue. Specifically, the enzymes differ in optimal pH, how they inhibit excess substrate, and in sensitivity to protease inhibitors (Inestrosa et al., 2008). These findings have implications for the effectiveness of a class of pharmaceuticals called acetylcholinesterase inhibitors (AChEIs) in the

treatment of AD (Dawbarn & Allen, 2007). AChE and Aβ form a stable complex that is highly neurotoxic and that is able to modify the biochemical and pharmacological properties of AChE (Cerpa et al., 2008). However, the extent of enhancement is dependent upon the type of Aβ peptide present (Inestrosa et al., 2008). The enhancement of the amyloid formation, as induced by AChE, is directly proportional to the lower amyloidogenic property of the Aβ peptides. Aβ40, for instance, has a lower amyloidogenic property so AChE increases the amyloid formation in this peptide (Inestrosa et al., 2008). However, even though Aβ42 has a higher amyloidogenic property, when AChE creates a formation with Aβ42, it increases the Aβ oligomeric formation that many recent studies have implicated as the dominant toxic species associated with AD (Armstrong et al., 2008; Inestrosa et al., 2008).

Additionally, a study involving prion pathology showed that AChE increased the altered scrapie prion protein (PrPsc) that is known to form amyloid prion which shares properties with Aβ peptides (Inestrosa et al., 2008). In vivo studies have shown that amyloid structures when combined with AChE cause a more neurodegenerative response than Aβ alone. This finding supports the hypothesis that these complexes are indeed made more neurotoxic and that AChE triggers some of the neurodegenerative changes in the AD brain (Cerpa et al., 2008).

Aβ may also contribute to the pathogenesis of AD by affecting the normal function of acetylcholine (ACh) neurons that project from the basal forebrain to cortical and hippocampal areas (Yan & Feng, 2004). Abnormalities of the cholinergic system were among the earliest pathological findings in AD (Dawbarn & Allen, 2007). ACh

neurons are crucial components of learning and memory (Boston et al., 2008), and ACh receptors (nicotinic and muscarinic) underlie many critical central nervous system (CNS) functions including attention, memory, and cognition (Tsang, Francis, Esiri, Wong, Chen, & Lai, 2008). Aβ peptides can disrupt muscarinic receptors, inhibit nicotinic receptor mediated currents in interneurons, and they are able to damage the cholinergic network of frontal cortices of transgenic mice. The latter is seen in the reduced density and size of cholinergic synapses in mice (Yan & Feng, 2004). Additionally, current studies suggest muscarinic receptor activation may regulate processing of APP, and many experts believe cholinesterase inhibitors might slow progression of AD by slowing production of Aβ (Dong, Csernansky, Martin, Bertchume, Vallera, & Csernansky, 2005).

Until recently AChEIs were the only class of pharmaceuticals used in the treatment of AD. However, AD patients treated with AChEIs have generally exhibited only moderate cognitive improvements and improvements in non-cognitive behaviors potentially related to enhancements in arousal and attention. Other neurotransmitter systems like serotonin and glutamate are being examined to get a more complete picture of the neurodegenerative effects of AD (Dawbarn & Allen, 2007).

Inflammation is described as the third hallmark of AD. Inflammatory processes are localized in areas containing Aβ plaques (Dawbarn & Allen, 2007). In neurodegenerative disorders like AD, neuron loss or death is referred to as excitotoxicity. This process is mediated by the activation of glutamate receptors. Hippocampal alterations following glutamate activation relate to a process of cell death that is different from necrosis or apoptosis; this has been potentially linked to decrease in ACh in AD,

and this excitotoxic process incites an inflammatory response (Scali, Prosperi, Vannucchi, Papeu, & Casamenti, 2000). Oxidative stress, cellular damage, and the presence of abnormal proteins are all capable of activating both innate and humoral inflammatory processes. Levels of various pro-inflammatory cytokines, proteases, and protease inhibitors involved in inflammatory processes are increased in plaque-associated cells in AD (Dawbarn & Allen, 2007). Microglia that respond to excitotoxic occurrences may lead to neurotoxic and inflammatory products (Scali et al., 2000). When microglia encounter the accumulating Aβ associated with AD, they become activated and increase their production of pro-inflammatory cytokines. One such cytokine called interleukin-1B (IL-1B) has been shown to impair long-term potentiation (LTP) of synaptic transmission in the hippocampus, suggesting a manner in which inflammation might lead to long-term memory deficits (Dawbarn & Allen, 2007).

Brain Injury and AD

Prior brain injury is a leading risk factor for AD. Brain injury can include any of the following: traumatic brain injury (TBI), stroke, ischemic brain injury, hypo-perfusion-reperfusion in cardiac arrest or cardiac bypass surgery, and hypo/hypertension (Frederickson, Cuajungco, & Frederickson, 2005). Ischemic stroke has been used as a model disease to uncover the role of tau concentration, Aβ peptides and Apo E in degenerative and regenerative brain processes (Hesse et al., 2000). In fact, brain injury or ischemia can directly contribute to the pathogenesis of AD. There is a significant increase for AD due to vascular risk factors linked to stroke in the elderly (Qi et al., 2007). It is

estimated that AD is three times more likely to occur in the elderly after a stroke. In addition to transporting lipids, Apo E has important roles in the recovery of the central nervous system from injury, which accounts for the increased expression of this protein after brain ischemia (Qi et al., 2007).

Hesse et al. (2000) studied 26 patients with cerebral infarctions. After the occurrence of acute ischemic stroke in these patients, consecutive CSF (cerebrospinal fluid) samples were analyzed for different CSF-biochemical markers for AD. These researchers found that CSF-tau and CSF-amyloid Aβ42 are possible biomarkers for AD. CSF-tau showed an increase after acute stroke, and the level of increase was positively correlated with the size of the brain infarctions. These results suggested that CST-tau level reflected the extent of neuronal damage after ischemic brain injury. Conversely, the levels of CSF-Aβ42 and CSF-Apo E did not change after acute stroke, although there was a correlation between the two. In AD, the CSF levels of both are reduced; this is most likely due to their accumulation into senile plaques.

Qi et al. (2007) examined the expression and distribution of Aβ40, Aβ42, and Apo E in the human hippocampus (HC) after cerebral ischemia, in order to uncover evidence of the link between brain ischemia and AD pathogenesis. These researchers concluded that Aβ40, Aβ42, and Apo E are upregulated in the HC after the occurrence of cerebral ischemia. Overexpression of Aβ40 and Aβ42 may contribute to the spread of the damage of the initial cerebral ischemia in addition to their neurotoxic contribution to AD onset. The researchers further concluded that ApoE may exhibit a more complex role because it affects various aspects of neurodegeneration and repair in addition to

involvement in fibrillar Aβ formation, Aβ clearance by astrocytes, formation of NFTs, and regulation of inflammatory responses. Although ApoE has a protective role in ischemia, its upregulation along with Aβ might explain the role of ischemia in AD onset.

Transgenic Mouse Model of AD

Transgenic (Tg) mice expressing amyloid precursor protein (APP) provide important information about the pathogenesis of Alzheimer's (Hsiao et al., 1995). The Tg2576 animal model is considered a standard in AD-related studies (Linkous, Adlard, Wanschura, Conko, & Flinn, 2009), and it is the most widely used model of Alzheimer's disease (Hsiao-Ashe, 2006). Specifically, Tg2576 is the mouse model of AD that overexpresses a mutant form of the human APP (Hsiao et al., 1996; Inestrosa et al., 2008), and the model was developed by Hsiao in 1996 (Horgan, Miguel-Hidalgo, Thrasher, & Bissette, 2007). The mutation exhibited in Tg2576 mice is derived from a large Swedish family with early onset AD. A hamster prion promoter is used to express high levels of the mutant APP protein in the mice (Horgan et al., 2007; Hsiao et al., 1996). These mice manifest an increase in Aβ deposits at fewer than 10 months of age and show deficits in memory and spatial learning (Hsiao et al., 1996; Linkous et al., 2009; Yan & Feng, 2004).

Transgenic murine models reiterate the finding that Aβ is not toxic until a threshold concentration is reached. When compared with non-transgenic mice, transgenic animals do not exhibit certain spatial learning and memory impairments until months after APP expression begins (Dawbarn & Allen, 2007). Additionally, studies involving

Tg2576 show that the impact of neuronal cell apoptosis may be exaggerated in AD. For instance, studies have shown that aged Tg2576 mice exhibit numerous Aβ plaques in cortical and limbic structures, but no cell death is seen in these areas (Yan & Feng, 2004). Cognitive deficits in these mice correlate to impaired hippocampal LTP (Dawbarn & Allen, 2007; Yan & Feng, 2004). Since no cell loss is seen even though the mice exhibit synaptic plasticity and spatial memory deficits, the results suggest that, in the presence of Aβ, the dysfunction of cortical and hippocampal neurons is responsible for the cognitive and memory impairments in AD, not their death (Yan & Feng, 2004).

In a study performed by Chauhan (2003), it was found that the detection of soluble Aβ is most sensitive when extracted by sodium dodesyl sulphate (SDS). SDS allows for detection of soluble Aβ peptids, whereas an SDS-resistant extraction method, formic acid, for instance, only detects insoluble Aβ peptides. According to Chauhan (2003), in Tg2576 mice, insoluble Aβ burden begins to develop at 10-months of age. It is at this point that SDS soluble Aβ is abundant and readily extractible. It is through use of transgenic mouse models that this order of events was discovered. Studies using transgenic mouse models have consistently shown that intracellular accumulation of Aβ occurs earlier in AD pathogenesis than extracellular plaque formation, and levels of intracellular Aβ decrease as extracellular plaques begin to form (Y. Zhang & Xu, 2007).

Horgan et al. (2007) used Tg2576 mice to study the fact that neuropeptides cortiocotropin releasing factor (CRF) and somatostatin (SRIF) are reduced in the cortical regions of AD inflicted brains, thus, implicating Aβ in this decrease. These neuropeptides perform as neurotransmitters in the hypothalamus, but their main role is to regulate

anterior pituitary hormone release. In AD, there is a known correlation between decreased SRIF, cognitive impairments, and plaque density. Horgan et al. (2007) found that the transgenic mice did not exhibit a decrease in CRF and SRIF as is the case in the human AD brain, but the mice did mimic the spatial memory deficits shown in humans. The implications of this study suggest the possible overexaggeration in implicating Aβ as the sole perpetrator of cognitive impairments in AD or a categorical difference in brain response of humans and mice in reaction to overproduction of Aβ.

According to Hsiao-Ashe (2006), Tg2576 mice exhibit memory impairments without the complex structural changes seen in human AD patients. For example, neuronal loss, including cholinergic neurons, is not seen in Tg2576 mice (Dong et al., 2005). Hsiao-Ashe and colleagues discovered that a soluble complex of Aβ called Aβ*56 in the brains of Tg2576 caused cognitive deficits without the presence of neurodegenerative changes like amyloidosis or neuronal loss. The discovery of Aβ*56 might help to uncover some of the human/mouse disparities in AD pathology, and as the initial entity causing dysfunction in transgenic animals it could lead to discovery of its homolog in the human AD brain and, thus, lead to early detection and possible treatment interventions (Hsiao-Ashe, 2006). Hsiao-Ashe summarizes that, "Tg2576 mice mimic pre-clinical Alzheimer's disease better than they resemble actual Alzheimer patients" (p. 125). This statement would account for the absence of some of the structural changes in Tg2576 mice without underestimating these structural changes in human AD patients.

Brain Regions Associated with AD

In AD, amyloid plaque congregation has been studied throughout the brain including in transition cortex, hippocampus, neocortex, amygdala, and basal ganglia. Each of these brain regions has been implicated in learning and memory. Autopsies show characteristic lesions in specific regions of the brain, most notably the hippocampus (HC), amygdala, and association cortices of the frontal, temporal, and parietal lobes of the cortex (Qi et al., 2007). Linking Aβ and AD pathology to neurodegeneration in these neuroanatomical regions could advance research into these regions and uncover their specific involvement in the underlying mechanisms of learning and memory.

Transition and Piriform Cortex

Transition and piriform cortex are part of the cerebral cortex but distinct from the neocortex. The areas of the transition cortex most notable in learning and memory are entorhinal cortex, perirhinal cortex, and insular cortex. These areas of the cortex have intimate connections with limbic structures and cortical association areas (Colurso, Nilson, & Vervoort, 2003) and are damaged early in the progression of AD (Braak & Braak, 1991).

The entorhinal cortex is located within the medial temporal lobe. It has been implicated in memory processes and is a key component of the cortico-hippocampal networks because it acts as an anatomical gateway through which most of the cortically processed information is presented to the hippocampus (Andersen, Morris, Amaral, Bliss, & O'Keefe, 2007; Squire & Zola, 1996; VanElzakker, Fevurly, Breindel, & Spencer,

2008). Neurons transfer cortical sensory information to the hippocampus via the perforant pathway (Andersen et al., 2007). Cortical information is relayed to CA1 of the hippocampus primarily from layer three of the entorhinal cortex and to CA3 of the hippocampus primarily from layer two of the entorhinal cortex. CA1 also receives cortical projects from layer two of the entorhinal cortex when it has first been processed by the dentate gyrus and CA3 via the trisynaptic loop (VanElzakker et al., 2008). Then deep entorhinal layers receive information back from the CA1 and subiculum of the HC (Andersen et al., 2007). The entorhinal cortex also receives nearly two-thirds of its cortical input from the adjacent perirhinal and parahippocampal cortices (Squire & Zola, 1996).

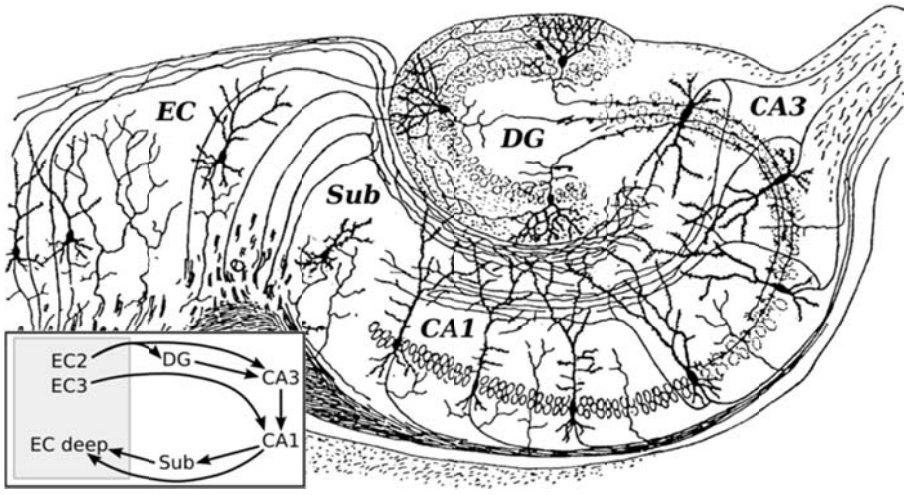

Figure 1.2: Neural Circuitry of the Rodent Entorhinal Cortex and Hippocampal Projections (Ramón y Cajal, 1911).

The perirhinal cortex is also located on the ventral surface of the temporal lobe, and it is adjacent to the entorhinal cortex (Murray & Richmond, 2001; Squire & Zola, 1996; Vargha-Khadem & Gadian, 1997). It plays an important role in declarative memory (Squire & Schacter, 2002) and object perception (Andersen et al., 2007; Murray & Richmond, 2001), and it receives visual projections from the neocortex (Squire & Zola, 1996). It is important in recognizing an object in its entirety, but it also has a role in distinguishing between objects and may even be implicated in memory storage (Murray & Richmond, 2001). The perirhinal cortex may also play a role in novelty detection. Neuronal activity in the perirhinal cortex may be linked to novel exposure to objects independent of their association with another object or particular context (VanElzakker et al., 2008).

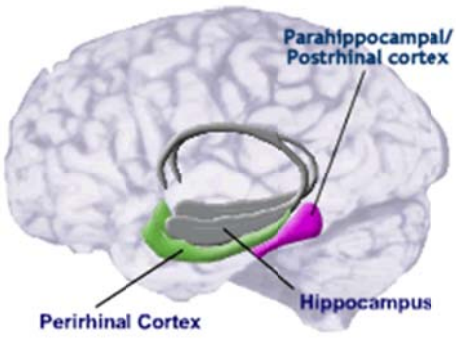

Figure 1.3: Location of Perirhinal Cortex (MRC Centre, 2011)

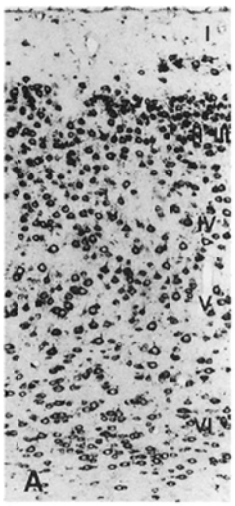

Figure 1.4: Perirhinal Cortex Layers II-VI (Kee et al., 2002).

The insular cortex is continuous, at the circular sulcus of the insula, with that of the adjacent frontal, parietal, and temporal lobes (Haines, 2006). In humans, the insular cortex plays a role in the processes associated with emotions, music, and language. It also plays a role in self/body recognition (Butti & Hof, 2010). Among mammals, the insular cortex varies greatly in regards to shape, function, and complexity. The insular cortex receives nociceptive (pain) visceromotor and viscerosensory input (Butti & Hof, 2010; Haines, 2006). It has intimate interconnections with limbic structures and cortical association areas that are damaged in AD (Colurso et al., 2003). In primates, the insular cortex is interconnected with the anterior cingulate cortex, the frontal pole and dorsolateral prefrontal cortex, the parietal and temporal lobes, and the entorhinal cortex. It also has reciprocal connections with the amygdala and dorsal thalamus, and several

intrainsular connections. In lab animals, such as mice, the insular cortex is organized into agranular, dysgranular, and granular fields (Butti & Hof, 2010).

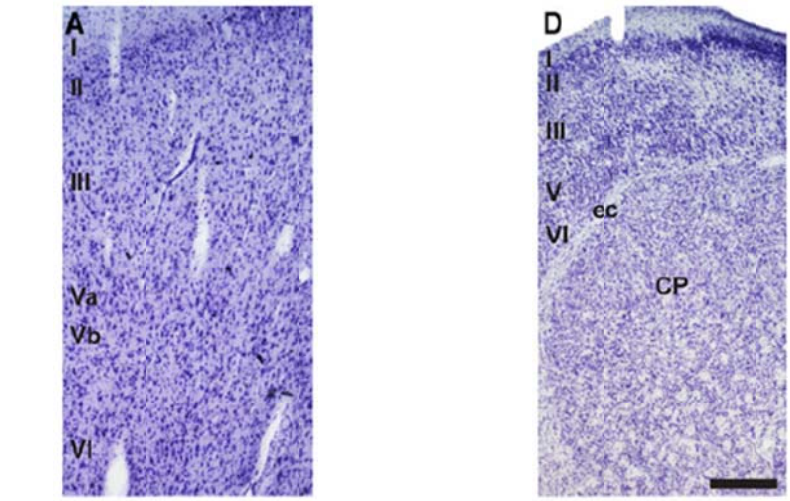

Figure 1.5: (A) Layers of the Human Insular Cortex; (B) Layers of the Mouse Insular Cortex (Butti & Hof, 2010).

The piriform cortex is a principle component of the olfactory cortex (Haines, 2006). The piriform cortex has extensive reciprocal connections with the entorhinal cortex, neocortical structures, and subcortical structures, including the amygdala and thalamus. The piriform cortex also receives excitatory afferent input from the olfactory bulb. Due to its structure and nature of its projections, the piriform cortex has been implicated in association memory (Ulinski, Jones, & Peters, 1999).

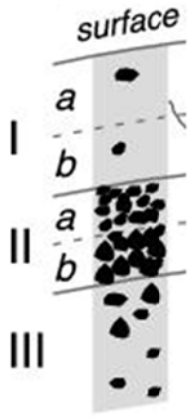

Figure 1.6: The Three Main Layers of the Piriform Cortex (Suzuki & Bekkers, 2007).

Aβ plaques in transition and piriform cortex. The entorhinal cortex and perirhinal cortex are implicated in the earliest pathological signs of AD (Braak & Braak, 1991; Thangavel, Van Hoesen, & Zaheer, 2009). Moreno-Gonzalez et al. (2009) discovered that, using the PS1xAPP murine model, the entorhinal cortex is affected by early NFTs and Aβ deposits, and it is also the site in the brain where the earliest apoptosis is detected. These early impairments block the continuous information transfer and contribute to the cognitive decline which occurs in early AD (Moreno-Gonzalez et al., 2009). Colurso et al. (2003) examined plaques (both diffuse and neuritic) in AD patients throughout cortical layers III, IV, and V of the insular cortex. The amount of diffuse Aβ plaques in these patients was significantly greater than in non-AD controls (non-AD elderly), and neuritic plaques were more localized in deeper cortical layers (2003). X.-M. Zhang et al., (2010) found evidence of plaques forming in the piriform

cortex of Tg2576 mice at 9 months of age and even more at 12 months of age with increases to 18-24 months of age.

Hippocampus

The hippocampus (HC) is located in the medial temporal lobe of the brain. Although it is relatively small in volume, it consists of complex structures called the cornu ammonis (CA fields 1-4), the dentate gyrus (DG), and the subiculum (Cho et al., 2010). The HC has been implicated in the acquisition of new memories (Barry & Doeller, 2010), spatial memory, storage of long-term memories, and maintenance of working memory for novel items and associations (Squire & Zola, 1996; Walker, Pavlov, & Kullmann, 2010).

Episodic and semantic components of cornitive memory are partly dissociable, and the HC is involved in memory systems that support episodic memory (Storandt, 2008; Vargha-Khadem & Gadian, 1997). The HC stores an index of components of complex information that is represented in different neocortical regions (Squire & Schacter, 2002). Celone et al. (2006) facilitated an fMRI study, using an associative memory task, comparing non-demented and AD diagnosed persons. In non-demented participants, hippocampal activity increased during the memory task and activity decreased in the resting areas of the brain (medial and parietal regions). In AD participants, hippocampal activity did not increase, and activity in the resting area did not decrease. This finding reinforces the attentional deficits in AD patients previously discussed, and accounts for the effect of early amyloid buildup in the parietal lobes and in

the medial prefrontal cortex (Celone et al., 2006). This reciprocal relationship can be blamed on either or both of the systems involved, but according to Storandt (2008), the HC has been blamed traditionally.

Spatial memory deficits have been examined in transgenic animals (Hsiao et al., 1995). Pyramidal cells in the CA3 and CA1 region of the HC have been implicated in spatial memory. These cells increase firing rate when a rodent is in a particular location in its environment and provide a representation of the rodent's position in its environment. Collectively, these pyramidal cells are called place fields, which were first discovered by O'Keefe and Dostrovsky (1971). Place fields change position relative to each other, and new representations are formed when an animal visits or is taken to a novel environment. This process is referred to remapping, and through this process, the HC establishes new and independent codes to present different spatial contexts (Barry & Doeller, 2010; O'Keefe & Dostrovsky, 1971).

The HC plays many crucial roles in brain functions, in addition to memory, such as mood regulation and stress (Fanselow & Dong, 2010; Hopkins, Abildskov, Bigler, & Weaver, 1997). Due to its multifunctionality, the HC can be broken down into distinct functional units, much like the neocortex. Fanselow and Dong (2010) support a functional segmentation of the HC into a dorsal, intermediate, and ventral component. The dorsal HC is strictly cognitive and involved in declarative memory regardless of emotional content; the ventral HC is tied to emotion and stress regulation responses, and the intermediate HC acts as a barrier between the other two regions with partly overlapping functional characteristics of each.

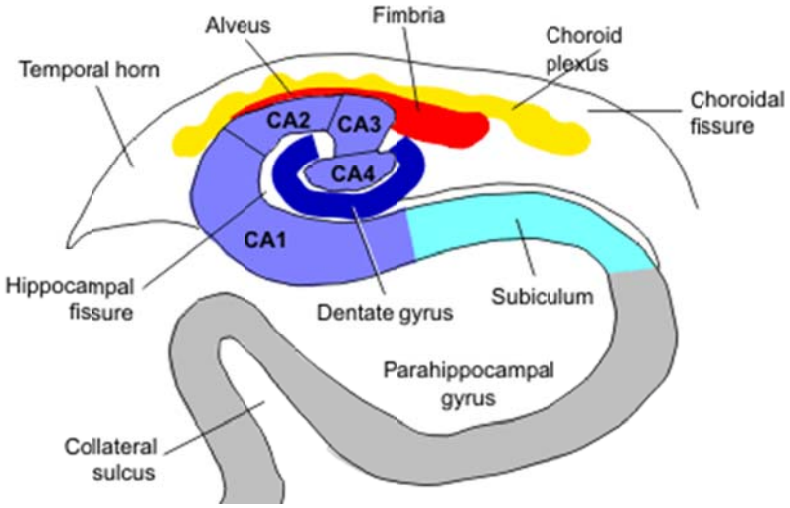

Figure 1.7: Hippocampal Anatomy (Hesselink, J., n.d.).

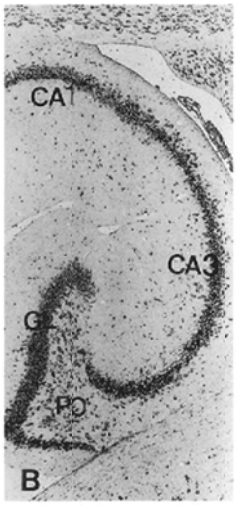

Figure 1.8: Hippocampal Anatomy, Stained Image (Kee et al., 2002).

Aβ plaques in hippocampus. The HC is significantly affected by neurodegeneration early in AD. Fukui, Takatsu, Shinkai, Suzuki, Abe, and Urano (2005), who examined learning and memory using the Morris water maze test, found Aβ congregated in the CA1 region of the HC of rats. Moreno-Gonzalez et al. (2009) studied early impairment of interneurons in the HC of PS1XAPP transgenic murine model. These mice develop Aβ plaques very early. Dense core Aβ plaques were detected by focal plane array maps (FTIR-FRA) and Synchrotron Fourier transform infrared and Raman analysis (sFTIR) in hippocampi of all TgCRND8 mice, which carry a double APP mutation, from 5 to 17 months (Kuzyk et al., 2010). Additionally, these plaques were found to be surrounded by diffuse, nonaggregated Aβ. Of the HC subfields, NFTs and amyloid plaque density is greatest in CA1 and the subiculum. In CA3 and CA4, only a small number of plaques have been observed, but the outer two-thirds of the dentate gyrus have exhibited a heavy neuritic plaque presence (Andersen et al., 2007).

Neocortex

The neocortex is believed to be the permanent repository of memory (Squire & Zola, 1996). In humans, the neocortex refers to the outermost layer of the cerebral cortex that is separated into the four lobes. The human neocortex is expanded and contains a significant increase in number of cortical areas as compared to other mammals. This expansion accounts for higher processing abilities including perception, cognition, language, and volitional motor responses. A relationship exists between the size, number,

and interconnectedness of cortical areas with the complexity of the species's perceptual, motor, language, and cognitive abilities (Cantania, 2004; Krubitzer & Huffman, 2000).

Brain size alone does not determine superior cognitive ability. A larger brain is needed to run a larger body in order to control more muscles and to process larger volumes of somatosensory inputs. Also, larger cell bodies are needed to support longer axons and dendrites in larger brains. However, more important is the number of cortical subdivisions and increase in connection length to maintain global connectivity. For instance, larger-brained mammals, like primates, have more cortical subdivisions than smaller-brained mammals, like rodents. Some primates can have as many as 20-30 visual areas, 15 auditory areas, and more than 10 motor areas. In contrast, examination of the organization of visual cortex in rodents suggests that they have a relatively simple visual system containing a primary and secondary visual cortex (V1 and V2) and few other areas. A benefit of additional neocortical subdivisions is the ability to process different aspects of sensory stimuli in different areas (Cantania, 2004).

Neocortex development can be affected by environmental factors. In the somatosensory system of rodents, each whisker is represented by a separate unit in their primary somatosensory cortex (S1). Development of the sensory system begins with the skin; it is through the whiskers' contact with the environment that cortical development is instructed. Damage to development of whiskers would, thus, halt formation of the corresponding S1 area (Cantania, 2004).

However, observation across mammals suggests that there is a common plan of neocortical structure organized around a network of thalamocortical and corticocortical

connectivity. The rostrocaudal and mediolateral organization of sensory systems and fine thalamocortical topography is conserved across species due to the conservation of the developmental mechanisms that create this organization. Thus, in general, the main topographic interactions between the thalamus and cortex are maintained. Support for this theory has been examined in animal studies in which the peripheral components of a particular sensory system have been lost or damaged. Despite this damage, evidence has revealed that the thalamocortical connections remain in place, even if cortical areas are diminished (Krubitzer & Huffman, 2000).

The neocortex is involved in complex information about episodes and facts (declarative memory). The posterior neocortex, a crucial component of the visual system, is likely involved in representing complex information at encoding and re-representing it, and in some areas it is involved in retrieval. The representation of complex information requires the encoder to attend to or become conscious of specific components. The frontal neocortex (prefrontal lobe) is implicated in this attentional mechanism through control of working memory (Squire & Schacter, 2002).

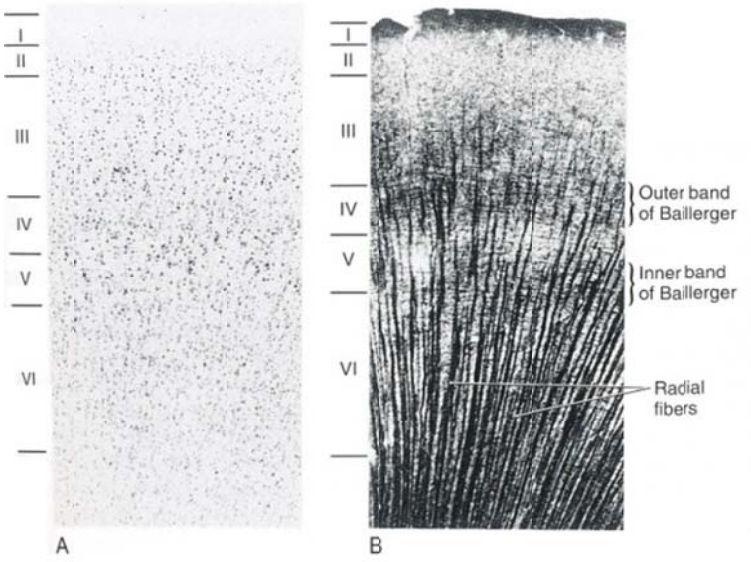

Figure 1.9: Nissl (A) and Myelin (B) Stains of adjacent sections of the Human Cerebral Cortex (Haines, 2006).

Aβ plaques in neocortex. The presence of extracellular Aβ that accumulates into plaques in AD is abundantly present in the cortex as evidenced by human and rodent studies (Braak et al., 1989; Braak et al., 1991 Echeverria et al., 2004; Hsiao et al., 1995). This physiological finding has behavioral implications. Behavioral and psychological symptoms of dementia (BPSD) include frequency of depression, psychosis, and aggression. (Tsang et al., 2008). In fact, transgenic mice have been known to exhibit aggressive behavior as well (Horgan et al., 2007). BPSD is considered to be directly linked to neuronal degeneration and altered neurotransmission.

Amygdala

Neuroanatomical evidence strongly suggests that the amygdala refers to arbitrarily defined heterogeneous nuclear groups referred to as the amygdalar nuclei or complex (Aggleton, 2000; Swanson & Petrovich, 1998) located in rostromedial part of the temporal lobe (Haines, 2006). The nuclear groups are largely categorized as basolateral nuclear group, the corticomedial nuclear group, and the central nucleus (Aggleton, 2000). These functionally different systems include a specialized expansion of the striatum (the central nucleus), components of the olfactory cortex (corticomedial nuclear group), and an extension of the claustrum (the basolateral nuclear group) (Aggleton, 2000; Swanson & Petrovich, 1998).

The amygdalar complex merges emotional and cognitive systems and, thus, impacts both learning processes and behavior (Aggleton, 2000). In addition to being implicated in emotional memory, the amygdala may also be involved in some of the behavioral changes exhibited in living AD patients (Storandt, 2008). Neuroimaging studies have further implicated the amygdala in AD. For instance, magnetic resonance imaging (MRIs) has shown decreased amygdala volume in AD patients (Hořínek et al., 2006) accounted for by neuronal loss, NFTs, neuritic plaques, diffuse plaques, and Lewy bodies (Aggleton, 2000). Damage to the amygdala has been associated with changes in eating habits, behavioral problems, inability to recognize emotion, and deficits in emotional memory processing (Aggleton, 2000; Hořínek et al., 2006). Hořínek et al. performed MRI measurements on the volume of the amygdala in AD patients to test the hypothesis that reduced volume may be associated with psychiatric symptoms. After

examining both AD and non-AD subjects, Hořínek et al. found that amygdala and HC volumes were reduced in the AD subjects. This study and other studies have been unable to definitively implicate the individual effect of damage to the amygdala on declarative memory, but the damage caused to the amygdala cannot be arbitrarily separated from the damage caused to the rest of the brain in AD.

The amygdala is particularly involved in fear conditioning and anxiety states and both the arousal and suppression response to both of these states (Kopell & Greenberg, 2008). Classical fear conditioning is impaired in AD patients (Storandt, 2008). The link between amygdala and fear conditioning deficits has been examined extensively in animal models with evidence showing the difficulty that animals experience when lesions are administered to their amygdala. Rabinak and Maren (2008) discussed a general history of these types of experiments where as a consequence of being paired with an unconditioned stimulus (US) (a shock), a conditioned stimulus (CS) (a tone) becomes feared. The conditioned fear response (CR) may manifest in the form of increased heart rate, increased blood pressure, stress hormone release, or freezing behavior. Animals with lesions to their amygdala may exhibit lower levels on measurements of the CR and may be slower to extinguish the CR.

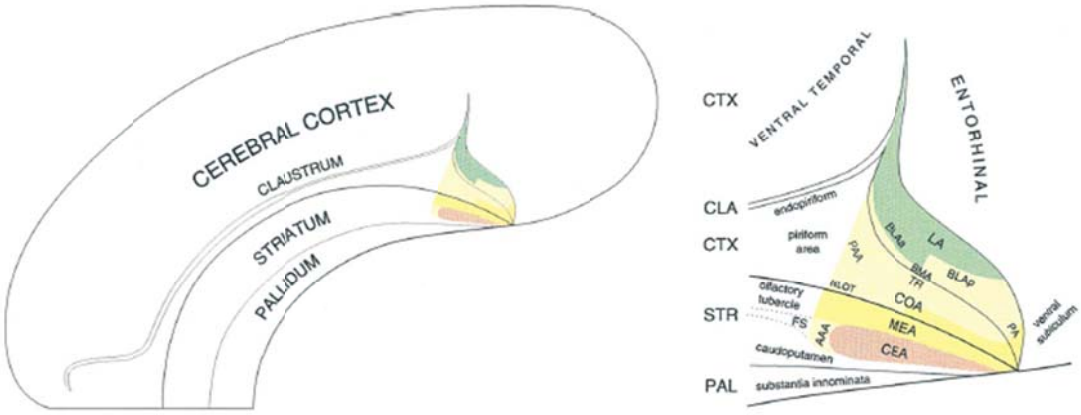

Figure 1.10: Structural Organization of Amygdalar Nuclear Groups (Swanson & Petrovich, 1998).

Aβ plaques in the amygdala. Although the amygdala is most commonly associated with NFTs, numerous amyloid plaques are found in the amygdala of Alzheimer's disease patients. Evidence suggests that amygdalar plaques form first in the corticomedial and central nuclear groups; then the process spreads to the basolateral areas (Aggelton, 2000). However, in the autopsied brains of AD patients, plaques are more prominently found in the accessory basal and medial basal nuclei and are least numerous in the medial, lateral, lateral basal, and central nuclei (Aggleton, 2000).

Basal Ganglia

The basal ganglia (BG) are a large system of neurons through which the cortex affects behavior. Specifically, these subcortical nuclei modulate signals that travel in parallel circuits from the cerebral cortex through the BG to the thalamus and then back to

the cortex. While the BG are largely associated with motor behavior, they are involved in various motor and affective behavior, in sensorimotor integration, and in cognitive functions (Haines, 2006).

The BG, in the telencephalon, comprise the dorsal and ventral striatopallidal complexes. The former consists of the dorsal striatum, the caudate nucleus and putamen, and the dorsal pallidum, the globus pallidus. The ventral striatopallidal complex consists of the ventral striatum, nucleus accumbens, the olfactory tubercle, and the ventral pallidum (largely synonymous with the substantia innominata). Some scientists include extratelencephalic components, such as the subthalamic nucleus (diencephalon) and substantia nigra (midbrain), in the term basal ganglia because of their structural and functional relationship with the dorsally located caudate and lenticular nuclei (putamen and globus pallidus) (Haines, 2006; Utter & Basso, 2008).

The globus pallidus can be broken down into the medially lying internal segment (GPi), which is referred to as the entopeduncular nucleus in rodents, and a laterally situated external segment (GPe), which is referred to as the globus pallidus in rodents. These two segments are divided by a sheet of white matter called the medullary lamina. The substantia nigra can be separated into the dopaminergic neurons of the pars compacta (SNc) and the more diffusely scattered GABAergic neurons of the pars reticulata (SNr). Most of these nuclei form circuits with thalamus and cortex (Haines, 2006; Utter & Basso, 2008). Of this network, the striatum and the subthalamic nucleus (STN) are the main input nuclei. These nuclei, along with SNc and SNr, receive input from throughout the cerebral cortex (Utter & Basso, 2008). The two nuclei that project outside of the BG

are the GPi and the SNr (Utter & Basso, 2008). The output nuclei of the BG innervate multiple regions of the brain, including the dorsal thalamus, superior colliculus, and pedunculopontine nucleus (PPN) (Utter & Basso, 2008).

The BG have long been associated with motor behavior. All straital neurons utilize GABA as a neurotransmitter, thus the BG circuits affect behavior through a disinhibition of signals. A balanced system of inhibition of striatal output systems is responsible for normal body movements (Wickens, 1993). This specifically refers to the dorsal striatopallidum loop system. In general, the direct loop facilitates a flow of information through the thalamus, and the indirect loop inhibits this flow of information. Movement is initiated through the direct loop and involves GPi, and movement is suppressed through the indirect loop and involves GPi, GPe, and the subthalamic nucleus. In the normal condition, these two loops are in balance by modulating the extent of inhibition (Haines, 2006).

The direct and indirect loops function via disinhibition (see Figure 1.10). Disinhibition is the release of cells from inhibition. The direct loop releases the thalamus from its pallidal inhibition by striatopallidal inhibition of pallidothalamic neurons. The indirect loop releases the subthalamic nucleus from inhibition from the lateral pallidal segment so that it can excite the inhibitory pallidothalamic cells. Therefore, the balance obtained in the normal condition is between the thalamic disinhibition by the direct loop and the subthalamic disinhibition by the indirect loop (Haines, 2006).

However, the BG are also associated with learning and memory, and with behavioral processes that are independent from motor behavior (Packard & Knowlton,

2002). Because the striatum specifically is located high in the hierarchy of brain control, it is involved in the control of many kinds of planning, decision-making, and action. The striatum has been implicated in internally directed choice behavior. When two choices are mutually exclusive, the striatum may be involved in assuring that one is chosen, and it may impact which one is chosen (Wickens, 1993).

The BG are also implicated in working memory along with the frontal lobes. Specifically, McNab and Klingberg (2008) showed that the BG mediated the input of only relevant information into working memory. This finding has implications for attention since the ability to control the encoding of new information is linked to working memory. The capacity to maintain working memory may be mediated by the ability to attend to relevant stimuli.

Additionally, the BG are also involved in memory organization or "habits." In this system, stimulus-response (S-R) associations are acquired incrementally. Animal studies implicate the BG in delayed alternation and response tasks; this system is distinguishable from the HC mediated associative learning system. Many researchers have concluded that these two systems are activated together in learning and memory (Packard & Knowlton, 2002). The BG's role in learning and memory has been examined though Parkinson's disease, Huntington's disease, dystonia, tourette syndrome, and obsessive-compulsive disorder (Utter & Basso, 2008).

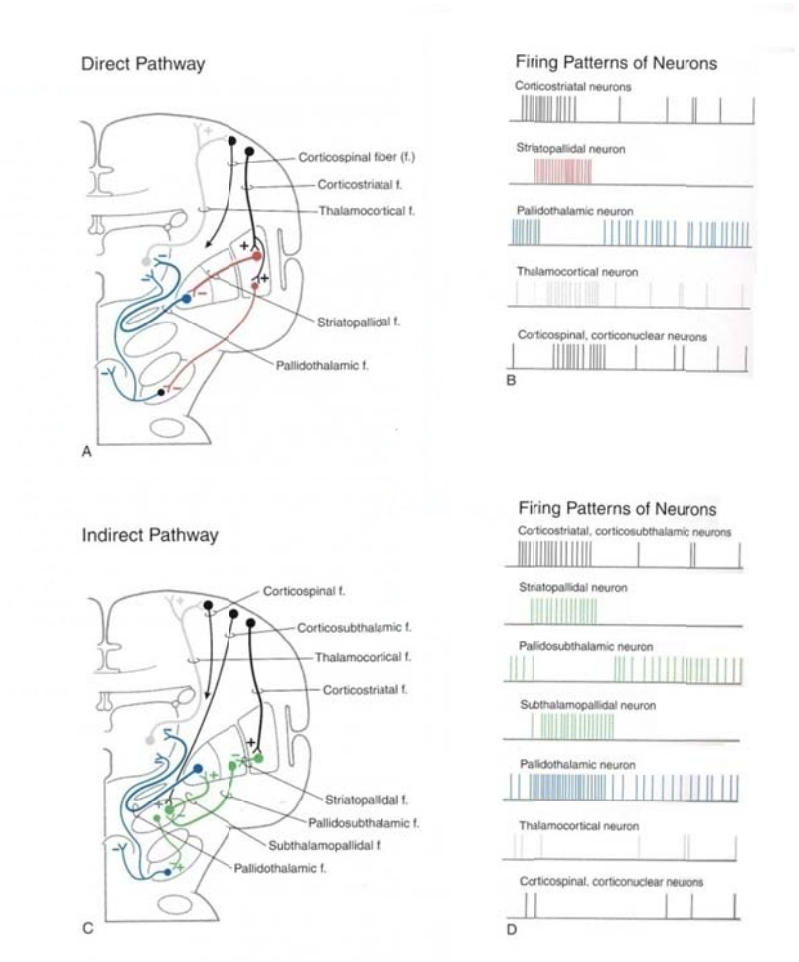

Figure 1.11: The Basal Ganglia Direct and Indirect Pathways (A, C) and the Corresponding Firing Patterns of Their Neurons (B, D). (The color of each fiber correlated with the color of the firing pattern [action potentials] of that neuron (B and D). The bold fibers in A and C represent the primary pathway in each example. +, excitatory synapse; -, inhibitory synapse) (Haines, 2006).

Aβ plaques in the basal ganglia. Studies have shown that the striatum is prone to AD pathology as amyloid depositions have been found in the striatum. Direct measurements of putamen in AD patients have revealed diminished volume of this structure. Data have been inconsistent in regards to atrophy of the caudate nucleus in AD.

Some studies have shown atrophy in this area associated with AD, but this is not the case in the study done by de Jong et al. (2008). Klunk et al. (2004) observed substantial amyloid in the striatum of AD patients. Striatal plaque deposition appears to occur early in the progression of AD and coincides with neocortical pathology and cognitive changes. However, most striatal AB deposits are not associated with dystrophic neurites. Neuritic plaques have been observed in the ventral striatum, but other striatal areas appear to be fibrillar (Klunk et al., 2004).

Metals Associated with AD

Metal ions contribute to important biological functions in the brain, such as nerve transmission, muscle contraction, and oxygen transport (Crichton, Dexter, & Ward, 2008). Zinc (Zn) plays an important role both in catalysis and in the stabilization of the structure of many proteins (Sever, 1975). Due to its ubiquitous nature, Zn homeostasis in humans requires the coordinated activity of members of several Zn transporter families, particularly those involved in Zn ingress and egress from cells and organelles. Metalloenzymes containing iron (Fe) or copper (Cu) are imperative in key metabolic pathways within nervous tissues. For example, they are involved in neurotransmitter synthesis and in neuroprotection. However, if there is a deficiency of these critical metals, then harmful consequences could ensue, and if these metals accumulate in excess, then they generally contribute to neurodegeneration (Crichton, Dexter, & Ward, 2008).

In addition, in vitro studies have characterized the interactions of these metals with APP, Aβ, and many enzymes and other proteins involved in AD-related pathways.

AB proteins are known to have metal ion binding sites (Falangola, Lee, Nixon, Duff, & Helpern, 2005). Zn, Cu, and Fe have been found in the brains of humans and transgenic mice in association with amyloid plaques (Linkous et al., 2009). It is not definitive whether these metals have an overall damaging or alleviatory role in AD progression, as evidence is varied, but each metal must be considered individually.

Zinc

Zinc (Zn) is required for the metabolism of nucleic acids and synthesis of protein (Sever, 1974). It is transported into the brain via the blood brain barrier (BBB) and blood cerebrospinal fluid barrier (BCB). To maintain homeostasis, brain capillary endothelial cells respond to changes in Zn status by increasing or decreasing Zn uptake. In the brain, Zn is distributed in three pools: (1) a membrane-bound metalloprotein involved in metabolic reactions and non-metabolic functions (biomembrane structure and support); (2) a vesicular pool in nerve terminal synaptic vesicles, and (3) an ionic pool of free or loosely bound ions in the cytoplasm. Zn concentrations, particularly vesicular Zn, are highest in the hippocampus, amygdala, and neocortex and are relatively low in cerebellum. In general, Zn homeostasis is maintained by three families of proteins called metallothioneins (MT), Zrt-Irt like proteins (ZIPs), and zinc transporter proteins (ZnT) (Lovell, 2009).

Zn is essential for brain metabolism (Heinitz, 2005; Sever, 1974) and remains relatively constant in the brain throughout adult life (Lovell, Robertson, Teesdale, Campbell, & Markesbery 1998). Zn is involved in glutamatergic functions in synaptic

vesicles, the synaptic gap, and the post-synaptic membrane (Heinitz, 2005). However, there is evidence to suggest that, like Cu, Zn ions are implicated in AD pathogenesis when bound to Aβ peptides. In most areas of the brain, extracellular levels of Zn ions are low. However, in some areas like the hippocampus, amygdala, and cortex, there are higher concentrations. Since these brain areas are consistently associated with AD, many researchers believe the Zn synapses located where these ions congregate are implicated in AD (Tõugu, Karafin, & Palumaa, 2008). Additionally, Zn binding to Aβ plaques makes the complexes more difficult to clear by the action of proteases due, in part, to the increases adhesiveness caused by this binding (Bush et al., 1994).

A study by Tõugu et al. (2008) focused on the complexes formed by Aβ and Cu and Aβ and Zn. These researchers were able to determine that the manner in which Zn and Cu ions interact with Aβ is very different. The complex formed by a Zn ion and Aβ tends to be formed very quickly and is very weak. Increased Zn has been found in AD patients in both the plaques and the cortical tissue (Danielsson, Pierattelli, Banci, & Gräslund, 2007). When Zn (or Cu) binds to the full-length Aβ peptide chain in high concentrations, aggregation of Aβ can be induced. However, when Zn (or Cu) binds in low concentrations, the Aβ oligomeric structure becomes less stable, and the Aβ aggregation is prevented. Therefore, the effect of metal on Aβ depends on factors such as pH, salt concentration, and metal concentration (Danielsson et al., 2007).

In vitro studies have shown that when Aβ binds with Zn leads to increased aggregation (Bush et al., 1994; Lovell et al., 1998). However, Linkous et al. (2009) researched the effect of Zn on plaque formation. Research using Tg2576 yielded results

that transgenic animals raised on Zn water had fewer and smaller plaques than transgenic animals raised on water with no deliberate metal content. Plaque location in this study referred specifically to the molecular and hilar areas of the hippocampal dentate gyrus. Both transgenic mice groups experienced impaired spatial memory on the Morris water maze experiment, and the animals raised on Zn water were the most impaired. Additionally, Bush et al (1994) found that soluble Aβ in humans is more likely to form toxic amyloid than soluble Aβ in rats in the presence of Zn. These results implicate a larger scope of neurodegeneration beyond plaque number and size in the behavior deficits associated with AD. Zinc may also have a role in the modulation of APP, thereby potentially leading to a greater deposition of Aβ (Lovell et al., 1998).

González et al. (1999) performed a study in order to uncover a potential relationship between serum Zn and Apo E polymorphism in AD. These researchers found that Zn concentrations are higher in AD patients who carry one Apo E4 allele than in control subjects who carried the same allele, and it could in fact act as an independent risk factor. Also, Zn that floods into the brain as a result of brain injury has been implicated in brain injury as a risk factor in AD (Frederickson et al., 2005).

Copper

Copper (Cu) is an essential element in health (Lovell et al., 1998). It is clear that Cu is heavily regulated in the body due to its importance in cellular function and its cytotoxic nature in oxidative stress. Imbalance of Cu homeostasis may result in a multitude of problems, including neurodegenesis, in AD. Cu ions absorbed from the

small intestine are transported in blood by binding to a protein called ceruloplasmin (Choi & Zheng, 2009; Lovell et al., 1998). Most of this Cu is distributed to the liver and kidneys. At the cellular level, the uptake of Cu into cells is thought to be mediated by two transporter proteins (Ctr1 and DMT1). The mechanism by which Cu is transported into the brain and the relative roles of the blood brain barrier (BBB) and cerebrospinal fluid (CSF) in regulated Cu homeostatis is not as clear. However, evidence suggests that it is the free form of Cu that enters the BBB, not the protein-bound Cu (Choi & Zheng, 2009).

Links have been made between Cu metabolism and late-onset neurodegenerative disorders (Macreadie, 2008). Cu is important for the function of many enzymes in living tissue. Cu in its free forms is toxic, so proteins in the body closely control its absorption, distribution and excretion. Cu is more toxic when ingested from water as opposed to food; in drinking water it has been known to exacerbate the inflammatory response in the aging brain (Campbell, 2006). Alterations of Cu homeostasis have been implicated in neurological disorders like AD. In AD, Cu has been associated with the aggregation of Aβ and plaque buildup in animal models and in vitro (Campbell, 2006; Pajonk et al., 2005). Furthermore, Cu may play a role in initiating the brain's inflammatory responses. However, its role in this response may have beneficial implications in the body's immune response if the response is not too prolonged (Campbell, 2006).

APP has been implicated in balancing Cu concentrations in cells (Bayer & Multhaup, 2005) because it can act as a metalloprotein and modulate Cu transport via its copper binding domain (CuBD) (Kong et al., 2008). Overexpression of APP in Tg2576 mice and postmortem AD brain tissue have shown reduced Cu levels (Bayer & Multhaup,

2005), whereas APP- and APLP2- knock-out mice have shown increased Cu levels in the cerebral cortex and liver (Pajonk et al., 2005). Conversely, Cu has been shown to influence APP processing in cells by reducing Aβ levels when it binds to CuBD (Kong et al., 2008; Pajonk et al. 2005).

These findings support the hypothesis of an inverse relationship between high Cu levels and Aβ production and accumulation (Bayer & Multhaup, 2005). Panjonk el al. (2005) showed that the cognitive disabilities in patients with mild to moderate AD correlate significantly with low to moderate serum Cu levels. They concluded that AD patients suffer from a mild Cu deficiency.

In vitro observations and in vivo data from APP mouse models show that APP overexpression allows for intracellular Cu to be transported out of the cell (Bayer & Multhaup, 2005). In Tg2576, overexpression leads to less Cu overall, but not Fe, just prior to onset of plaques. Bayer and Multhaup (2005) concluded that high Cu levels in plaques and low cellular Cu lead to the progression of AD in those inflicted.

Iron

Iron (Fe) is essential for a multitude of functions in the CNS, including DNA synthesis, gene expression, myelination, neurotransmission, and mitochondrial electron transport (Benarroch, 2009; Falangola et al., 2005). Homeostasis of Fe is important because either excess accumulation or depletion of Fe could impair normal function and promote cell death. Fe transportation in the brain depends on interactions between the endothelial cells and astrocytes. Brain endothelial cells express the transferrin receptor 1

(TfR1) in their luminal membrane (Benarroch, 2009). The best-known mechanism for Fe transport into the brain involves the binding of iron-containing transferrin to its receptor and its translocation to the intracellular compartment (Hirsch, 2009). Transferrin is the main source of Fe for neurons, which express high levels of TfR1 (Benarroch, 2009). Transferrin receptors have been found on the plasma membrane of neurons and glial cells. Another transfer protein that carries iron into the brain is called lactoferrin (Hirsch, 2009).

Fe is also a key component of many proteins that are important for brain function, including the proteins that compose the mitochondrial electron transport chain (Ong & Farooqui, 2005). The level of brain Fe is controlled by the blood brain barrier (BBB) and proteins that mediate Fe control. Increased Fe levels have occurred in AD, and certain free forms of Fe can cause neuronal injury in neurodegenerative diseases (Lovell et al., 1998). A relationship has been found between disturbed Fe homeostasis, APP synthesis and processing, and Aβ accumulation (Reznichenko et al., 2006).

Increased Fe levels in NFT, glial cells, and plaques have been noted in AD (Benarroch, 2009; Dawbarn & Allen, 2007; Lovell, Ehmann, Butler, & Markesbery, 1995; Ong & Farooqui, 2005); this is likely due to its increased uptake into the brain (Ong & Farooqui, 2005). Fe has been reported to accumulate in neurons with NFTs and cause the aggregation of tau (Yamamoto et al., 2002). In a study by Yamamoto et al., it was established that Fe can bind to hyperphosphorylated *t* (PHF*t*) and induce its aggregation. Analysis into the cortical structures of Tg2576 mice shows significant increase in Fe and Zn (but not copper [Cu]) in amyloid plaques as compared to

surrounding tissue. In these cases, five times as much Fe and six times as much Zn has been reported (Ong & Farooqui, 2005).

The complete role of Fe in the pathogenesis of AD is unclear. Studies have shown that Aβ and Fe are involved in the formation of free radicals and oxidative stress in the AD brain (Falangola et al., 2005). Fe can facilitate aggregation of Aβ into oligomers, and Fe can interact with Aβ to generate reactive oxygen species (Ong & Farooqui, 2005). Oxidative stress changes have been determined to precede the primary neurodegenerative occurrences in AD (Waugh, 2008).

There is an overabundance of Fe found in the hippocampus, cerebral cortex, and basal nucleus of AD patients (Collingwood & Dobson, 2006), and the presence of Fe in and around Aβ plaques in the brain has been studied post-mortem in the human brain. MRI is an important tool in locating region-specific Fe accumulation in the brain. More study into Fe could result in it being classified as a possible biomarker for AD and possibly other neurodegenerative diseases. Being able to locate altered regional Fe levels and to differentiate between Fe compounds in living patients could become more of a reality (Collingwood & Dobson, 2006; Falangola et al., 2005).

Interdependence of Metals Associated with AD

Various levels of Fe, Cu, and Zn have been found with Aβ42 within plaques in AD (House, Collingwood, Khan, Korchazkina, Berthon, & Exley, 2004; Lovell et al., 1998). A current theory implies that the initial accumulation of Aβ into a soluble, toxic form is due to the additive effect of Aβ42, zinc, and copper (Bush, 2008). Because each

of the metals has been observed interacting with Aβ42 in vitro, metal chelation has been suggested as a possible AD therapy in vivo. Bush et al. (1994) discuss the lack of evidence demonstrating the benefit of metal chelation in AD subjects. Adlard et al. (2008) echo this finding and suggest that chelators that lower tissue metal levels are unlikely to be helpful in remedying amyloid pathology. However, these researchers propose that a substance which inhibits metal-induced Aβ aggregation and/or reactive oxygen species generation could have AD treatment implications.

Such therapy has been delayed because experimental results have varied. In various experiments, different metals have been shown to interact with Aβ42 and contribute to plaque formation, while others have not (House et al., 2004; Linkous et al., 2009). For instance, House et al. (2004) found that Fe promoted aggregation of Aβ42 into β-pleated sheets, but Zn did not, and Cu was found to have protective effects. Metal chelation therapy was suggested for the former two metals, but a Cu chelator was deemed detrimental. Treatment interventions related to metal ions continues to be explored (Adlard et al., 2008).

Furthermore, the manner in which these metals affect each other is notable. Increased intake of Zn can cause Cu deficiency because intestinal absorption of Cu is inhibited by Zn. Cu is involved in the transport and metabolism of Fe via ceruloplasmin. Therefore, reduced Cu can lead to reduced Fe. Lab animals raised on Zn have exhibited reduced levels of Cu in their blood and have exhibited reduced absorption and retention of Fe. Lab animals who are given water that contains both Cu and Zn have exhibited improvements in spatial memory and fear conditioning. Reduced Cu levels caused by

increased Zn levels may be an important factor in the role of Zn in AD pathology (Linkous et al., 2009). Additionally, Zn and Cu are enriched in plaque amyloid where they directly aggregate Aβ. However, intracellular Cu is deficient in AD and could facilitate generation of Aβ, leading to a vicious cycle (Adlard et al., 2008). Potential drug therapies that target metals may be ineffective due to the interdependent nature of metals associated with AD and due to the importance of maintaining their homeostasis (Linkous et al., 2009).

Histological Data and Image Analysis

Amyloid plaques can be divided into two types: diffuse plaques and neuritic plaques. Diffuse plaques are composed of homogeneous deposits of fibrillary material but only contain a small amount of amyloid fibrils. Conversely, neuritic plaques are heterogeneous with a dense amyloid core in the form of insoluble and potentially neurotoxic β-pleated sheets. Neuritic plaques appear red when stained with Congo red and examined post-mortem (Andersen et al., 2007; Braak et al., 1989).

A significant breakthrough in understanding the neuropathology of AD would be the ability to detect and measure amyloid deposits in the living AD brain. This specifically applies to regions of amyloid-rich grey matter that can be viewed consistent with AD pathology. In vivo amyloid imaging would be crucial for confirming the presence of amyloid deposits, and as a byproduct, it could be instrumental in preventing, stopping, and/or reversing the formation of amyloid deposits (Wei et al., 2005).

Advancements have been made to histological analysis and imaging used to examine amyloid plaque load in transgenic mice. For instance, Wengenack, Jack, Garwood, and Poduslo (2008) developed MRI techniques to detect amyloid plaques throughout the cerebral cortex and hippocampus of the transgenic mouse brain. Additionally, Klunk et al. (2004) used the Pittsburgh Compound-B(PIB)—a prototypical benzothiazole amyloid binding agent—as a tool for in vivo brain imaging. The Pittsburgh Compound-B binds selectively to aggregated fibrillar Aβ deposits, but not to amorphous Aβ deposits like those found in the cerebellum. In this study, PIB was found to bind to AD cortical areas containing amyloid deposits, but not to the cortex of control subjects.

Breakthroughs such as this continue to be important in uncovering more information about Aβ, plaques, and cognitive deficits using mouse models. However, definitive diagnosis of AD in humans still requires postmortem examination of the brain through histological staining of amyloid plaques and neurofibrillary tangles (Wei et al., 2005). The current study uses post-mortem histological examination of neuritic plaques from the Tg2576 transgenic mouse in order to examine the effects of raising Tg mice on water with different metal content.

CHAPTER 2

METHODS

Experiment

The purpose of the current study was to examine amyloid plaque buildup in transgenic Tg2576 mouse raised on drinking water with different metal content. Previous research using the same group of transgenic animals focused on behavior, examining freezing behavior (evaluated by genotype) for two types of fear conditioning (contextual and cued) and for spatial memory assessed with the Morris water maze (MWM) (Burns, 2008; Railey, Groeber, & Flinn, 2011). The parameters for this group were:

Water type: lab water, iron, zinc, and zinc + copper

Genotype: transgenic Tg2576, wildtype Wt2576

The animals were separated by genotype—Tg2576 transgenic mice and the Wt2576 wildtype mice. The wildtype animals were used as a control group in the original fear conditioning experiment. This group of animals did not express the human APP gene and as a result did not have amyloid plaques. Therefore, Wt2576 mice were not used for the histological examination in the current study. In the Tg2576 mice, histological data concerning the amount of amyloid plaques found in different brain regions was examined.

It was expected that all Tg2576 transgenic mice would exhibit plaque formation, given the overexpression of the human APP gene. However, an expressed difference wasexpected between the mice raised on lab water and the mice raised on water with a metal content (Fe, Zn, Zn + Cu). This difference was expected due to the likelihood of the metals combining with Aβ. However a caveat was that copper was expected to reduce plaque buildup (Bayer & Multhaup, 2005).

Once behavioral tests that involved fear conditioning and spatial memory were performed on the animals, the mice were sacrificed at approximately 18 months of age (Burns, 2008; Railey, Groeber, & Flinn, 2011). Using standard protocol, the brains were sliced into coronal sections on a cryostat. Congo red staining techniques were used to locate and mark amyloid in the brain. Under a light microscope, neuritic amyloid plaques appear red. The images were captured by a digital camera mounted on a microscope.

The specific aim of this research was to (1) expand analysis of amyloid deposits in Tg2576, (2) contribute to research on the interaction of metals in the brain with amyloid and the implications of this interaction for cognition, and (3) determine if metal intake correlates to varying plaque concentration in specific brain regions.

Hypotheses

It was predicted that transgenic mice raised on Zn water would have the greatest amount of plaque burden since Zn has been shown to facilitate the accumulation of amyloid into plaques (Burns, 2008). Furthermore, it was predicted that transgenic mice raised on Zn + Cu water would exhibit a smaller amount of plaques than those raised on

Zn water due to the protective qualities of Cu in the accumulation of plaques (Bayer & Multhaup, 2005), and that transgenic mice raised on lab water (LH_2O) would exhibit the smallest amount of plaques. LH_2O was obtained directly from the faucet and had an insignificant metal content as compared to the other groups. However, given the results of the experiment by Burns (2008) on the same animal group, an alternative hypothesis was that Fe was expected to have less plaque burden than all other water groups including lab water.

Subjects

Eighty-three total female mice were obtained from Taconic Farms (Germantown, NY) at approximately three months of age, 40 of which were transgenic (Burns, 2008). From their inception into the lab, the animals were raised on plain lab water, iron water, zinc water, or zinc + copper water. The current study involves brain tissue extracted from 36 Tg2576 mice.

The 10ppm $Fe(NO_3)_2$ iron mixture was made by adding 10mL of $Fe(NO_3)_2$ to 10L of water. The zinc water was 10ppm $Zn(CO_3)$, which was made by adding 10mL of $Zn(CO_3)$ to 10L of water. The zinc + copper water was made by adding 10mL of $Zn(CO_3)$ and 250*u*L of $CuCO_3$ to 10L of water. Table 2.1 lists the original assignment of animal groups that were to be involved in both experimental runs (Groups a and b) during the study. However, one mouse died, 10 were removed from the study because of a genetic disposition to blindness, and one mouse was reassigned due to incorrect genotyping, leaving 72 total mice, 36 of which were transgenic. Table 2.2 lists the

combined census of Groups a and b. This table only includes the transgenic mice used in the current study, as the wildtype mice were excluded (Burns, 2008).

Table 2.1: Animal Groups for Both Experimental Runs.

(Original distribution of animals before death and removal of blind animals)

Group a	**Zinc**	**Zn + Cu**	**Iron**	**Lab/Plain**
Transgenic (Tg)	5	5	6	6
Wildtype (Wt)	6	5	5	4
Group b	**Zinc**	**Zn + Cu**	**Iron**	**Lab/Plain**
Transgenic (Tg)	5	4	5	4
Wildtype (Wt)	5	6	5	7

Table 2.2: Animal Groups for Histological and Statistical Analysis.

(Number of transgenic animals used, excluding the removed animals and wildtype animals)

Group a	**Zinc**	**Zn + Cu**	**Iron**	**Lab/Plain**
Transgenic (Tg)	7	9	10	10

Histological Tool

The histological tool used to analyze amyloid plaque buildup in Tg2576 brain tissue was the BioQuant NOVAPRIME image analysis system. BioQuant analyzes 24-bit color or black and white images. The system previously used for amyloid computation was called ImageJ. ImageJ was vulnerable to user error because it required the user to identity and circle amyloid plaques. BioQuant can be calibrated using RGB thresholding to select pixels that match amyloid criteria set by a user or group via automatic measurement.

The BioQuant system used for the histological analysis was located in David King Hall on the George Mason University Campus in Fairfax, Virginia. The computer installed with the BioQuant software was only used to examine brain tissue photographs.

Anatomical Definitions

The brain regions examined in the Tg2576 mice were transition and piriform cortex, hippocampus, neocortex, amygdala, and basal ganglia. For the purpose of the current study, anatomical regions were defined according to Franklin and Paxinos (2008). In this experiment, each section was obtained according to a specific distance from bregma. Bregma refers to the junction of the anterior sagittal and coronal sutures. Sections were obtained on the coronal plane (also called transverse or cross-section). Specifically, sections were taken at approximately 0.74mm (5), -0.70mm (4), -1.46mm (3), -1.94mm (2), and -3.16mm (1).

Transition and Piriform Cortex

Transition and piriform cortex, as defined by this study, was visible in all five sections. These areas included granular, dysgranular, and agranular dorsal, ventral and posterior insular cortices; piriform cortex; ectorhinal cortex; perirhinal cortex; dorsolateral and dorsal intermediate entorhinal cortex. Concurrently, these cortical areas were referred to as transition and piriform cortex in this study.

Hippocampus

In four of the sections (1, 2, 3 and 4), components of the hippocampus were visible. These include: alveus HC, oriens layer HC, pyramidal cell HC, radiatum layer HC, fimbria HC, dorsal hippocampal commissure, field CA1, CA2, and CA3 HC, molecular, granular, and polymorph layer of dentate gyrus, straitum lucidum HC, lacunosum moleculare, hippocampal fissure, dorsal subiculum (Franklin & Paxinos, 2008). Collectively, these groups were referred to as hippocampus for this study.

Neocortex

Neocortical areas were clearly defined in all five sections. These areas included primary and secondary motor cortices; primary and secondary somatosensory cortices; medial, lateral and posterior (rostral) parietal association cortices; ventral auditory cortex; primary and secondary auditory cortices; primary and secondary visual cortices; and temporal association cortex (Franklin & Paxinos, 2008). Concurrently these cortical areas were referred to as neocortex in this study.

Amygdala

In four of the sections (1, 2, 3 and 4), components of the amygdalar complex were visible, including the central and medial extended amygdala; anterior amygdala area; central amygdala nucleus; anterior, posteriolateral and posteriomedial cortical amygdaloid nucleus; intercalated nuclei of the amygdala; lateral and medial amygdaloid nuclei; basolateral amygdaloid nuclei; basomedial amygdaloid nucleus; posteriolateral and anterior cortical amygdaloid nuclei; medial amygdaloid nuclei; bed nucleus of the stria terminalis; intraamygdaloid division; lateral, medial, and capsular part of central amygdaloid nucleus; rostral amygdalopiriform; and lateral olfactory tract (Franklin & Paxinos, 2008). These nuclear groups were referred to as the amygdala in this study.

Basal Ganglia

In four of the sections (2, 3, 4 and 5), there were clearly defined basal ganglia nuclear groups. These groups included: dorsal and ventral striatum (caudate and putamen), lateral accumbens shell, accumbens nucleus shell and core, and pallidum. These nuclear groups were referred to as basal ganglia in this study (Franklin & Paxinos, 2008).

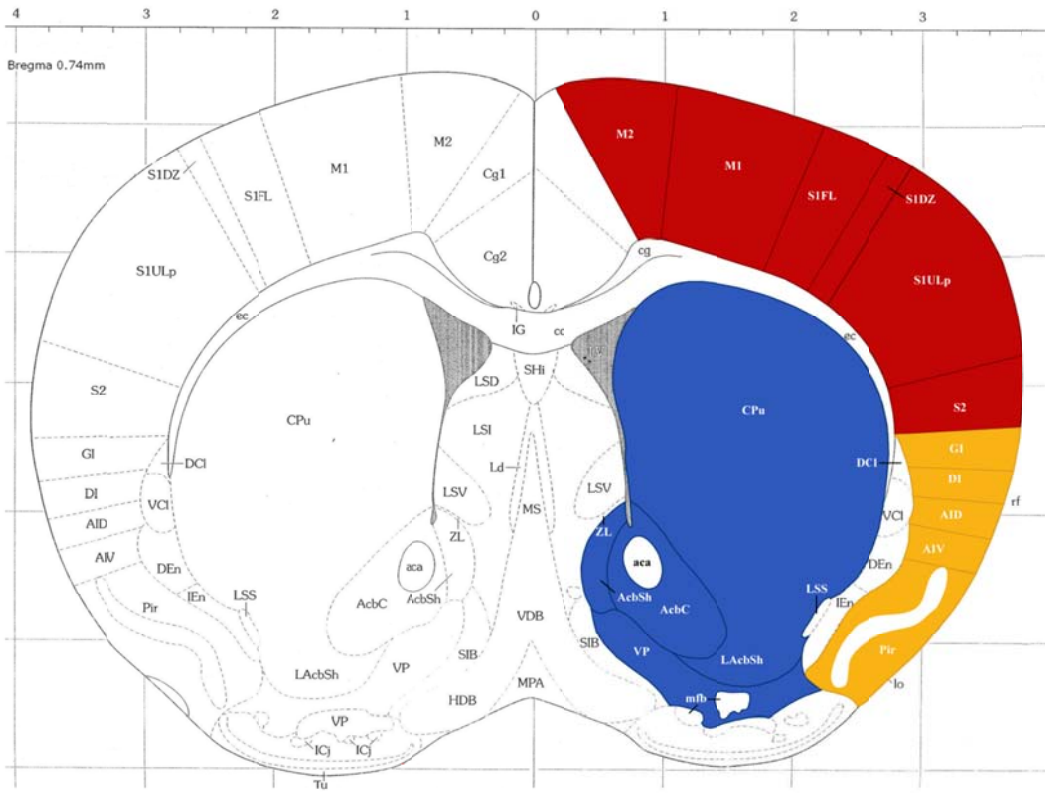

Figure 2.1: Anatomical Definition of Brain Regions for Bregma 0.74mm; blue = basal ganglia; red = neocortex; orange = association cortex (Franklin & Paxinos, 2008).

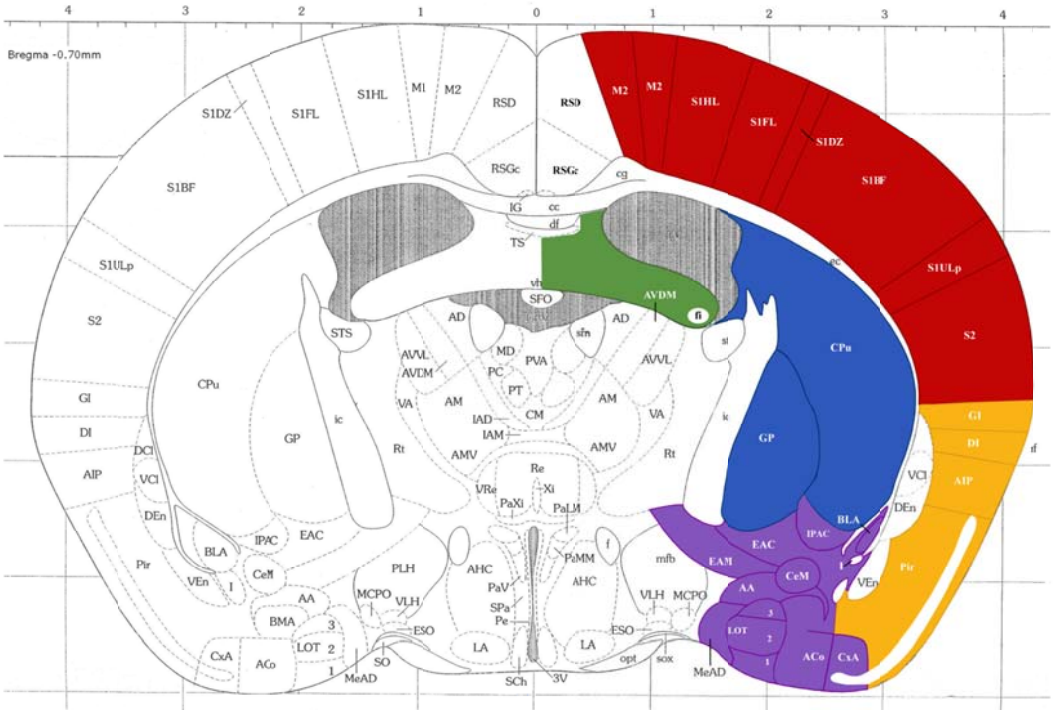

Figure 2.2: Anatomical Definition of Brain Regions for Bregma -0.74mm; blue = basal ganglia; red = neocortex; orange = association cortex; purple = amygdala ((Franklin & Paxinos, 2008).

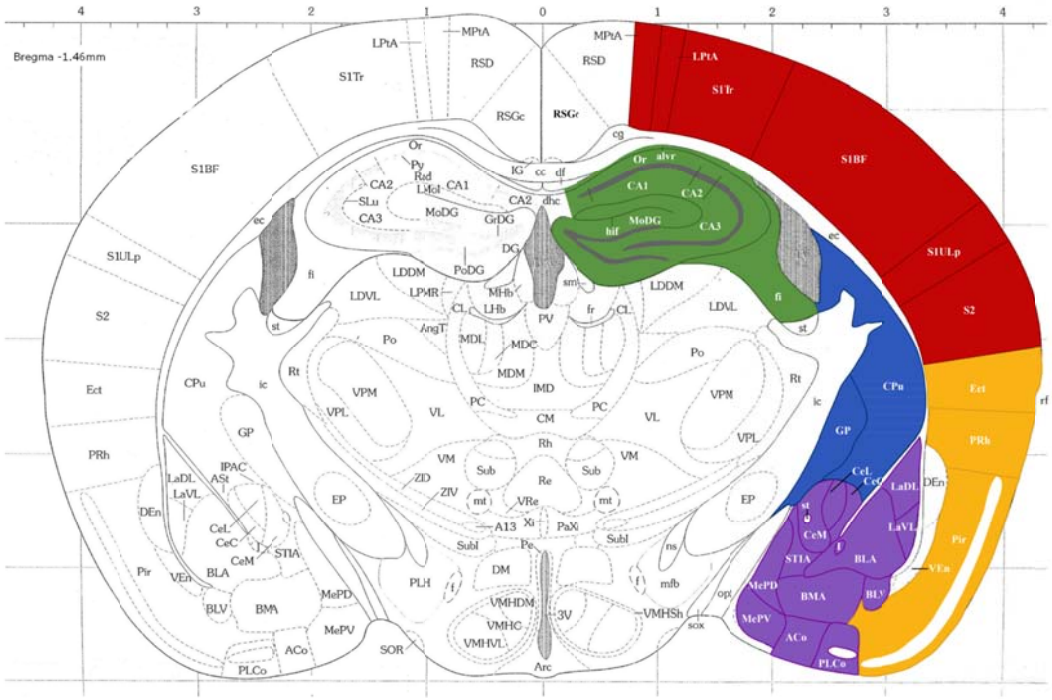

Figure 2.3: Anatomical Definition of Brain Regions for Bregma -1.46mm; blue = basal ganglia; red = neocortex; orange = association cortex; purple = amygdala; green = hippocampus (Franklin & Paxinos, 2008).

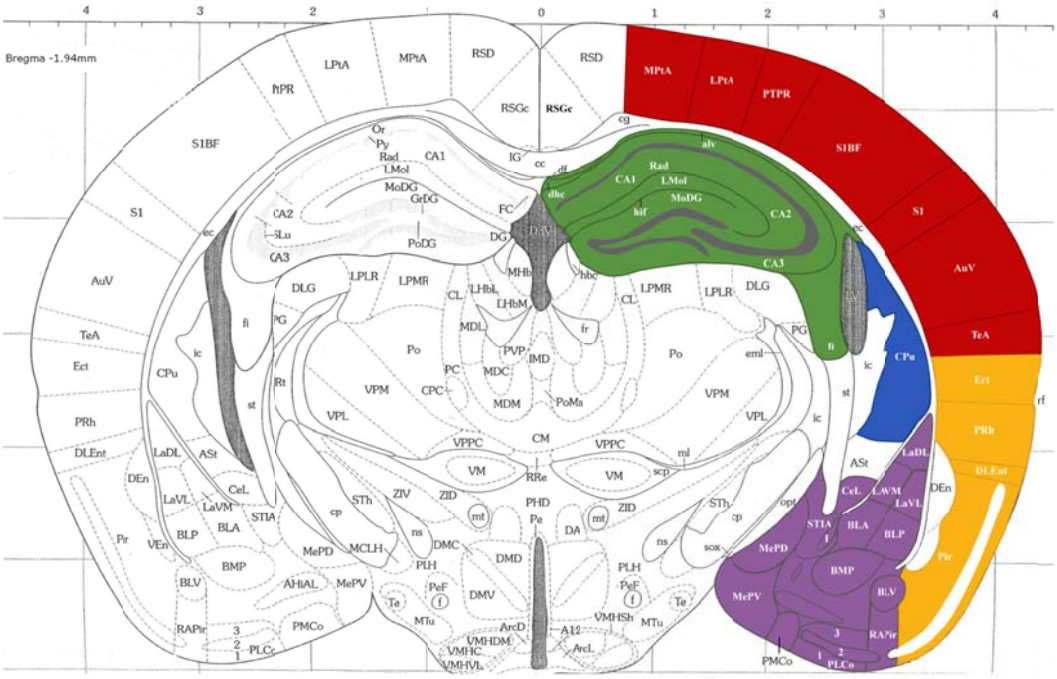

Figure 2.4: Anatomical Definition of Brain Regions for Bregma -1.94mm; blue = basal ganglia; red = neocortex; orange = association cortex; purple = amygdala; green = hippocampus (Franklin & Paxinos, 2008).

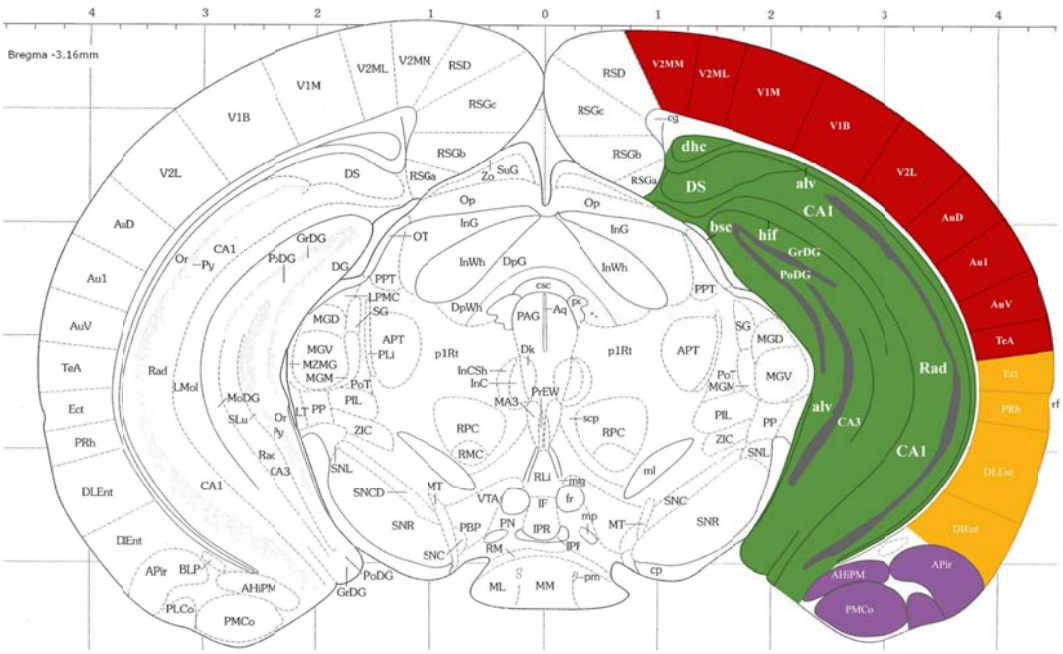

Figure 2.5: Anatomical Definition of Brain Regions for Bregma -3.16mm; red = neocortex; orange = association cortex; purple = amygdala; green = hippocampus (Franklin & Paxinos, 2008).

Histological Procedure

BioQuant was calibrated for use in this study by Lloyd Kinzer using images from the actual study. Lloyd Kinzer was employed by the BioQuant Image Analysis Corporation and acted as the liaison between the company and George Mason University. The system calibration included: calibrating at the highest camera calibration resolution (4048 x 3072), setting a region of interest that would apply to each image, and setting up measurement parameters (object count: count the number of plaques; area: calculate the area of each individual plaque). Each photograph containing congo red stained plaques

was loaded into BioQuant and measurement analysis was run to compute each parameter as outlined above.

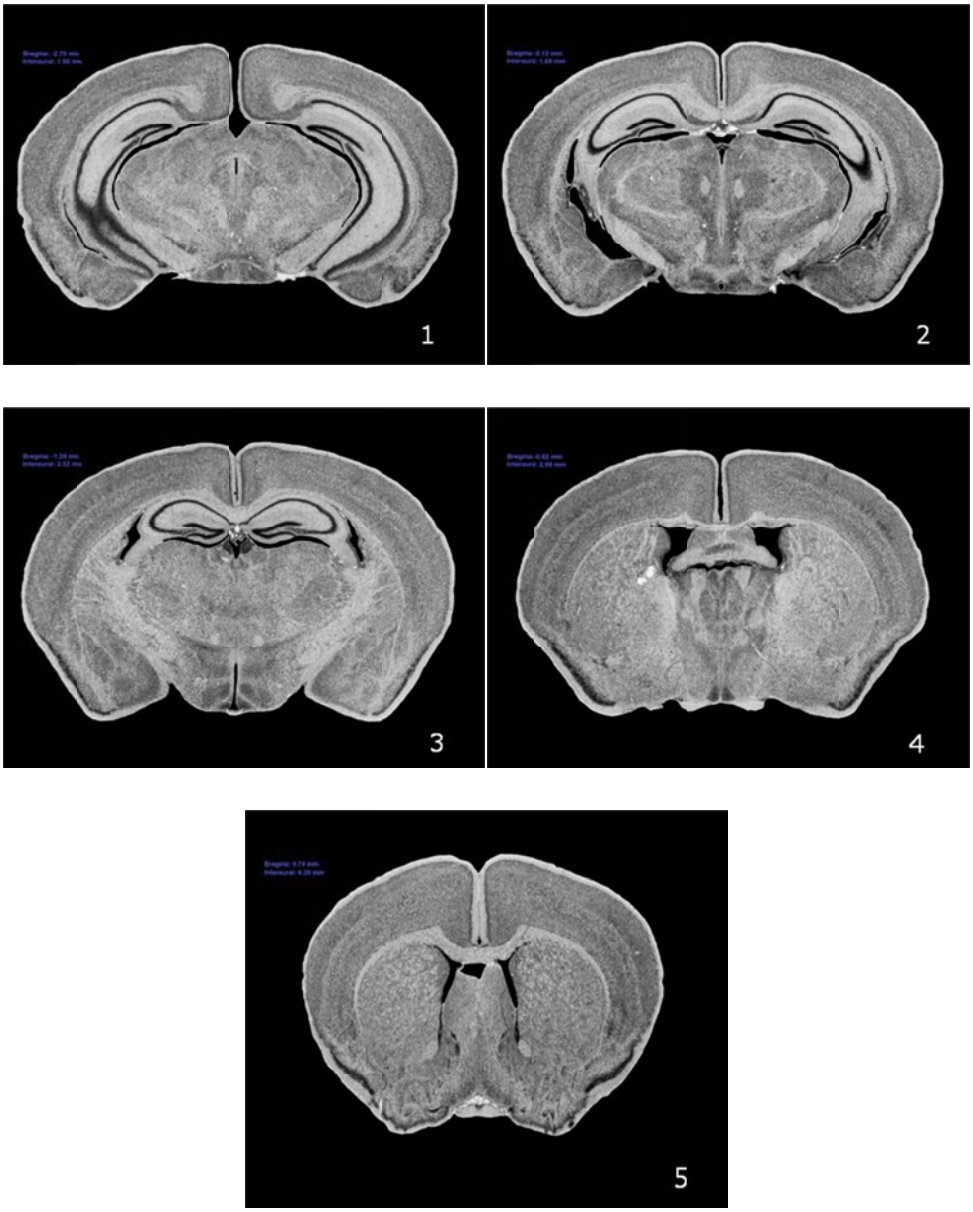

Figure 2.6: Nissl Tissue Examples: **1.** Bregma -3.16mm, **2**. Bregma -1.94mm, **3**. Bregma -1.46mm,, **4**. Bregma -0.70mm, **5**. 0.74mm (Burns, 2008).

Data from the plaque images was collected for each water group for the transgenic animals. The average area of plaques and number of plaques was analyzed in each brain region. The area of each brain region was also analyzed. The normalized area measurement was obtained from these numbers. Table 2.3 represents the number of measurements taken in each group. For each measurement, a normalized area value, an average individual plaque area value, and a plaque number value was obtained; there were a total of 1,454 values for each measurement parameter.

Table 2.3: Numbers of Measurements by Group.

Metal Type	**Number of Measurements**					
	TPC	**HC**	**NC**	**AMG**	**BG**	**Total**
Zinc	89	75	87	58	74	383
Zinc & Copper	84	65	84	54	66	353
Iron	90	75	96	58	79	398
LH_2O	64	68	77	45	66	320
Total	327	283	344	215	285	1454

TPC = transition and piriform cortex, HC = hippocampus, NC = neocortex, AMG = amygdala, BG = basal ganglia

CHAPTER 3

RESULTS

The current study addressed three research questions. Do certain metals exacerbate plaque load? Are plaques more heavily associated with particular brain regions? Is plaque load affected by a relationship between metal type and location within the brain? In this study, plaque load was examined using three different measurement parameters (normalized area, average area, and plaque number). Normalized area was derived by dividing the total area of plaques by the total area of the brain region in which the plaques were located. The average plaque area was derived by dividing the sum of all area measurements of plaques in each brain region by the number of plaques in that region. Plaque number represented the quantity of plaques in each region. Each of these measurement parameters was taken in five brain regions (transition and piriform cortex, hippocampus, neocortex, amygdala, and basal ganglia) grouped by type of water (iron, zinc, zinc + copper, lab water) on which animals were raised. Three two-way analyses of variance (ANOVA) were used to examine plaque load as affected by water/metal type and brain region. Each ANOVA was analyzed using a 4 (water/metal type) x 5 (brain region) ANOVA.

Each ANOVA produced significant results on Levene's Test of Equality of Error Variances. Because this ANOVA assumption was violated, the Welch-Aspin F approximation and the Brown-Forsythe F approximation were computed (Alexander & Govern, 1994) for each one-way analysis, but the results of each were also significant in all cases. Due to heterogeneity of variances, the significance values obtained in this study reflect corrected tests. This violation is less important because SPSS uses the regression approach to calculate ANOVAs (Leech, Barrett & Morgan, 2005). Games-Howell post hoc comparisons were computed to assess specific differences for each ANOVA because this post hoc test does not rely on homogeneity of variance. For each ANOVA, there were main effects by water/metal type (Fe, Zn, Zn + Cu, LH_2O) and by brain region (transition and piriform cortex, hippocampus, neocortex, amygdala, and basal ganglia). Excluding average area, there were significant interactions between water/metal type and brain region.

Relationship Between Certain Metals and Plaque Burden

It was predicted that transgenic mice raised on Zn water would have the greatest amount of plaque burden since Zn has been shown to facilitate the accumulation of amyloid into plaques (Burns, 2008). Furthermore, it was predicted that transgenic mice raised on Zn + Cu water would have a smaller amount of plaques than those raised on Zn water due to the protective qualities of Cu in the accumulation of plaques (Bayer & Multhaup, 2005), and that transgenic mice raised on lab water (LH_2O) would exhibit the smallest amount of plaques. However, given the results of the experiment by Burns on

the same animal group, an alternative hypothesis was proposed that mice raised on Fe water were expected to exhibit less plaque burden than all other water groups including LH_2O.

The normalized area ANOVA produced a significant main effect of water/metal type ($F(3,1434)=8.43$, $p=0.00$) (see Table 3.4). However, only 1.7% of the variance in the normalized area measurement can be accounted for by water/metal type. This small effect size does not represent a meaningful difference. The biggest mean difference was between Fe and Zn (see Figures 3.1A and 3.1B). Games-Howell post hoc comparisons were computed to assess specific mean differences. The results for Fe were significantly different from Zn ($p=0.000$) and Zn + Cu ($p=0.001$) but were not significantly different from LH_2O ($p=0.804$). Furthermore, Zn was significantly different from LH_2O ($p=0.002$), but not Zn + Cu ($p=0.823$). Also, Zn + Cu was significantly different from LH_2O ($p=0.014$) (see Table 3.7). Fe had the least plaque burden overall, and Zn had the largest (refer to Table 3.3 and Figures 3.1A and 3.1B).

For average area, there was a significant main effect of water type ($F(3,1434)=3.234$, $p=0.00$) (see Table 3.5). However, given the small Eta Squared value (0.007), the average area was not meaningfully different across water/metal type. Games-Howell post hoc comparisons showed the only significant difference across water/metal types was between Fe and Zn + Cu ($p = 0.039$) (see Table 3.8). Fe had the least plaque burden overall, and Zn + Cu had the largest (refer to Table 3.3; Figures 3.2A and 3.2B).

For plaque number, there was a significant main effect of water type ($F(3,1434)=19.652$, $p=0.00$) (see Table 3.6). However, the small effect size (eta = 0.039)

suggested that the number of plaques was not meaningfully different across water/metal type. Games-Howell post hoc comparisons showed the specific differences across water/metal types. Both Fe and LH_2O were significantly different from Zn ($p = 0.000$ and $p = 0.000$ respectively) and Zn + Cu ($p = 0.000$ and $p = 0.001$ respectively), although they (Fe and LH_2O) were not significantly different from each other (see Table 3.9). Fe had the smallest number of plaques overall, and Zn + Cu had the most (refer to Table 3.3; Figures 3.3A and 3.3B).

Regarding the normalized area analysis, Zn raised mice had the most plaque burden, but the Zn + Cu raised mice had the most plaque burden on the average area and plaque number analyses. This finding may challenge the hypothesis that Cu provides some protection from plaque formation. Furthermore, across all measurements of the dependent variable (normalized area, average area, and plaque number), Fe was the water/metal type with the smallest quantifiable plaque load overall (Table 3.1; Table 3.2; Table 3.3). In fact, Fe had the smallest quantifiable plaque load in almost all comparisons with the other water/metal types (Figure 3.1B; Figure 3.2B; Figure 3.3B). This finding confirms the results of Burns (2008).

Relationship Between Brain Region and Plaque Burden

It was predicted that plaque burden would be significantly different across brain regions. Additionally, the animals used in the current study were sacrificed at approximately 18 months of age (Burns, 2008). It was predicted that plaque burden would be more apparent in transition and piriform cortex, which is associated with

earliest amyloidosis. Conversely, it was predicted that less plaque burden would be evident in the basal ganglia because plaque formation in this brain region occurs later in neurodegeneration.

The normalized area ANOVA produced a significant main effect by region ($F(4,1434)=79.57$, $p=0.00$), but the effect was not big enough to implicate a specific region(s) in correlation with a quantifiable plaque load (Eta=0.182, see Table 3.4). Games-Howell post hoc comparisons were computed to assess specific mean differences. The neocortex significantly differed from the transition and piriform cortex, hippocampus, and basal ganglia. The transition and prirform cortex was significantly different from the hippocampus, basal ganglia, and amygdala in addition to the neocortex. The basal ganglia were significantly different from the hippocampus and amygdala (see Table 3.10). The basal ganglia had the least plaque burden, and the transition and piriform cortex had the largest (refer to Table 3.3; Figures 3.1A and 3.1B).

For average area, there was a significant main effect by brain region ($F(4,1434)=63.048$, $p=0.00$) (see Table 3.5). Although the small effect size (eta = 0.150) prevents drawing strong correlational conclusions. Games-Howell post hoc comparisons showed that neocortex and transition and piriform cortex were not significantly different, but they were both significantly different from hippocampus, basal ganglia, and amygdala. Also, hippocampus and basal ganglia were significantly different (see Table 3.11). The basal ganglia had the least plaque burden, and the transition and piriform cortex had the largest (refer to Table 3.3; Figures 3.2A and 3.2B).

For plaque number, there was a significant main effect by region ($F(4,1434)=96.686$, $p=0.00$) (see Table 3.6). Although this difference also had a small effect size (eta = 0.212), it was larger than any other effect size measurement obtained in analysis. Games-Howell post hoc comparisons showed that neocortex was significantly different from transition and piriform cortex, hippocampus, basal ganglia, and amygdala. Both the transition and piriform cortex and hippocampus were significantly different from basal ganglia and amygdala but not significantly different from each other. The basal ganglia and amygdala were significantly different (see Table 3.12). The basal ganglia had the smallest number of plaques, and the neocortex had the most number of plaques (refer to Table 3.3; Figures 3.3A and 3.3B).

Regarding the normalized area and average area measurements, the transition and piriform cortex was the brain region with the largest quantifiable plaque load overall. However, regarding the plaque number measurement, the neocortex was the region with the largest plaque load. Across all measurements of the dependent variables (normalized area, average area, and plaque number), the basal ganglia were the brain region with the smallest quantifiable plaque load overall. In fact, the basal ganglia had the smallest plaque load in all comparisons with the other brain regions.

Interaction Between Water/Metal Type and Location Within the Brain

For each measurement parameter, an interaction between water/metal type and brain region was assessed. The normalized area ANOVA produced a significant interaction between the two independent variables ($F(12, 1434)=5.42$, $p=0.00$) (see Table

3.4). Although a difference in the means existed, the effect of water/metal type on normalized area was too small to implicate brain region as a predictor of plaque load (Eta=0.043, see Table 3.4).

For average area, there was no significant interaction between the two independent variables (F(12, 1434)=1.362, p=0.178) (see Table 3.5). Therefore, the effect of water/metal type was independent of brain region, and the effect of brain region was independent of water/metal type. For plaque number, there was a significant interaction between the two independent variables (F(12, 1434)=3.520, p=0.000) (see Table 3.6). The small effect size (eta = 0.029) showed that this difference did not warrant meaningful interpretation (see Table 3.6).

Regarding normalized area, transition and piriform cortex always had the largest plaque load across water/metal type, and basal ganglia had the smallest plaque load (see Table 3.1). Across all water/metal types, Fe-raised mice had the least plaque load in the neocortex, transition and piriform cortex, hippocampus, and basal ganglia. Zn-raised mice had the highest plaque load in the transition and piriform cortex. Zn + Cu-raised mice had the highest plaque load in the neocortex and amygdala (see Table 3.2).

Regarding average area, cortical brain regions (neocortex and transition and piriform cortex) always had the largest plaque load across water/metal groups (see Table 3.1). According to Table 3.2, Fe-raised mice had the least plaque load in the cortical brain regions (neocortex and transition and piriform cortex). Zn raised mice had the highest plaque load in the transition and piriform cortex, and Zn + Cu raised animals had the highest plaque load in the neocortex, basal ganglia, and amygdala (Table 3.2).

Regarding plaque number, when comparing brain regions across water/metal groups, neocortex always had the highest number of plaques followed by the hippocampus, except for in Zn-raised animals (see Table 3.1). According to Table 3.2, Fe-raised mice had the fewest number of plaques in the neocortex, transition and piriform cortex, hippocampus, and basal ganglia. Zn-raised mice had the largest number of plaques in the transition and piriform cortex, the basal ganglia, and the amygdala, and Zn + Cu raised mice had the largest number of plaques in the neocortex and hippocampus (Table 3.2).

Table 3.1: Means and Standard Deviations Measurement Parameters by Water/Metal Type.

Metal	Brain Reg.	Normalized Area		Average Area		Plaque Number	
		Mean (mm^2)	**SD** (mm^2)	**Mean** (mm^2)	**SD** (mm^2)	**Mean**	**SD**
Zn	TPC	3.66×10^{-3}	3.56×10^{-3}	1.01×10^{0}	6.49×10^{-1}	5.76	4.34
	HC	1.04×10^{-3}	1.10×10^{-3}	6.83×10^{-1}	5.25×10^{-1}	4.99	6.54
	NC	1.31×10^{-3}	1.48×10^{-3}	8.76×10^{-1}	5.17×10^{-1}	5.75	4.70
	AMG	1.29×10^{-3}	1.42×10^{-3}	7.12×10^{-1}	7.41×10^{-1}	1.78	1.39
	BG	5.80×10^{-5}	1.97×10^{-4}	8.80×10^{-2}	3.15×10^{-1}	0.22	0.65
Zn & Cu	TPC	2.65×10^{-3}	2.17×10^{-3}	9.40×10^{-1}	5.40×10^{-1}	4.82	3.44
	HC	9.35×10^{-4}	1.37×10^{-3}	5.89×10^{-1}	5.52×10^{-1}	5.17	7.98
	NC	1.52×10^{-3}	1.44×10^{-3}	9.64×10^{-1}	6.08×10^{-1}	6.67	5.03
	AMG	1.56×10^{-3}	2.26×10^{-3}	8.41×10^{-1}	1.10×10^{0}	1.44	1.40
	BG	1.17×10^{-4}	4.82×10^{-4}	2.63×10^{-1}	7.80×10^{-1}	0.17	0.38
Fe	TPC	1.61×10^{-3}	1.80×10^{-3}	7.86×10^{-1}	7.91×10^{-1}	2.41	2.22
	HC	7.79×10^{-4}	8.98×10^{-4}	6.94×10^{-1}	7.55×10^{-1}	2.67	3.27
	NC	8.35×10^{-4}	1.04×10^{-3}	7.44×10^{-1}	6.08×10^{-1}	3.50	2.80
	AMG	1.52×10^{-3}	2.61×10^{-3}	6.03×10^{-1}	8.04×10^{-1}	1.53	1.80
	BG	2.80×10^{-5}	9.99×10^{-4}	9.54×10^{-2}	3.79×10^{-1}	0.10	0.34
LH_2O	TPC	1.81×10^{-3}	1.80×10^{-3}	8.22×10^{-1}	6.18×10^{-1}	2.80	1.75
	HC	1.01×10^{-3}	1.29×10^{-3}	7.17×10^{-1}	5.96×10^{-1}	3.32	3.55
	NC	1.27×10^{-3}	1.40×10^{-3}	8.76×10^{-1}	5.44×10^{-1}	5.00	4.10
	AMG	9.22×10^{-4}	1.44×10^{-3}	4.71×10^{-1}	7.22×10^{-1}	1.04	1.17
	BG	1.41×10^{-4}	4.82×10^{-4}	1.65×10^{-1}	5.76×10^{-1}	0.18	0.55

SD = standard deviation, mm – millimeters, Zn = zinc, Cu = copper, Fe = iron, LH_2O = lab water, TPC = transition and piriform cortex, HC = hippocampus, NC = neocortex, AMG = amygdala, BG = basal ganglia

Table 3.2: Means and Standard Deviations for All Measurement Parameters by Brain Region.

Brain Reg.	Metal	Normalized Area		Average Area		Plaque Number	
		Mean (mm^2)	**SD** (mm^2)	**Mean** (mm^2)	**SD** (mm^2)	**Mean**	**SD**
TPC	Zn	3.66×10^{-3}	3.56×10^{-3}	1.01×10^{0}	6.49×10^{-1}	5.76	4.34
	ZnCu	2.65×10^{-3}	2.17×10^{-3}	9.40×10^{-1}	5.40×10^{-1}	4.82	3.44
	Fe	1.61×10^{-3}	1.80×10^{-3}	7.86×10^{-1}	7.91×10^{-1}	2.41	2.22
	LH_2O	1.81×10^{-3}	1.80×10^{-3}	8.22×10^{-1}	6.18×10^{-1}	2.80	1.75
HC	Zn	1.04×10^{-3}	1.10×10^{-3}	6.83×10^{-1}	5.25×10^{-1}	4.99	6.54
	ZnCu	9.35×10^{-4}	1.37×10^{-3}	5.89×10^{-1}	5.52×10^{-1}	5.17	7.98
	Fe	7.79×10^{-4}	8.98×10^{-4}	6.94×10^{-1}	7.55×10^{-1}	2.67	3.27
	LH_2O	1.01×10^{-3}	1.29×10^{-3}	7.17×10^{-1}	5.96×10^{-1}	3.32	3.55
NC	Zn	1.31×10^{-3}	1.48×10^{-3}	8.76×10^{-1}	5.17×10^{-1}	5.75	4.70
	ZnCu	1.52×10^{-3}	1.44×10^{-3}	9.64×10^{-1}	6.08×10^{-1}	6.67	5.03
	Fe	8.35×10^{-4}	1.04×10^{-3}	7.44×10^{-1}	6.08×10^{-1}	3.50	2.80
	LH_2O	1.27×10^{-3}	1.40×10^{-3}	8.76×10^{-1}	5.44×10^{-1}	5.00	4.10
AMG	Zn	1.29×10^{-3}	1.42×10^{-3}	7.12×10^{-1}	7.41×10^{-1}	1.78	1.39
	ZnCu	1.56×10^{-3}	2.26×10^{-3}	8.41×10^{-1}	1.10×10^{0}	1.44	1.40
	Fe	1.52×10^{-3}	2.61×10^{-3}	6.03×10^{-1}	8.04×10^{-1}	1.53	1.80
	LH_2O	9.22×10^{-4}	1.44×10^{-3}	4.71×10^{-1}	7.22×10^{-1}	1.04	1.17
BG	Zn	5.80×10^{-5}	1.97×10^{-4}	8.80×10^{-2}	3.15×10^{-1}	0.22	0.65
	ZnCu	1.17×10^{-4}	4.82×10^{-4}	2.63×10^{-1}	7.80×10^{-1}	0.17	0.38
	Fe	2.80×10^{-5}	9.99×10^{-4}	9.54×10^{-2}	3.79×10^{-1}	0.10	0.34
	LH_2O	1.41×10^{-4}	4.82×10^{-4}	1.65×10^{-1}	5.76×10^{-1}	0.18	0.55

SD = standard deviation, mm – millimeters, Zn = zinc, Cu = copper, Fe = iron, LH_2O = lab water, TPC = transition and piriform cortex, HC = hippocampus, NC = neocortex, AMG = amygdala, BG = basal ganglia

Table 3.3: Means Totals for All Measurement Parameters for Metal/Water Type and Brain Region.

		Normalized Area		Average Area		Plaque Number	
		Mean (mm^2)	**SD** (mm^2)	**Mean** (mm^2)	**SD** (mm^2)	**Mean**	**SD**
Metal Type	Zn	1.56×10^{-3}	2.35×10^{-3}	6.93×10^{-1}	6.44×10^{-1}	3.93	4.81
	Zn+Cu	1.43×10^{-3}	1.85×10^{-3}	7.39×10^{-1}	7.59×10^{-1}	3.94	5.15
	Fe	9.39×10^{-4}	1.56×10^{-3}	5.95×10^{-1}	7.22×10^{-1}	2.14	2.61
	LH_2O	1.04×10^{-3}	1.45×10^{-3}	6.63×10^{-1}	6.99×10^{-1}	2.65	3.25
Brain Reg.	TPC	2.47×10^{-3}	2.60×10^{-3}	8.94×10^{-1}	6.64×10^{-1}	4.02	3.47
	HC	9.41×10^{-4}	1.17×10^{-3}	6.72×10^{-1}	6.14×10^{-1}	4.01	5.71
	NC	1.22×10^{-3}	1.36×10^{-3}	8.61×10^{-1}	5.75×10^{-1}	5.18	4.35
	AMG	1.34×10^{-3}	2.02×10^{-3}	6.65×10^{-1}	8.62×10^{-1}	1.47	1.47
	BG	8.20×10^{-5}	3.38×10^{-4}	1.48×10^{-1}	5.34×10^{-1}	0.16	0.49

SD = standard deviation, mm – millimeters, Zn = zinc, Cu = copper, Fe = iron, LH_2O = lab water, TPC = transition and piriform cortex, HC = hippocampus, NC = neocortex, AMG = amygdala, BG = basal ganglia

Table 3.4: Significance Test for Simple Effects and Interaction for Normalized Area.

Source	Type III Sum of Squares	df	Mean Square	F	Sig.	Partial Eta Squared
Corrected Model	.001[a]	19	6.159×10^{-5}	22.820	.000	.232
Intercept	.002	1	.002	752.741	.000	.344
Water Type	6.822×10^{-5}	3	2.274×10^{-5}	8.425	.000	.017
Region	.001	4	.000	79.573	.000	.182
Water Type * Region	.000	12	1.463×10^{-5}	5.419	.000	.043
Error	.004	1434	2.699×10^{-6}			
Total	.007	1454				
Corrected Total	.005	1453				

a. R Squared = .232 (Adjusted R Squared = .222); df = degrees of freedom, F = Fisher statistic, Sig = significance

Table 3.5: Significance Test for Simple Effects and Interaction for Average Area.

Source	Type III Sum of Squares	df	Mean Square	F	Sig.	Partial Eta Squared
Corrected Model	117.231[a]	19	6.170	14.922	.000	.165
Intercept	587.457	1	587.457	1420.741	.000	.498
Water Type	4.011	3	1.337	3.234	.022	.007
Region	104.279	4	26.070	63.048	.000	.150
Water Type * Region	6.758	12	.563	1.362	.178	.011
Error	592.939	1434	.413			
Total	1349.327	1454				
Corrected Total	710.170	1453				

a. R Squared = .165 (Adjusted R Squared = .154) ; df = degrees of freedom, F = Fisher statistic, Sig = significance

Table 3.6: Significance Test for Simple Effects and Interaction for Plaque Number.

Source	Type III Sum of Squares	df	Mean Square	F	Sig.	Partial Eta Squared
Corrected Model	6495.893[a]	19	341.889	26.238	.000	.258
Intercept	12340.437	1	12340.437	947.041	.000	.398
Water Type	768.239	3	256.080	19.652	.000	.039
Region	5039.471	4	1259.868	96.686	.000	.212
Water Type * Region	550.338	12	45.862	3.520	.000	.029
Error	18685.769	1434	13.031			
Total	39703.000	1454				
Corrected Total	25181.662	1453				

a. R Squared = .258 (Adjusted R Squared = .248) ; df = degrees of freedom, F = Fisher statistic, Sig = significance

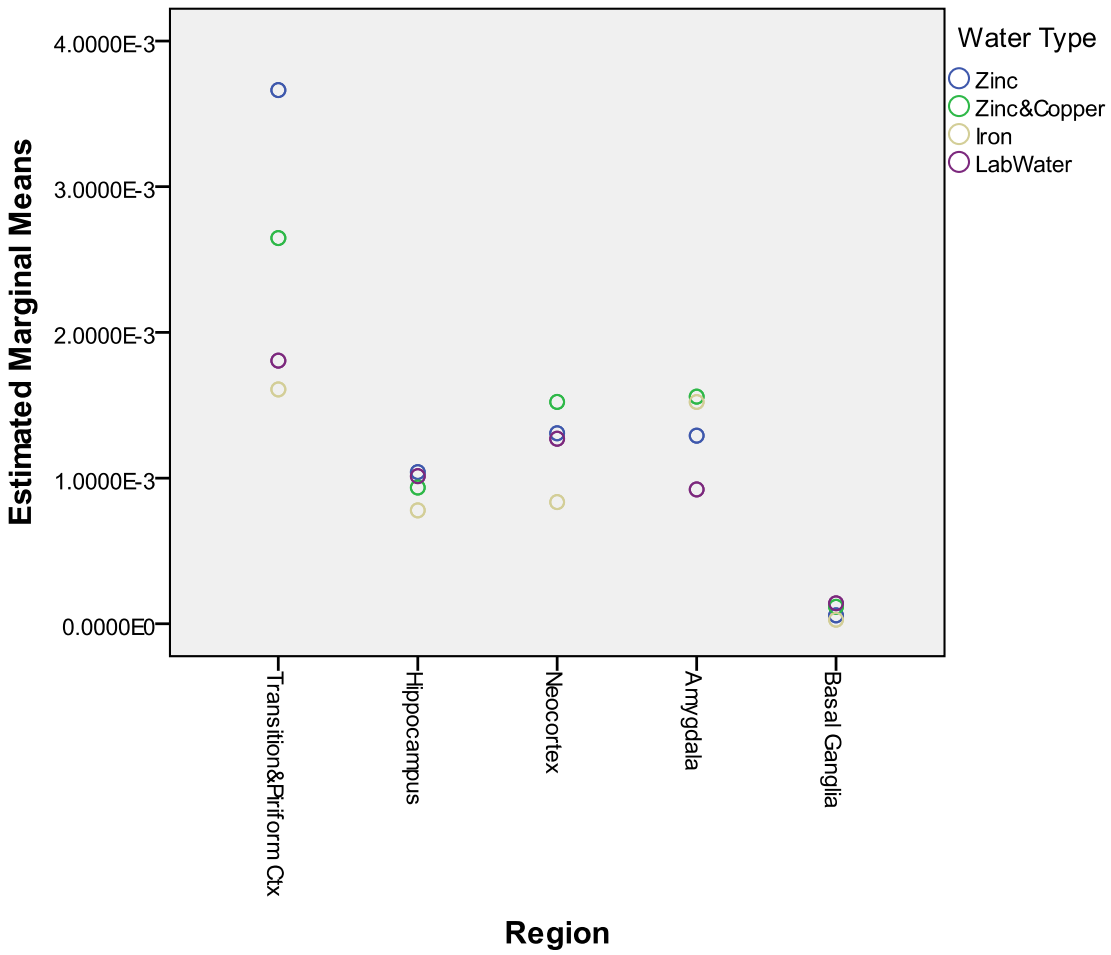

Figure 3.1A: Dot Graph: Normalized Area Means by Region and Water/Metal Type.

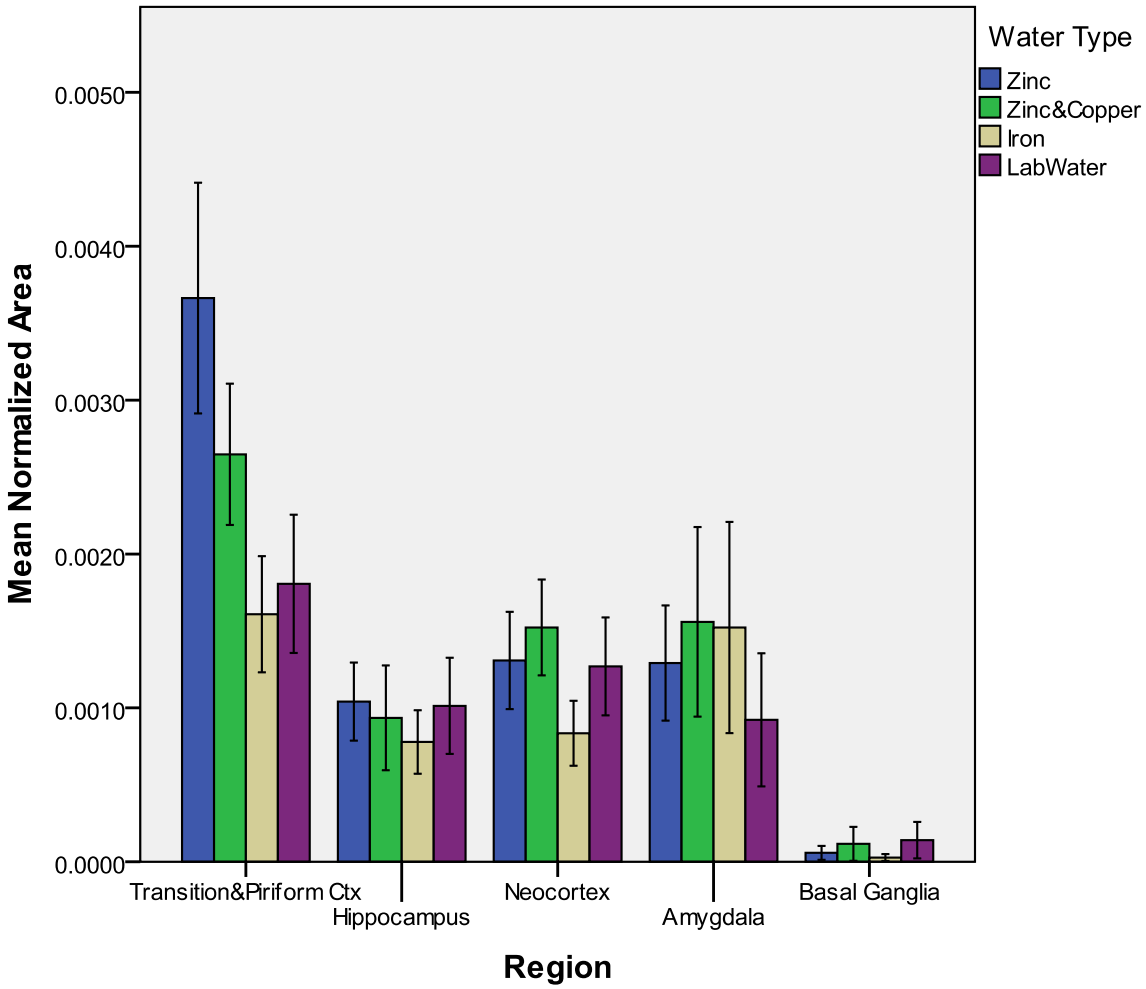

*Error bars represent 95% confidence interval

Figure 3.1B: Bar Graph: Normalized Area Means by Region and Water/Metal Type.

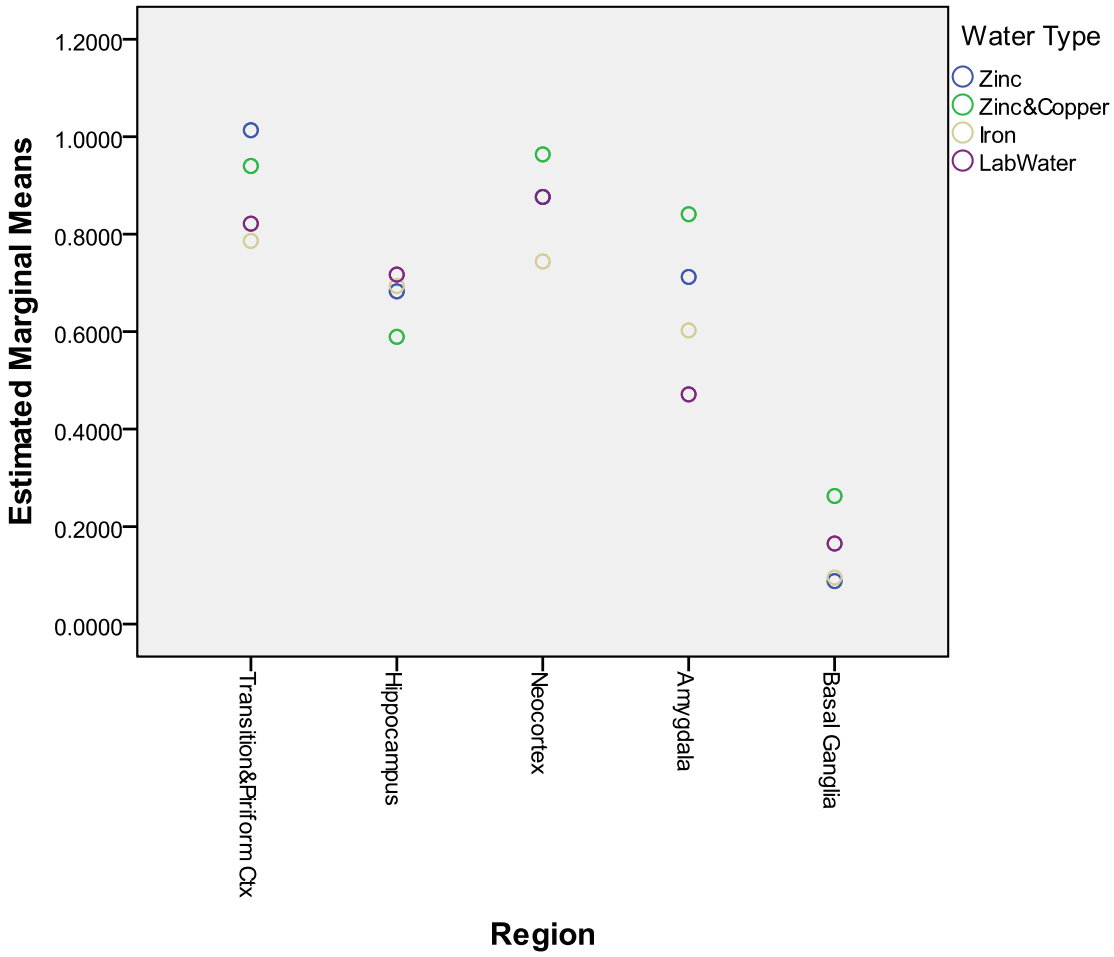

Figure 3.2A: Dot Graph: Average Area Means by Region and Water/Metal Type.

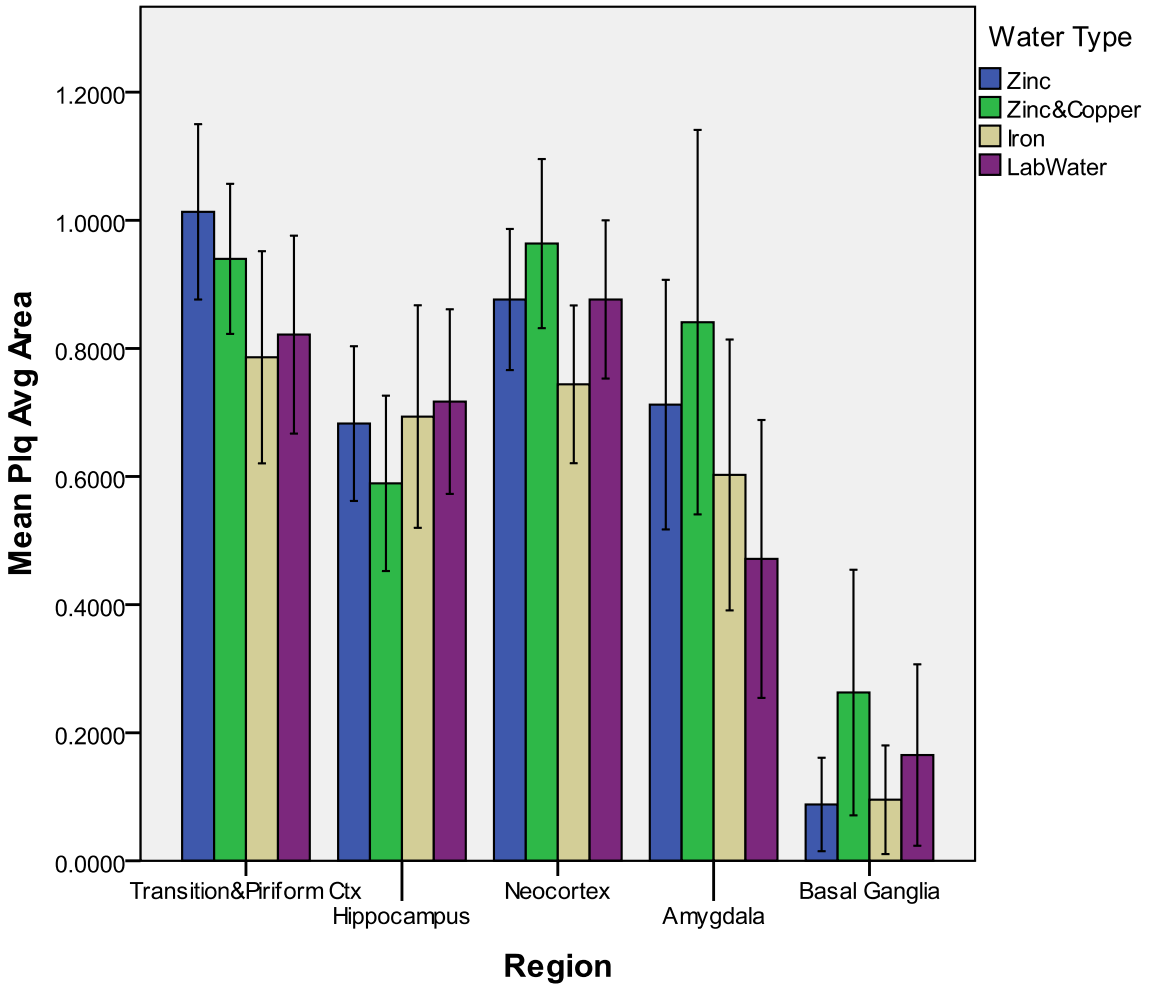

*Error bars represent 95% confidence interval

Figure 3.2B: Bar Graph: Average Area Means by Region and Water/Metal Type.

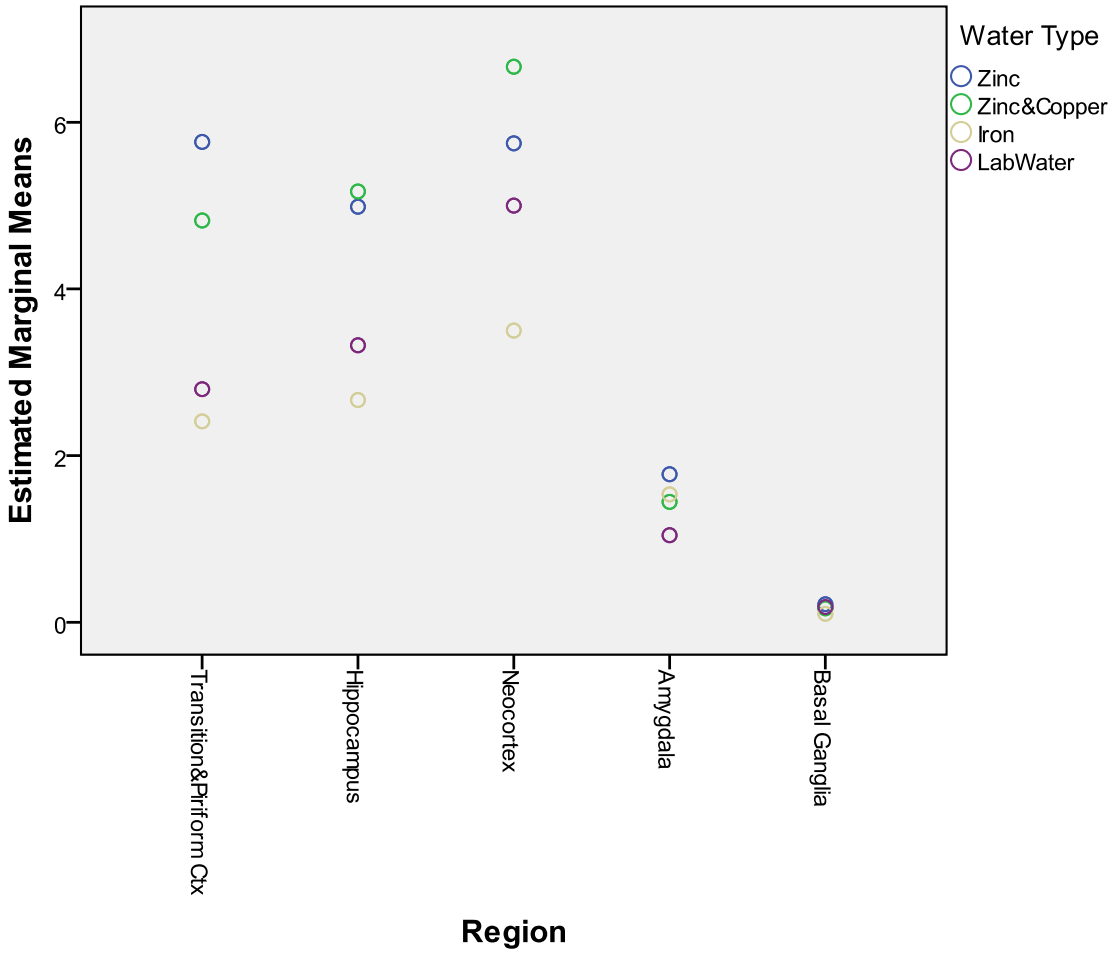

Figure 3.3A: Dot Graph: Plaque Number Means by Region and Water/Metal Type.

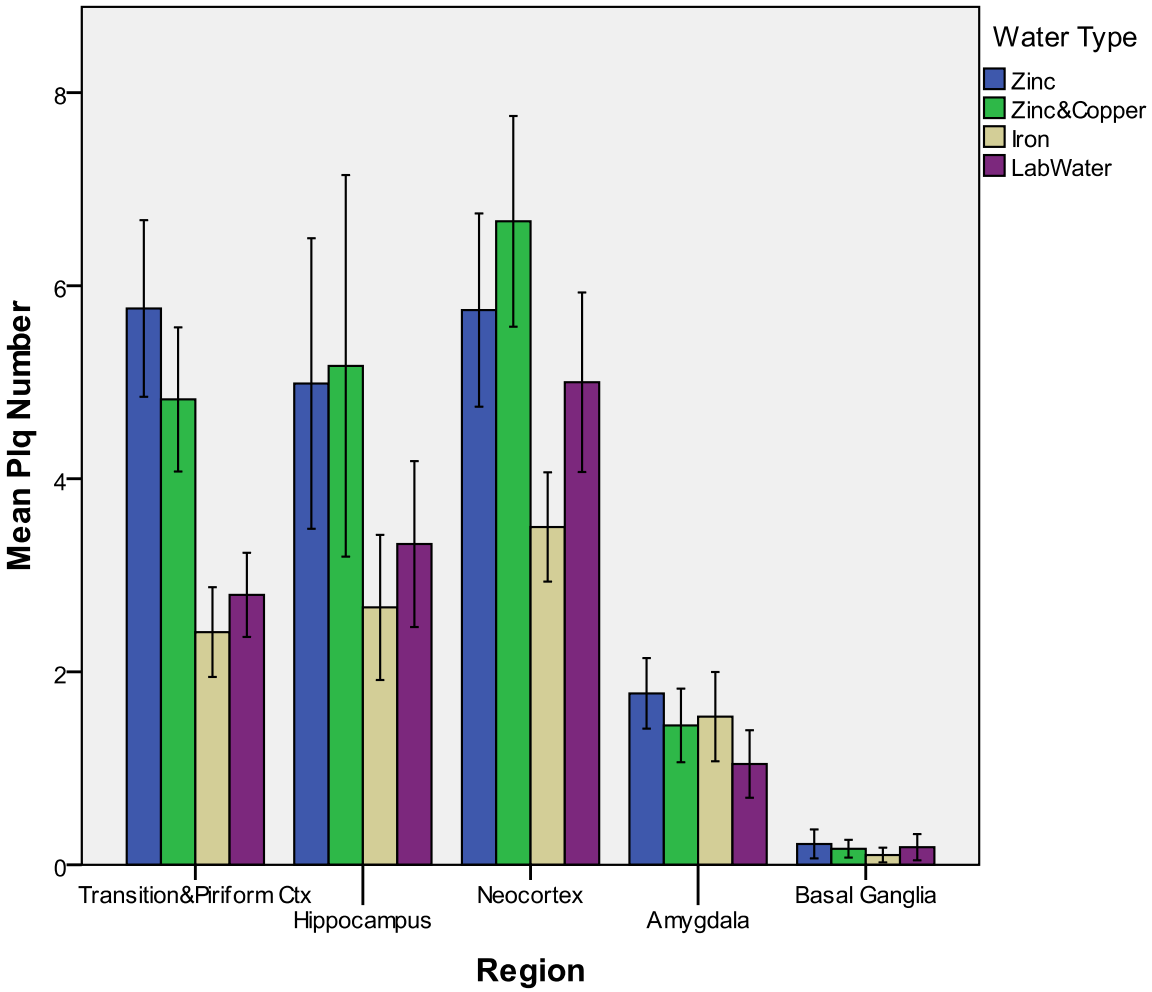

*Error bars represent 95% confidence interval

Figure 3.3B: Bar Graph: Plaque Number Means by Region and Water/Metal Type.

Table 3.7: Games-Howell Post Hoc Comparisons Between Metal/Water Types for Normalized Area.

	Metal/Water Type			
	Zinc	Zinc & Copper	Iron	Lab Water
Zinc	--	0.823	0.000	0.002
Zinc & Copper	0.823	--	0.001	0.014
Iron	0.000	0.001	--	0.804
Lab Water	0.002	0.014	0.804	--

Table 3.8: Games-Howell Post Hoc Comparisons Between Metal/Water Types for Average Area.

	Metal/Water Type			
	Zinc	Zinc & Copper	Iron	Lab Water
Zinc	--	0.811	0.184	0.550
Zinc & Copper	0.811	--	0.039	0.175
Iron	0.184	0.039	--	0.917
Lab Water	0.550	0.175	0.917	--

Table 3.9: Games-Howell Post Hoc Comparisons Between Metal/Water Types for Plaque Number.

	Metal/Water Type			
	Zinc	Zinc & Copper	Iron	Lab Water
Zinc	--	1.000	0.000	0.000
Zinc & Copper	1.000	--	0.000	0.001
Iron	0.000	0.000	--	0.097
Lab Water	0.000	0.001	0.097	--

Table 3.10: Games-Howell Post Hoc Comparisons Between Brain Regions for Normalized Area.

	Brain Region				
	TPC	HC	NC	AMG	BG
TPC	--	0.000	0.000	0.000	0.000
HC	0.000	--	0.046	0.071	0.000
NC	0.000	0.046	--	0.933	0.000
AMG	0.000	0.071	0.933	--	0.000
BG	0.000	0.000	0.000	0.000	--

TPC = transition and piriform cortex, HC = hippocampus, NC = neocortex, AMG = amygdala, BG = basal ganglia

Table 3.11: Games-Howell Post Hoc Comparisons Between Brain Regions for Average Area.

	Brain Region				
	TPC	HC	NC	AMG	BG
TPC	--	0.000	0.957	0.009	0.000
HC	0.000	--	0.001	1.000	0.000
NC	0.957	0.001	--	0.028	0.000
AMG	0.009	1.000	0.028	--	0.000
BG	0.000	0.000	0.000	0.000	--

TPC = transition and piriform cortex, HC = hippocampus, NC = neocortex, AMG = amygdala, BG = basal ganglia

Table 3.12: Games-Howell Post Hoc Comparisons Between Brain Regions for Plaque Number.

	Brain Region				
	TPC	HC	NC	AMG	BG
TPC	--	1.000	0.001	0.000	0.000
HC	1.000	--	0.040	0.000	0.000
NC	0.001	0.040	--	0.000	0.000
AMG	0.000	0.000	0.000	--	0.000
BG	0.000	0.000	0.000	0.000	--

TPC = transition and piriform cortex, HC = hippocampus, NC = neocortex, AMG = amygdala, BG = basal ganglia

CHAPTER 4

DISCUSSION

Relationship Between Certain Metals And Plaque Burden

In researching the relationship between certain metals and plaque burden, an unexpected result was that transgenic mice raised on Fe-content water were not significantly different from mice raised on LH_2O. As hypothesized, these animals produced the fewest amyloid plaques overall. All ANOVAs showed that Fe produced the fewest quantifiable amount of plaque burden as compared to the results for the other metals. These results may be, in part, due to the specific iron ion involved. The mice studied in this experiment were administered iron (II) nitrate or ferrous nitrate (Burns, 2008). The Fe administered to these mice breaks down to Fe^{2+} as opposed to Fe^{3+}. Melega, Laćan, Harvey, and Way (2007) conducted drug induced Fe experiments on rodents. These researches noted that Fe increases might not have as much of a negative consequence if the additional Fe was ferritin-bound as Fe^{3+}. Fe^{2+} ions are bound much more weakly to transferrin than the Fe^{3+} ion. It is more likely that Fe^{2+} ions are released into the cell due to reductive processes and transport of Fe^{2+} increases bioavailability of extracellular Fe. Additionally, Fe^{2+} is more soluble and more mobile (Bertini, Gray, Stiefel, & Valentine, 2007).

Fe can generate reactive oxygen species (ROS)—O_2 or one of its derivatives can be converted into a reactive free radical that is capable of attacking and damaging biological molecules including DNA, lipids, and proteins (Lovell et al., 1998). These ROS can also promote dopamine system pathology (Melega et al., 2007). ROS directly oxidize proteins. Oxidative modification of proteins includes protein side chains, backbone cleavage, and protein-protein dimerization (Bertini et al., 2007). It is possible that the ROS produced by the excess Fe^{2+} in the brains of the Tg2576 mice could have caused the breakdown of the amyloid plaques. For instance, Fe activates microglial cells (oxidation) that restrict plaque formation by phagocytosis (Moreno-Gonzalez et al., 2009). This might also explain why studies have shown a disconnect between plaque burden and cognition (Linkous et al., 2009). Such reactive free radicals are believed to be responsible for much of the cellular injury resulting from acute and chronic iron overload (Melega et al., 2007).

It was hypothesized that animals raised on Zn + Cu water would have less amyloid plaques than animals raised on Zn water. However, there was no discernable difference between Zn and Zn + Cu for any of the measurements. It was also hypothesized that animals raised on Zn water would have the most plaques overall. This hypothesis was not upheld as Zn + Cu had the most plaques in more cases (refer to Tables 3.1, 3.5, and 3.9).

Prior research has been inconsistent regarding increased Zn intake and plaque burden. Histological analysis by Linkous et al. (2009) showed that Tg2576 mice raised on Zn water had fewer and smaller plaques (specifically in the hippocampus) than

transgenic mice raised on lab water. These researchers suggested that this finding is due to reduced brain Cu levels because ingested Zn leads to decreased absorption of Cu. Additionally, Cu has been shown to have some alleviatory effects in AD pathology. However, research has shown that Cu is more toxic when ingested from water, as is the case in the current study (Burns, 2008; Campbell, 2006). For the animals raised on Zn + Cu water, zinc carbonate—$Zn(CO_3)$—was combined with copper (II) carbonate—$CuCO_3$ (Burns, 2008). Free Cu is extremely efficient in the generation of free radicals and has been shown to induce partial aggregation of Aβ, although unlink the other metals this aggregation does not form fibrils (Lovell et al., 1998).

When Cu^{2+} binds Aβ, it may cause an increase in insolubility and also induce a series of electron transfers that result in ROS, such as H_2O_2 and hydroxyl radicals. These ROS are capable of short-range damage on proteins, lipids, sterols, and nucleic acids. Zn is not known to cause the type of ROS associated with Fe and Cu (Dawbarn & Allen, 2007; Linkous et al., 2009). The results of the current study suggest that the ROS produced by Fe and Cu affect plaque formation differently. It is possible that because the ROS produced by the two metal ions are different chemicals, the damage caused by one ROS could be more catastrophic and/or have farther-reaching effects than another.

Since metal ions can be both essential and damaging, a homeostasis must be upheld to keep metal ion levels at an optimal range. These levels are kept in place by mechanisms that control transporters, storage molecules, and detoxifying enzymes. These mechanisms react to an excess in metal ions by slowing uptake and expanding the storage capability (Bertini et al., 2007). It is unclear how these processes are affected regarding

the specific metal ions given to the transgenic mice in the present study. The effects of these metals are complex, interdependent, and inconsistent.

Relationship Between Plaque Burden and Brain Region

Uncovering a relationship between plaque burden and brain region might reveal how and to what extent plaque aggregation affects specific brain regions. This study explored plaque burden in order to postulate a potential relationship with brain region. For example, the measurements used in the present study might uncover evidence about whether plaque size or plaque number correlates more strongly with damage associated with amyloid plaques.

The normalized area measurement takes into account the quantity of plaques present, given the size of the region in which they are located. Given these results, at 18 months of age, as predicted, plaques occupy the most space in the transition and piriform cortex followed by the neocortex. As predicted, plaques occupy the lease amount of space in the basal ganglia. The average area measurement provided information about the size of the plaques in a given region. As hypothesized, the transition and piriform cortex had the largest plaques followed by the neocortex. As expected, the basal ganglia had the smallest plaques. The plaque number measurement provided a count of the plaques in a given region, regardless of their size. The neocortex had the highest number of plaques, but the data suggest that these plaques are smaller on average than those in the transition and piriform cortex, given the average area results. Also, as predicted, the basal ganglia had the fewest number of plaques. Research has shown that amyloid buildup begins in

transition cortex, affecting behavior associated with this area of the brain. Corresponding behavioral data might suggest that the number of plaques is not as damaging as size of the plaques.

The order of neuropathological changes in AD is widely thought to begin in the entorhinal cortex, then progress to the hippocampus with increasing involvement of the neocortex as the disease progresses, and then neurodegeneration continues onto the amygdala, and finally to the basal ganglia (Andersen et al., 2007). Moreno-Gonzalez et al. (2009) describe AD neurodegeneration as occurring with a regional and temporal defined pattern of susceptible brain regions. Early in amyloidosis, the entorhinal cortex is affected by NFTs and Aβ deposits, and then these lesions spread to the hippocampus and neocortex. These researchers studied amyloidosis in the PS1xAPP transgenic mice model, which develop plaques at a very early age. A significant loss of neurons was found in the entorhinal cortex of these animals at six months of age. However, significant neuron loss in the hippocampus was not seen until 17-18 months of age. Since substantially more Aβ plaques were observed in the entorhinal cortex and hippocampus than other brain areas, the researchers correlate the early neurodegeneration with extracellular Aβ accumulation rather than intracellular Aβ and cytotoxic inflammatory response (Moreno-Gonzalez et al., 2009).

A few plaques are visible in Tg2576 mice at about 9 months old in the cortical areas and hippocampus (X.-M. Zhang et al., 2010). Additionally, at this age, β-secretase-1 and Aβ-immunoreactive profiles resembling plaques were found in the piriform cortex. From 12 months to 24 months of age, plaque-like profiles increased in the piriform

cortex. The Tg2576 animals used in the present study were sacrificed at 18 months of age (Burns, 2008).

Interaction Between Water/Metal Type and Location Within the Brain

Results regarding the relationship between water/metal type and brain region show that no concrete predictions can be made. However, there are two brain regions in particular that have been associated with particular metal ions in previous studies. The basal ganglia, particularly the substantia nigra and globus pallidus, contain the highest levels of iron in the brain (Falangola et al., 2005; Melega et al., 2007). This Fe level has been shown to increase in aging and neurodegeneration (Falangola et al., 2005), and as suggested above, it has been associated with oxidative stress. This might account for the minimal plaque burden in the basal ganglia overall.

In the normal condition, the highest levels of Zn are found in the hippocampus (Bush et al., 1994). An interesting observation from this study is that the mice raised on water that contained a Zn content (Zn and Zn + Cu) had smaller plaques (normalized area, average area) in the hippocampus than in the amygdala. For animals raised on Fe water and LH_2O, this was the opposite (see Table 3.1). Given the amyloid cascade hypothesis, it is expected that hippocampus would exhibit a larger plaque burden prior to the amygdala. Evidence has suggested that Zn can destabilize Aβ plaques and lead to fibril formation (Lovell et al., 1998). If it is indeed the fibril formation that is more hazardous than plaque formation, this might account for studies in which elevated Zn levels correspond with memory and learning deficits, but decreased plaque formation.

Additionally, signs of altered Zn metabolism are evident in the AD brain. These alterations seen in areas of the brain associated with Zn may implicate an abnormality in the uptake and distribution of Zn in the AD brain (Bush et al., 1994). It is probable that the complex relationship between the hippocampus and Zn levels is relevant here.

Future Research

An addendum to this study might be the way in which anatomical boundaries are defined. For instance, in future study, the transition cortex might be viewed as distinct from piriform cortex, especially regarding the normalized area measurement, which accounts for the size of the region being examined. Uncovering potential associations might result in more information about the order of amyloidosis, extent of damage in specific brain regions, and implications in learning and memory.

More research into the metal ions associated with AD is necessary. The present study involved the chemical compounds $Fe(NO_3)_2$, $Zn(CO_3)$, and $CuCO_3$. The anions associated with the Zn, Cu, and Fe—nitrate, for instance—could play a role in the effects seen in the current study. More research into these specific compounds, the implications of their interactions, and the implications of their absorption in water might better uncover the way in which these metal ions are involved in amyloid plaque aggregation and/or degradation. Also, it might be pertinent to quantify the amyloid plaques visible under polarized light to determine if a particular metal(s) is associated with plaque aggregation into β-pleased sheets.

Furthermore, directly examining behavioral results and histological results from the same animal group could contribute to research on the relationship between memory impairments and amyloid plaque burden. For instance, Railey, Groeber, & Flinn (2011) examined spatial memory deficits in the same Tg2576 mice whose brain tissue was examined in the current study. Results of this study showed that increased long-term Zn and Fe consumption can impair spatial memory and learning in Tg2576. The deficits seen in the mice which consumed Zn water were alleviated when they were administered Cu. The memory deficits seen in mice given Zn or Fe water differed significantly from those given Zn + Cu or lab water. These behavioral results do not exhibit the same pattern as the histological results obtained in the current study.

Additionally, this study raised a question that might be explored in the future. Based on behavioral experiments, what implications can be drawn about the damaging effects of plaque size versus plaque number? Research has shown that Aβ burden and plaque count are not well correlated with cognitive decline and neuronl loss in AD (Colurso et al., 2003; Linkous et al., 2009).

Finally, the animals used for this study were sacrificed at 18 months of age. It might be interesting to examine the brains of animals sacrifice at different ages to note any correlation between age and plaque formation in different brain regions. Taking age into consideration might uncover more information about the order of amyloidogenesis, and it could lead to further explanation of the differences between groups.

APPENDIX A

DIAGNOSTIC CRITERIA FOR ALZHEIMER'S-TYPE DEMENTIA

A. Multiple cognitive deficits in both

    1. Memory and

    2. One or more of the following

        a. Aphasia

        b. Apraxia

        c. Agnosia

        d. Executive function

B. Impairment in social or occupational function that represents a decline from previous levels

C. Gradual onset and continued cognitive decline

D. Deficits not due to other causes

(Storandt, 2008).

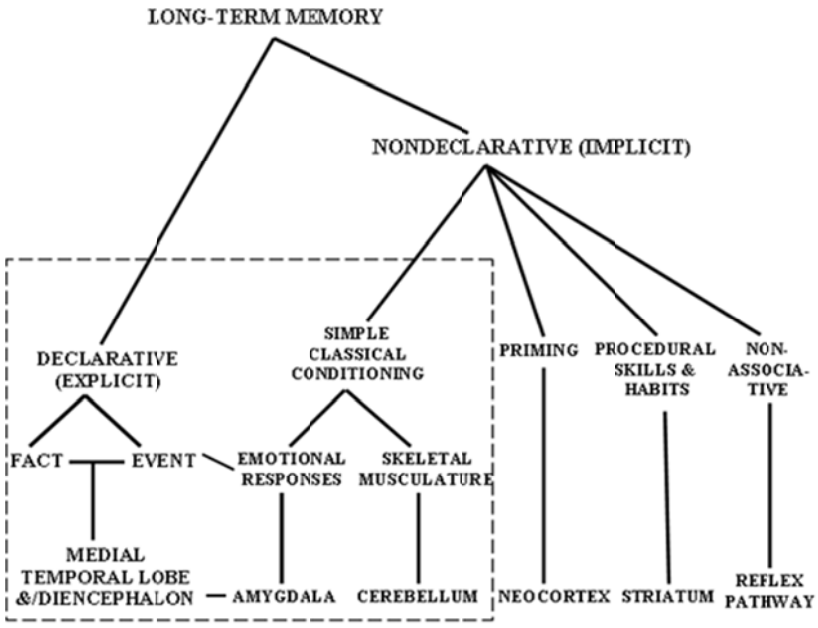

Figure A.1: Long-Term Memory Map (Squire, 2004).

APPENDIX B

BIOQUANT PROTOCOL

Figure B.1 depicts how BioQuant (BQ) appears when it is first opened. The **Unsaved Image** screen is where the image will populate. This screen should never be manually moved because this will skew measurements.

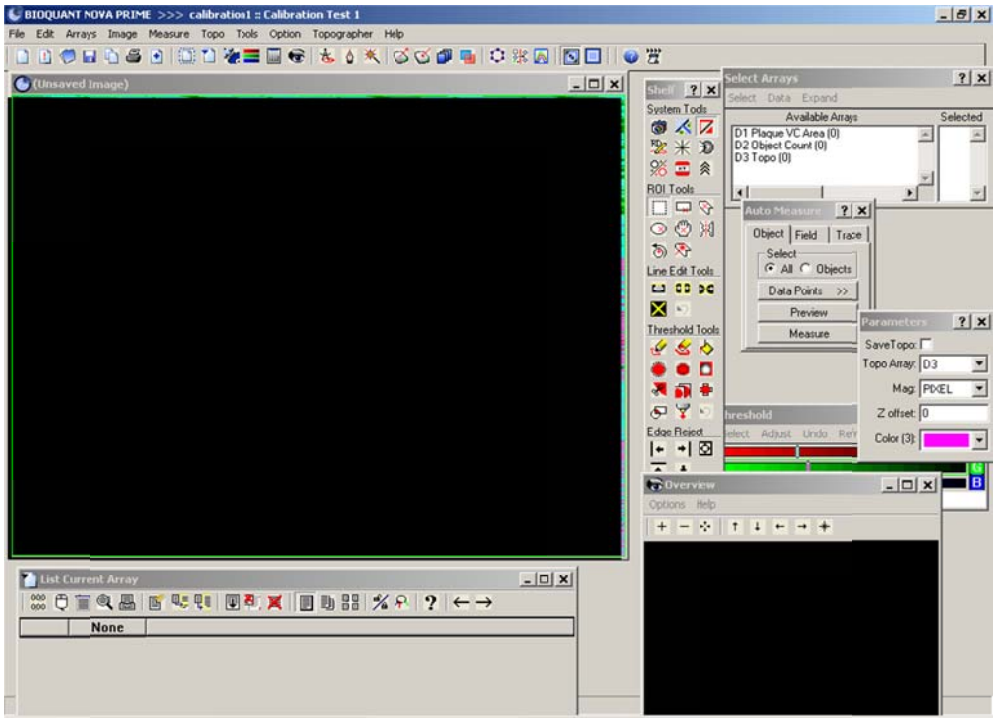

Figure B.1: BioQuant Screenshot.

Before use, the system calibration must be checked. Once the system is calibrated it will automatically populate the same way each time the system is opened, so calibration will only need to be done once. To calibrate the system, navigate to the Measure option and select Calibration (see Figure B.2). Navigate to Measure again and select Parameters to set the magnification level to 40X (see Figure B.3). All other options should populate automatically—including the magnification factor. Under Measure, select Data Points. On this menu, set the smoothing limit to 2, the low filter to 1, and the high filter to 9999 (See Figure B.4).

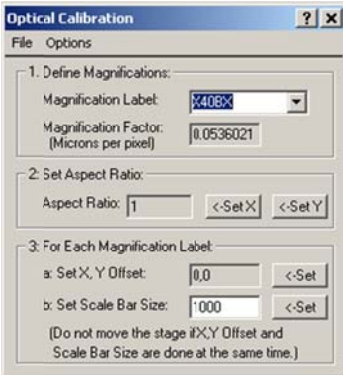

Figure B.2: BioQuant Optical Calibration Screen.

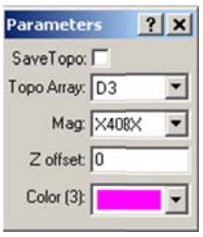

Figure B.3: BioQuant Parameters Screen.

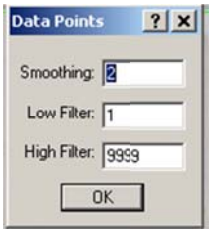

Figure B.4: BioQuant Data Points Screen.

For plaque analysis, open three arrays: Plaque VC Area, Object Count, and Topo. Plaque VC Area gives you the area of each plaque selected (NOTE – BioQuant will not give you a total area using this feature). Object Count will count the number of 'objects' (in this case plaques) selected. Topo will give you 3-D topographical data (X, Y, Z axis). In the Select Arrays, type the following syntax (in each) to set the measurement threshold:

"COL3;MAG6;TR(177,134);TG(96,39);TB(117,32);CHA7;FLT1;DFH9999;DFL1;SMO 2;". You can do this by selecting expand at the top-right of the window (Refer to Figure B.5).

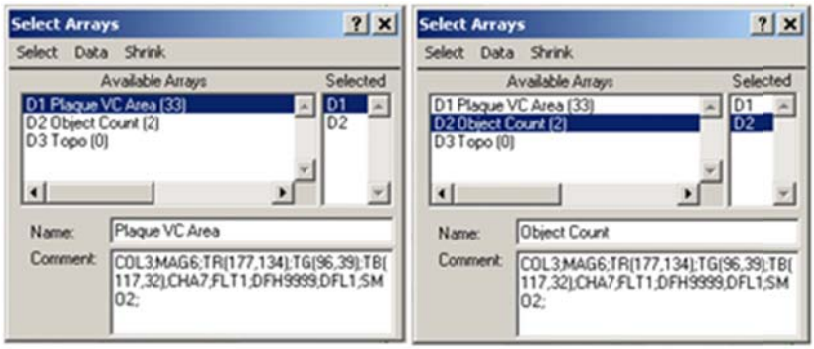

Figure B.5: BioQuant Select Arrays Screen.

To begin plaque analysis, select File – Load Image(s) - Load Single Image. Images should be in "tiff" format. The image will populate like Figure B.6. Do not move the image screen.

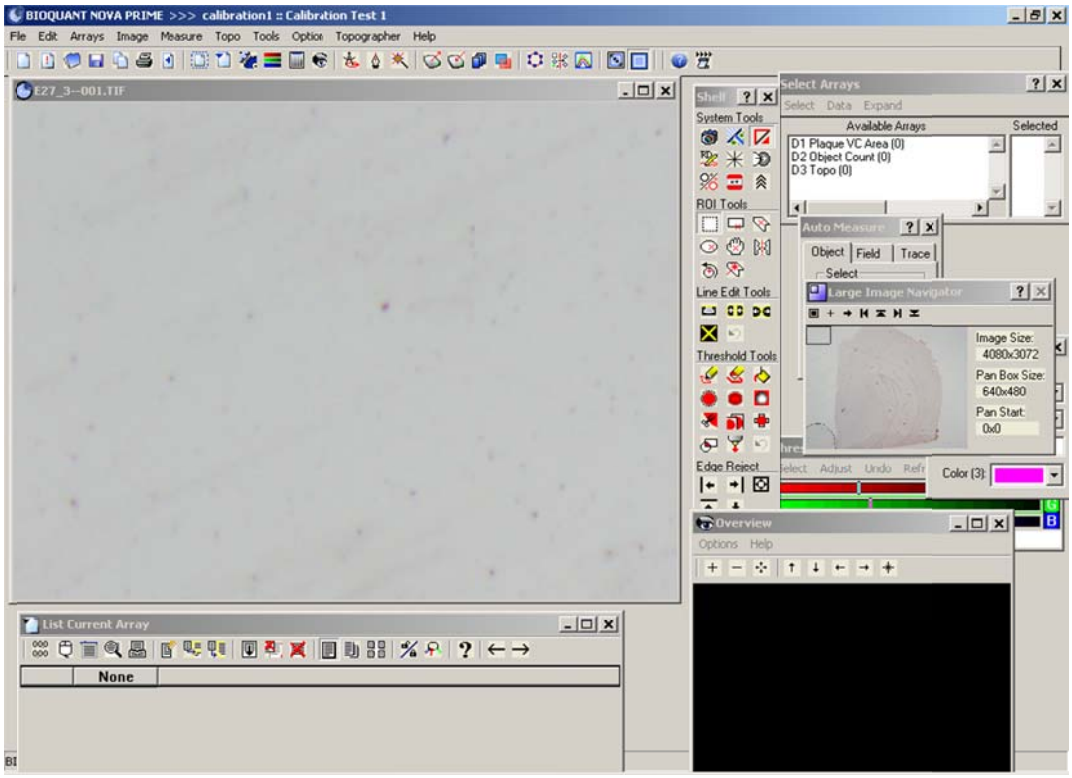

Figure B.6: BioQuant Navigation Sample Screen.

Use the Large Image Navigator to view the entire image (the square-shaped button on the far left of the window). When the threshold and calibration parameters are set, plaques can be measured. First, use the Region of Interest (ROI) tool to select the portion of the image under investigation. Generally the entire picture is the ROI. However, if there are slices with folded edges, then the ROI should be set to exclude these edges, or if only certain brain regions are being investigated, then select and measure the plaques in those regions one region at a time.

Double click each array in the Select Arrays menu. This must be done before selecting objects or BQ will clear prior selections. On the Threshold menu, click Select.

As plaques are chosen, BQ will 'color' objects of the same RGB threshold in yellow. Users should be conservative when clicking plaques because the BQ system is temperamental, and it will select unwanted items or the user may accidentally click a color outside of the plaques.

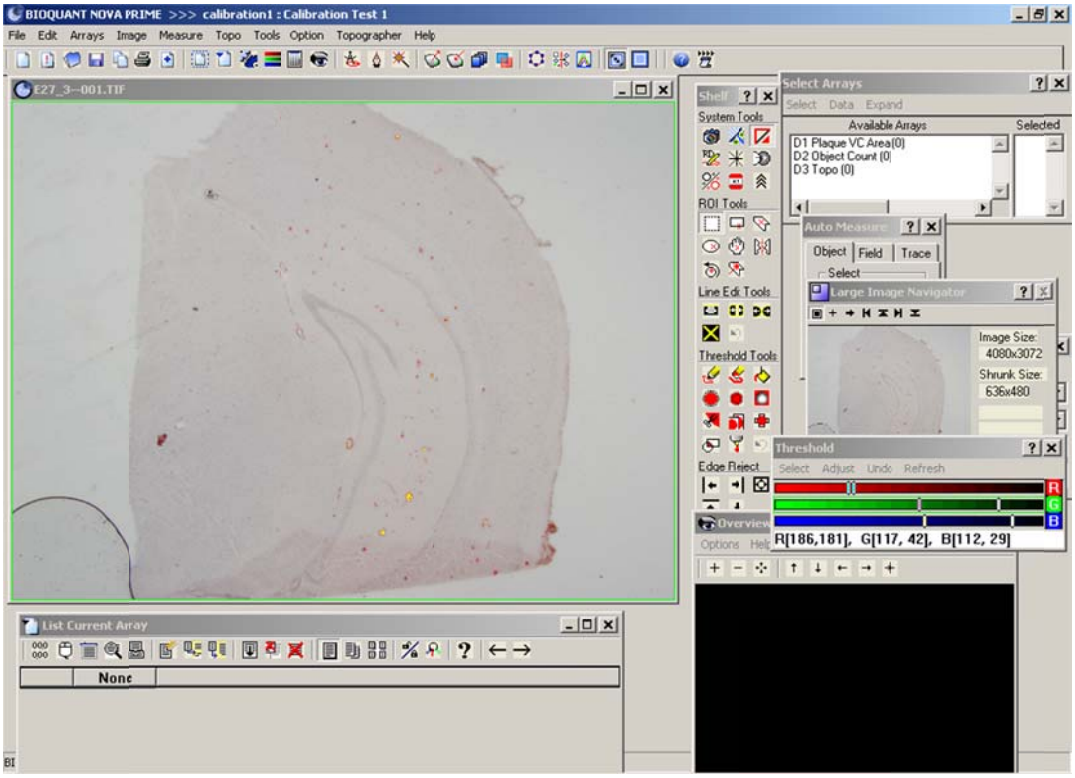

Figure B.7: BioQuant Plaque Selection Sample Screen.

Use Control + Z to zoom the image to select smaller plaques, and use the arrow keys to move around the image (do NOT use the mouse). Do not use the mouse to click

outside of the image window because prior selections will be lost. The zoomed in selection will appear like Figure B.8.

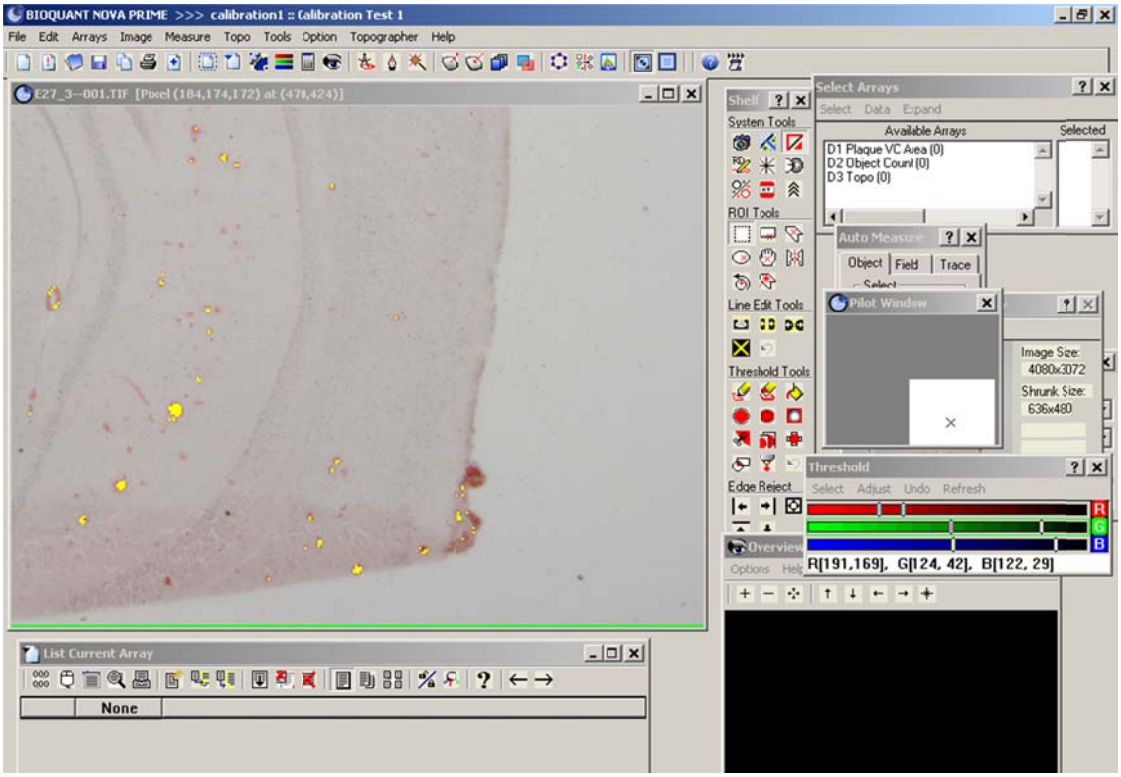

Figure B.8: BioQuant Plaque Selection Zoomed-In Sample Screen.

Once plaques have been selected, click the dilate button once. This button is located on the Shelf under Threshold Tools (left side, one down). This is to ensure that the entire plaque is selected. To toggle back to the large view, continue using Control + Z (there is no 'unzoom' option in BQ). Figure B.9 shows a sample of image where the dilate feature has been used.

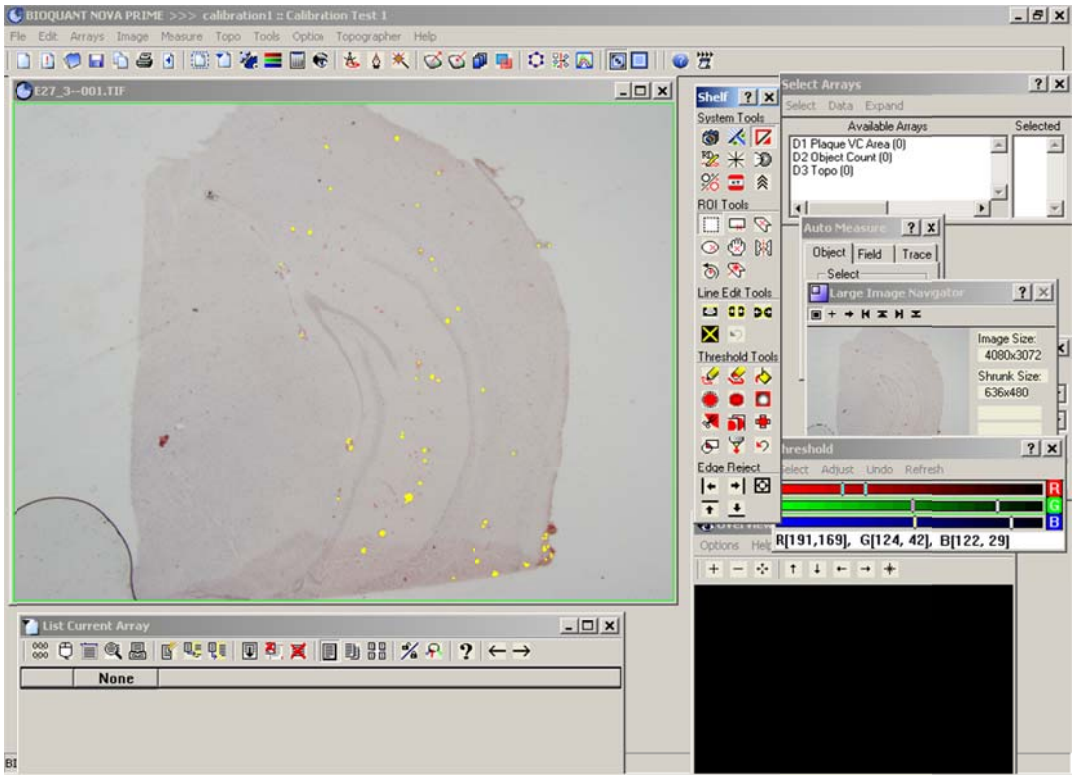

Figure B.9: BioQuant Plaque Selection Dilate Sample Screen.

Next, on the Auto Measure window (under the Objects tab) click Preview. Refer to Figure B.10. Notice that all objects that BQ considers plaques are highlighted in blue (this color is set by the user). Next, select Measure (below Preview). BQ will them give measurement data for all selected plaques. This is shown in Figure B.11. The precision has been set to "4" so that BQ produces numbers that have been rounded to the nearest ten-thousandth decimal place. Notice that the area measurements (in microns) are populated in the List Current Array menu at the bottom of the screen. In this example, there are thirty-three plaques, and there is an area measurement for each. To export this data to excel, select Edit, Copy Data, and then Current array (see Figure B.12). Right

click in excel and select paste. The data will paste wherever you choose (see Figure B.13). To count the number of objects, click on object count. This number will populate in the D2 column in the List Current Arrays menu. The number of objects should match the number of area measurements.

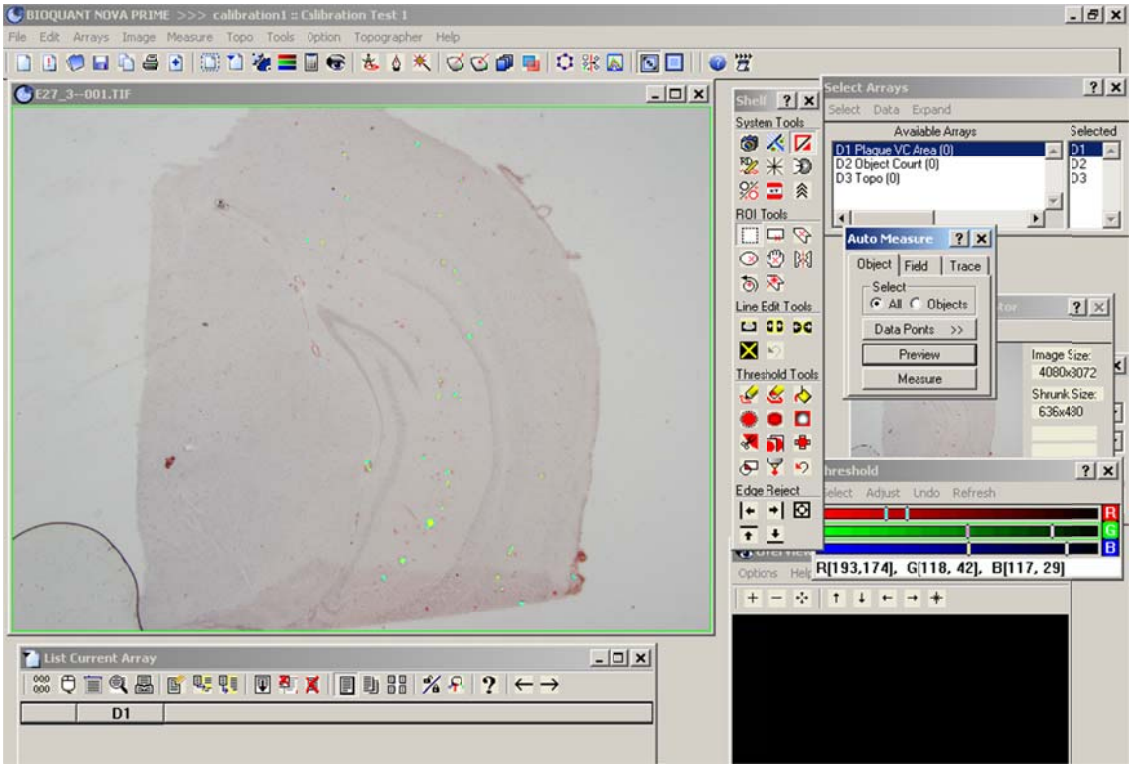

Figure B.10: BioQuant Plaque Selection Preview Sample Screen.

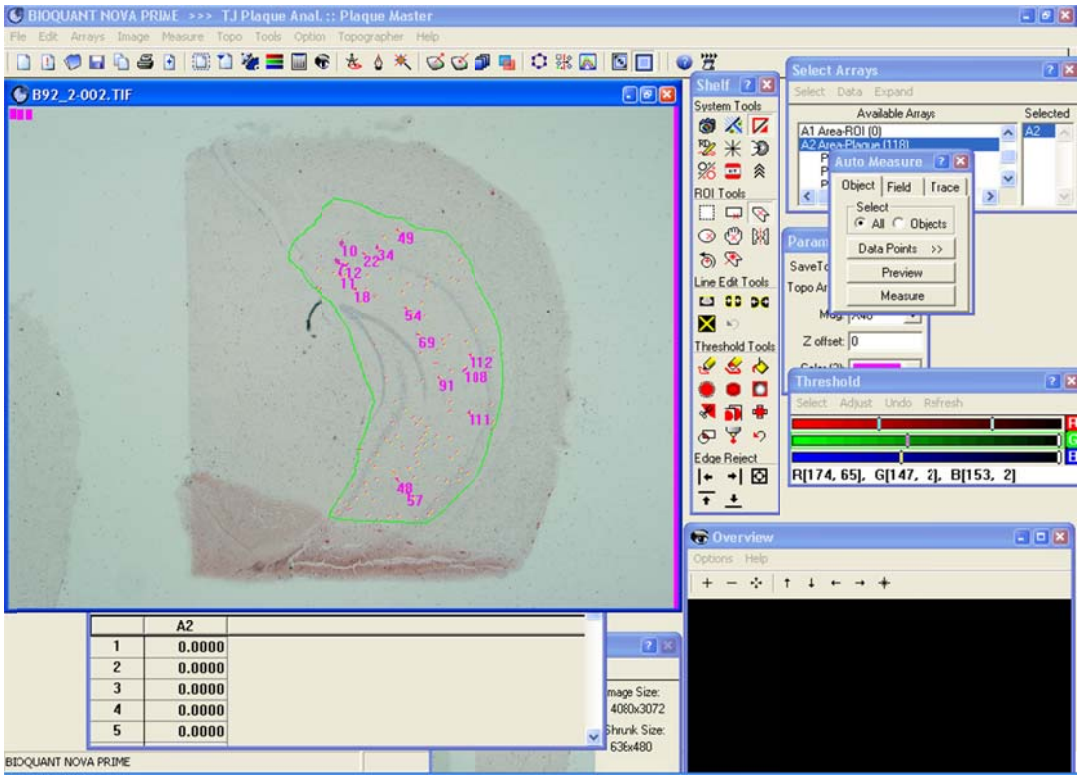

Figure B.11: BioQuant Plaque Measurements Sample Screen.

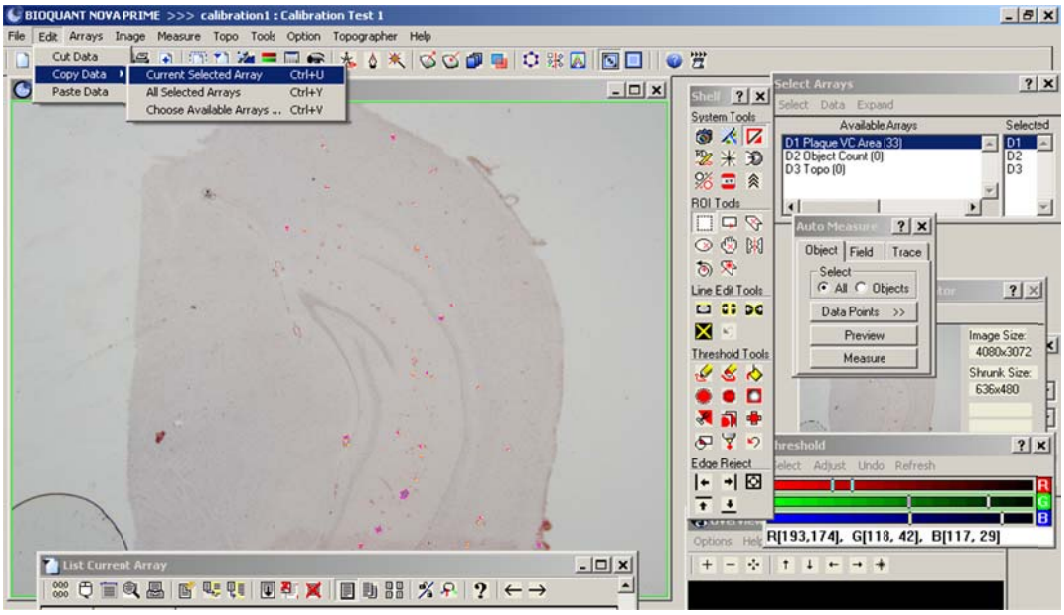

Figure B.12: BioQuant Plaque Copy Data Screen.

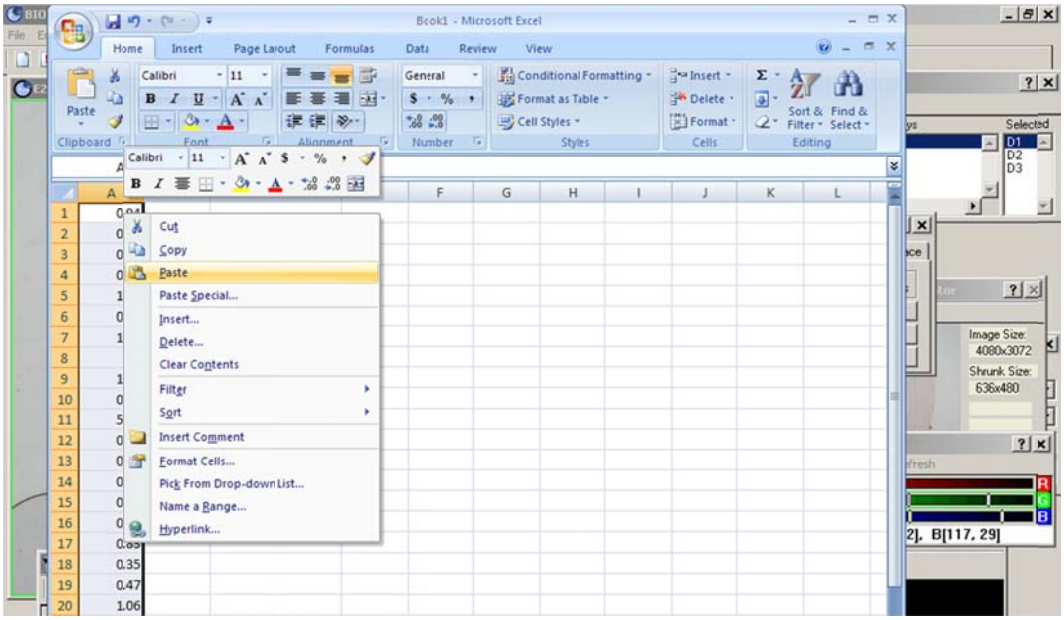

Figure B.13: Microsoft Excel Paste Data Screen.

REFERENCES

REFERENCES

Adlard, P., Cherny, R., Finkelstein, D., Gautier, E., Robb, E., Cortes, M., Volitakis, I., Liu, X., Smith, J., Perez, K., Laughton, K., Li, Q.-X., Charman, S., Nicolazzo, J., Wilkins, S., Deleva, K., Lynch, T., Kok, G., Ritchie, C., Tanzi, R., Cappai, R., Masters, C., Barnham, K., Bush, A. (2008). Rapid Restoration of Cognition in Alzheimer's Transgenic Mice with 8-Hydroxy Quinoline Analogs Is Associated with Decreased Interstitial Aβ. *Neuron*, *59*, 43-55.

Aggleton, J. (2000) *The amygdala, a functional analysis* (2nd ed.). New York, NY: Oxford University Press.

Alexander, R., & Govern, D. (1994). A new and simpler approximation for ANOVA under variance heterogeneity. *Journal of Educational and Behavioral Statistics*, *19*(2), 91-101.

Andersen, P., Morris, R., Amaral, D., Bliss, T., & O'Keefe, J. (2007). *The hippocampus book.* New York, NY: Oxford University Press.

Armstrong, R., Lantos, P., & Cairns, N. (2008). What determines the molecular composition of abnormal protein aggregates in neurodegenerative disease? *Neuropathology, 28*, 351–365.

Barry, C., & Doeller, C. (2010). Conjunctive representations in the hippocampus: What and where? *The Journal of Neuroscience*, *30*(3), 799-801.

Bayer, T., & Multhaup, G. (2005). Involvement of amyloid *β* precursor protein (A*β*PP) modulated copper homeostasis in Alzheimer's disease. *Journal of Alzheimer's Disease*, *8*, 201-206.

Becaria, A., Bondy, S., & Campbell, A. (2003). Aluminum and copper interact in the promotion of oxidative but not inflammatory events: Implications for Alzheimer's disease. *Journal of Alzheimer's Disease*, *5*, 31–38.

Benarroch, E. (2009). Brain iron homeostasis and neurodegenerative disease. *Neurology*, *72*, 1436-1440.

Bertini, I., Gray, H., Stiefel, E., & Valentine, J. (2007). Biological inorganic chemistry: structure and reactivity. Sausalito, CA: University Science Books.

Boston, P., Gopalkaje, K., Manning, L., Middleton, L., & Loxley, M. (2008). Developing a simple laboratory test for Alzheimer's disease: measuring acetylcholinesterase in saliva - a pilot study. *International Journal of Geriatric Psychiatry*, *23*, 439–440.

Braak, H., & Braak, E. (1991). Neuropathological stageing of Alzheimer-related changes. *Acta Neuropathologica*, *82*, 239-259.

Braak, H., Braak, E., Ohm, T., & Bohl, J. (1989). Alzheimer's disease: mismatch between amyloid plaques and neuritic plaques. *Neuroscience Letters*, *103*, 24-28.

Burns, A. (2008) *Fear conditioning as a measuring tool for cognitive deficits related to amyloid burden coupled with iron, zinc, and copper in the transgenic tg2576 mouse model for Alzheimer's disease*." MA thesis, George Mason University, Fairfax, VA.

Bush, A. (2008). Drug Development Based on the Metals Hypothesis of Alzheimer's Disease. *Journal of Alzheimer's Disease*, *15*, 223-240.

Bush, A., Pettingell, W., Multhaup, G., d.Paradis, M., Vonsattel, J.-P., Gusella, J., Beyreuther, K., Masters, C., & Tanzi, R. (1994). Rapid Induction of Alzheimer Aβ Amyloid Formation by Zinc. *Science*, *265*, 1464-1467.

Butti, C., & Hof, P. (2010). The insular cortex: a comparative perspective. *Brain Structure and Function*, *214*, 477-493.

Campbell, A. (2006). The role of aluminum and copper on neuroinflammation and Alzheimer's disease. *Journal of Alzheimer's Disease*, *10*, 165-172.

Cantania, K. (2004). Correlates and possible mechanisms of neocortical enlargement and diversification in mammals. *International Journal of Comparative Psychology*, *17*(1), 71-91.

Castel A., Balota, D., & McCabe, D. (2009). Memory efficiency and the strategic control of attention at encoding: impairments of value-directed remembering in Alzheimer's disease. *Neuropsychology*, *23*(3), 297-306.

Celone, K., Calhoun, V., Dickerson, B., Atri, A., Chua, E., Miller, S., DePeau, K., Rentz, D., Selkoe, D., Blacker, D., Albert, M., & Sperling, R. (2006). Alterations in memory networks in mild cognitive impairment and Alzheimer's disease: An

independent component analysis. The *Journal of Neuroscience*, *26*(40), 10222-10231.

Cerpa, W., Dinamarca, M., & Inestrosa, N. (2008). Structure-function implications in alzheimer's disease: effect of aβ oligomers at central synapses. *Current Alzheimer Research*, *5*, 233-243.

Chauhan, N. (2003). Anti-amyloidogenic effect of allium sativumin Alzheimer's transgenic model Tg2576. *Journal of Herbal Pharmacotherapy*, *3*(1), 95-107.

Cho, Z.-H., Han, J.-Y., Hwang, S.-I., Kim, D.-S., Kim, K.-N., Kim, N.-B., Kim, S. Chi, J.-G., Park, C.-W., & Kim, Y.-B. (2010). Quantitative analysis of the hippocampus using images obtained from 7.0 T MRI. *NeuroImage*, *49*, 2134-2140.

Choi, B.-S., & Zheng, W. (2009). Copper transport to the brain by the blood-brain barrier and blood-CSF barrier. *Brain Research*, *1248*, 14-21.

Collingwood, J., & Dobson, J. (2006). Mapping and characterization of iron compounds in Alzheimer's tissue. *Journal of Alzheimer's Disease*, *10*, 215-222.

Colurso, G., Nilson, J., & Vervoort, L. (2003). Quantitative assessment of DNA fragmentation and beta-amyloid deposition in insular cortex and midfrontal gyrus from patients with Alzheimer's disease. *Life Sciences*, *73*, 1795-1803.

Crichton, R., Dexter, D., & Ward, R. (2008). Metal based neurodegenerative disease—From molecular mechanisms to therapeutic strategies. *Coordination Chemistry Reviews*, *252*(10/11), 1189-1199.

Danielsson, J., Pierattelli, R., Banci, L., & Gräslund, A. (2007). High-resolution NMR studies of the zinc-binding site of the Alzheimer's amyloid β-peptide. *FEBS Journal*, *274*, 46-59.

Dawbarn, D., & Allen, S. (2007). *Neurobiology of Alzheimer's disease* (3rd ed.). New York, NY: Oxford University Press.

de Jong, L., van der Hiele, K., Veer, I., Houwing, J., Westendorp, R., Bollen, E., de Bruin, P., Middlekoop, H., van Buchem, M., & van der Grond, J. (2008). Strongly reduced volumes of putamen and thalamus in Alzheimer's disease: An MRI study. *Brain*, *131*, 377-3285.

Dong, H., Csernansky, C., Martin, M., Bertchume, A., Vallera, D., & Csernansky, J. (2005). Acetylcholinesterase inhibitors ameliorate behavioral deficits in the Tg2576 mouse model of Alzheimer's disease. *Psychopharmacology*, *181*, 145–152.

Echeverria, V., Ducatenzeiler, D., Alhonen, L., Janne, J., Grant, S., Wandosell, F., Muro, A., Baralle, F., Li, H., Duff, K., Szyf, M., & Cuello, C. (2004). Rat transgenic models with a phenotype of intracellular A*β* accumulation in hippocampus and cortex. *Journal of Alzheimer's Disease*, *6*, 209–219.

Falangola, M., Lee, S.-P., Nixon, R., Duff, K., & Helpern, J. (2005). Histological Co-Localization of Iron in Aβ Plaques of PS/APP Transgenic Mice. *Neurochemical Research*, *30*(2), 201-205.

Fanselow, M., & Dong, H.-W. (2010). Are the dorsal and ventral hippocampus functionally distinct structures? *Neuron*, *65*(1), 7-19.

Franklin, K., & Paxinos, G. (2008). *The mouse brain in stereotaxic coordinates* (3rd ed.). New York, NY: Elsevier.

Frederickson, C., Cuajungco, M., & Frederickson, C. (2005). Is zinc the link between compromises of brain perfusion (excitotoxicity) and Alzheimer's disease? *Journal of Alzheimer's Disease*, *8*, 155–160.

Fukui, K., Takatsu, H., Shinkai, T., Suzuki, S., Abe, K., & Urano, S. (2005). Appearance of amyloid *β*-like substances and delayed-type apoptosis in rat hippocampus CA1 region through aging and oxidative stress. *Journal of Alzheimer's Disease*, *8*, 299-309.

Gandy, S., Zhang, Y., Ikin, A., Schmidt, S., Levy, E., Sheffield, R., Nixon, R., Liao, F.-F., Mathews, P., Xu, H., & Ehrlich, M. (2007). Alzheimer's presenilin 1 modulates sorting of APP and its carboxyl-terminal fragments in cerebral neurons in vivo. *Journal of Neurochemistry*, *102*, 619–626.

González, C., Martín, T., Cacho, J., Breñas, M., Arroyo T., García-Berrocal, B., Navajo, J., & González-Buitrago, J. (1999). Serum zinc, copper, insulin and lipids in Alzheimer's disease epsilon 4 apolipoprotein E allele carriers. *European Journal of Clinical Investigation*, *29*, 637-642.

Haines, D. (2006). *Fundamental neuroscience for basic and clinical applications* (3rd ed.). Philadelphia, PA: Elsevier.

Heinitz, M. (2005). Alzheimer's disease and trace elements: Chromium and zinc. *Journal of Orthomolecular Medicine*, *20*(2), 89-92.

Hesse, C., Rosengren, L., Vanmechelen, E.,Vanderstichele, H., Jensen, C., Davidsson, P., & Blennow, K. (2000). Cerebrospinal fluid markers for Alzheimer's disease evaluated after acute ischemic stroke. *Journal of Alzheimer's Disease*, *2*, 199-206.

Hesselink, J. (n.d.). *The temporal lobe & limbic system*. Retrieved from http://spinwarp.ucsd.edu/NeuroWeb/Text/br-800epi.htm

Hirsch, E. (2009). Iron transport in Parkinson's disease. *Parkinsonism and Related Disorders*, *1553*, S209-S211.

Hopkins, R., Abildskov, T., Bigler, E., & Weaver, L. (1997). Three dimensional image reconstruction of neuroanatomical structures: Methods for isolation of the cortex, ventricular system, hippocampus, and fornix. *Neuropsychology Review*, *7*(2), 87-104.

Horgan, J., Miguel-Hidalgo, J., Thrasher, M., & Bissette, G. (2007). Longitudinal brain corticotropin releasing factor and somatostatin in a transgenic mouse (tg2576) model of Alzheimer's disease. Journal *of Alzheimer's Disease*, *12*, 115-127.

.

Hořínek, D., Petrovický, P., Hort, J., Krásenský, J., Brabec, J., Bojar, M., Veněčková, M., & Seidl, Z. (2006). Amygdalar volume and psychiatric symptoms in Alzheimer's disease: An MRI analysis. *Acta Neurol Scand*, *113*, 40-45.

House, E., Collingwood, J., Khan, A., Korchazkina, O., Berthon, G., & Exley, C. (2004). Aluminum, iron, zinc and copper influence the *in vitro* formation of amyloid fibrils of Aβ42 in a manner which may have consequences for metal chelation therapy in Alzheimer's disease. *Journal of Alzheimer's Disease*, *6*, 291-301.

Hsiao, K., Borchelt, D., Olson, K., Johannsdottir, R., Kitt, C., Yunis, W., Xu, S., Eckman, C., Younkin, S., Price, D., Iadecoia, C., Clark, H., Carlson, G. (1995). Age-Related CNS Disorder and Early Death in Transgenic FVB/N Mice Overexpressing Alzheimer Amyloid Precursor Proteins. *Neuron*, *15*, 1203-1218.

Hsiao, K., Chapman, P., Nilsen, S., Eckman, C., Harigaya, Y., Younkin, S., Yang, F., Cole, G. (1996). Cognitive Memory Deficits, Aβ Elevation, and Amyloid Plaques in Transgenic Mice. *Science*, *274*, 99-102.

Hsiao-Ashe, K. (2006). Molecular basis of memory loss in the Tg2576 mouse model of Alzheimer's disease. *Journal of Alzheimer's Disease*, *9*, 123-126.

Inestrosa, N., Dinamarca, M., & Alvarez, A. (2008). Amyloid–cholinesterase interactions: Implications for Alzheimer's disease. *FEBS Journal*, *275*, 625-632.

Kee, H., Koh, J., Kim, M.-Y., Ahn, K., Kim, J., Bae, C., Park, S., Kim, K. (2002). Expression of brain-specific angiogenesis inhibitor 2 (BAI2) in normal and ischemic brain: Involvement of BAI2 in the ischemia-induced brain angiogenesis. *Journal of Cerebral Blood Flow & Metabolism*, *22*, 1054-1067.

Klunk, W., Engler, H., Nordberg, A., Wang, Y., Blomqvist, G., Holt, D., Bergström, M., Savitcheva, I., Huang, G.-F., Estrada, S., Ausén, B., Debnath, M., Barletta, J., Price, J., Sandell, J., Lopresti, B., Wall, A., Koivisto, P., Antoni, G., Mathis, C., & Långström, B. (2004). Imaging Brain Amyloid in Alzheimer's Disease with Pittsburgh Compound-B. *American Neurological Association*, *55*, 306-319.

Kong, G., Miles, L., Crespi, G., Morton, C., Ng, H., Barnham, K., McKinstry, W., Cappai, R., & Parker, M. (2008). Copper binding to the Alzheimer's disease amyloid precursor protein. *European Biophysics Journal*, *37*, 269-279.

Kopell. B., & Greenberg, B. (2008). Anatomy and physiology of the basal ganglia: Implications for DBS in psychiatry. *Neuroscience and Biobehavioral Reviews*, *32*, 408-422.

Krubitzer, L., & Huffman, K. (2000). Arealization of the neocortex in mammals: Genetic and epigenetic contributions to the phenotype. *Brain, Behavior and Evolution*, *55*, 322-335.

Kuzyk, A., Kastyak, M., Agrawal, V., Gallant, M., Sivakumar, G., Rak, M., Del Bigio, M., Westaway, D., Julian, R., & Gough, K. (2010). Association among amyloid plaque, lipid, and creatine in hippocampus of TgCRND8 mouse model for Alzheimer disease. *The Journal of Biological Chemistry*, *41*, 31202-31207.

Leech, N., Barrett, K., & Morgan, G. (2005). *SPSS for intermediate statistics: Use and interpretation*. Mahwah, New Jersey: Erlbaum.

Linkous, D., Adlard, P., Wanschura, P., Conko, K., & Flinn, J. (2009). The effects of enhanced zinc on spatial memory and plaque formation in transgenic mice. *Journal of Alzheimer's Disease*, *18*, 565-579.

Lovell, M. (2009). A potential role for alterations of zinc and zinc transport proteins in the progression of Alzheimer's disease. *Journal of Alzheimer's Disease*. *16*, 471-483.

Lovell, M., Ehmann, W., Butler, S., Markesbery, W. (1995). Elevated thiobarbituric acid-reactive substances and antioxidant enzyme activity in the brain in Alzheimer's disease. *Neurology*, *45*, 1594-1601.

Lovell, M., Robertson, J., Teesdale, W., Campbell, J., Markesbery, W. (1998). Copper, iron and zinc in Alzheimer's disease senile plaques. *Journal of the Neurological Sciences*, *158*, 47-52.

Macreadie I. (2008). Copper transport and Alzheimer's disease. *European Biophysics Journal*, *37*, 295-300.

McNab, F., & Klingberg, T. (2008). Prefrontal cortex and basal ganglia control access to working memory. *Nature Neuroscience*, *11*, 103-107.

Mehta, P. (2007). Amyloid beta protein as a marker or risk factor of Alzheimer's disease. *Current Alzheimer Research*, *4*, 359-363.

Melega, W., Laćan, G., Harvey, D., & Way, B. (2007). Methamphetamine increases basal ganglia iron to levels observed in aging. *Neuropharmacology and Neurotoxicology*, *18*(16), 1741-1745.

Moreno-Gonzalez, I., Baglietto-Vargas, D., Sanchez-Varo, R., Jimenez, S., Trujillo-Estrada, L., Sanchez-Mejias, E., Carlos Del Rio, J., Torres, M., Romero-Acebal, M., Ruano, D., Vizuete, M., Vitorica, J., & Gutierrez, A. (2009). Extracellular amyloid-β and cytotoxic glial activation induce significant entorhinal neuron loss in young $PS1^{M146L}$/APP^{751SL} mice. *Journal of Alzheimer's Disease*, *18*, 755-776.

MRC Centre for Synaptic Plasticity, University of Bristol (2011). *Hippocampal pathways*. Retrieved from http://www.bristol.ac.uk/synaptic/pathways/

Murray, E., & Richmond, B. (2001). Role of perirhinal cortex in object perception, memory, and associations. *Current Opinion in Neurobiology*, *11*, 188-193.

O'Keefe, J., & Dostrovsky, J. (1971). The hippocampus as a spatial map. Preliminary evidence from unit activity in the freely-moving rat. *Brain Research*, *34*, 171-175.

Ong, W., & Farooqui, A. (2005). Iron, neuroinflammation, and Alzheimer's disease. *Journal of Alzheimer's Disease*, *8*, 183–200.

Packard, M., & Knowlton, B. (2002). Learning and memory functions of the basal ganglia. *Annual Review of Neuroscience*, *25*, 563–593.

Pajonk, F.-G., Kessler, H., Supprian, T., Hamzei, P., Bach, D., Schweickhardt, J., Herrmann, W., Obeid, R., Simons, A., Falkai, P., Multhaup, G., & Bayer, T. (2005). Cognitive decline correlates with low plasma concentrations of copper in patients with mild to moderate Alzheimer's disease. *Journal of Alzheimer's Disease*, *8*, 23-27.

Pierrot, N., & Octave, J.-N. (2008). Processing of amyloid precursor protein and amyloid peptide neurotoxicity. *Current Alzheimer Research*, *5*, 92-99.

Qi, J., Wu, H., Yang, Y., Wang, D., Chen, Y., Gu, Y., & Liu, T. (2007). Cerebral ischemia and Alzheimer's disease: The expression of amyloid-β and apolipoprotein e in human hippocampus. *Journal of Alzheimer's Disease*, *12*, 335-341.

Rabinak, C., & Maren, S. (2008). Associative structure of fear memory after basolateral amygdala lesions in rats. *Behavioral Neuroscience*, *122*(6), 1284-1294.

Railey, A., Groeber, C., Flinn, J. (2011). The Effect of Metals on Spatial Memory in a Transgenic Mouse Model of Alzheimer's Disease. J*ournal of Alzheimer's Disease*, *23*, 1-7.

Ramón y Cajal, S. (1911). *Histologie du système nerveux de l'homme et des vertébrés*. Paris, France: Maloine.

Reznichenko, L., Ami, T., Zheng, H., Avramovich-Tirosh, Y., Youdim, M., Weinreb, O., & Mandel, S. (2006). Reduction of iron-regulated amyloid precursor protein and b-amyloid peptide by (–) epigallocatechin-3-gallate in cell cultures: Implications for iron chelation in Alzheimer's disease. *Journal of Neurochemistry*, *97*, 527-536.

Scali, C., Prosperi, C., Vannucchi, M., Papeu, G., & Casamenti, F. (2000). Brain inflammatory reaction in an animal model of neuronal degeneration and its modulation by an anti-inflammatory drug: implication in Alzheimer's disease. *European Journal of Neuroscience*, *12*, 1900-1912.

Sergeant, N., David, J., Champain, D., Ghestem, A., Wattez, A., & Delacourte, A. (2002). Progressive decrease of amyloid precursor protein carboxy terminal fragments (APP-CTFs), associated with tau pathology stages, in Alzheimer's disease. *Journal of Neurochemistry*, *81*, 663-672.

Sever, L. (1975). Zinc and Human Development: A Review. *Human Ecology*, *3*(1), 43-57.

Squire, L. (2004). Memory systems of the brain: A brief history and current perspective. *Neurobiology of Learning and Memory*, *82*(3), 171-177.

Squire, L., & Schacter, D. (2002) *Neuropsychology of memory* (3rd ed.). New York, NY: The Guilford Press.

Squire, L., & Zola, S. (1996). Structure and function of declarative and nondeclarative memory systems. *Proceedings of the National Academy of Sciences of the United States of America*, *93*, 13515-13522.

Storandt, M. (2008). Cognitive deficits in the early stages of Alzheimer's disease. *Current Directions in Psychological Science*, *17*, 198-202.

Swanson, L., & Petrovich, G. (1998). What is the amygdala? *Trends in Neuroscience*, *21*(8), 323-331.

Suzuki, N., & Bekkers, J. (2007). Inhibitory interneurons in the piriform cortex. *Proceedings of the Australian Physiological Society*, *38*, 9-14.

Thangavel, R, Van Hoesen, G., & Zaheer, A. (2009). The abnormally phosphorylated tau lesion of early Alzheimer's disease. *Neurochemistry Research*, *34*, 118-123.

Tõugu, V., Karafin, A., & Palumaa, P. (2008). Binding of zinc(II) and copper(II) to the full-length Alzheimer's amyloid-β peptide. *Journal of Neurochemistry*, *104*, 1249-1259.

Tsang, S., Francis, P., Esiri, M., Wong, P., Chen, C., & Lai, M. (2008). Loss of [3H]4-DAMP binding to muscarinic receptors in the orbitofrontal cortex of Alzheimer's disease patients with psychosis. *Psychopharmacology*, *198*, 251–259.

Ulinski, P., Jones, E., & Peters, A. (1999). *Cerebral cortex: Volume 13 models of cortical circuits*. New York, NY: Kluwer Academic/Plenum.

Utter, A., & Basso, M. (2008). The basal ganglia: An overview of circuits and function. *Neuroscience and Biobehavioral Reviews*, *32*, 333-342.

VanElzakker, M., Fevurly, R.,Breindel, T., & Spencer, R. (2008). Environmental novelty is associated with a selective increase in Fos expression in the output elements of the hippocampal formation and the perirhinal cortex. *Learning & Memory*, *15*, 899-908.

Vargha-Khadem, F., & Gadian, D. (1997). Differential effects of early hippocampal pathology on episodic and semantic memory. *Science*, *277*(5324), 376-381.

Walker, M., Pavlov, I., & Kullmann, D. (2010). A 'sustain pedal' in the hippocampus? *Nature Neuroscience, 13*(2), 146-148.

Waugh, W. (2008). Inhibition of iron-catalyzed oxidations by attainable uric acid and ascorbic acid levels: Therapeutic implications for Alzheimer's disease and late cognitive impairment. *Gerontology*, *54*, 238-243.

Wei, J., Wu, C., Lankin, D., Gulrati, A., Valyi-Nagy, T., Cochran, E., Pike, V., Kozikowski, A., & Wang, Y. (2005). Development of novel amyloid imaging agents based upon thioflavin s. *Current Alzheimer Research*, *2*, 109-114.

Wengenack, T., Jack, C., Jr., Garwood, M., & Poduslo, J. (2008). MR microimaging of amyloid plaques in Alzheimer's disease transgenic mice. *European Journal of Nuclear Medicine and Molecular Imaging*, *35*, 82-88.

Wickens, J. (1993). *A theory of the striatum*. New York, NY: Pergamon Press.

Willems, S., Salmon, E., & Van der Linden, M. (2008). Implicit/explicit memory dissociation in Alzheimer's disease: The consequence of inappropriate processing? *Neuropsychology*, *22*(6), 710-717.

Yamamoto, A., Shin, R.-W., Hasegawa, K., Naiki, H., Sato, H., Yoshimasu, F., & Kitamoto, T. (2002). Iron (III) induces aggregation of hyperphosphorylated *t* and its reduction to iron (II) reverses the aggregation: implications in the formation of neurofibrillary tangles of Alzheimer's disease. *Journal of Neurochemistry*, *82*, 1137-1147.

Yan, Z., & Feng, J. (2004). Alzheimer's disease: Interactions between cholinergic functions and β-amyloid. *Current Alzheimer Research*, *1*, 241-248.

Zhang, X.-M., Xiong, K., Cai, Y., Cai, H., Luo, X.-G., Feng, J.-C., Clough, R., Patrylo, P., Struble, R., Yan, X.-X. (2010). Functional deprivation promotes amyloid plaque pathogenesis in Tg2576 mouse olfactory bulb and piriform cortex. *European Journal of Neuroscience*, *31*, 710-721.

Zhang, Y., & Xu, H. (2007). Molecular and cellular mechanisms for alzheimer's disease: Understanding APP metabolism. *Current Molecular Medicine*, *7*, 687-696.

CURRICULUM VITAE

Everett-Teejay Brown graduated from Hermitage High School, Glen Allen, Virginia, in 2001. He received his Bachelor of Science in Psychology with minors in Biology and English from George Mason University in 2005. He has been employed with George Mason University since 2001. He is currently the Office/Program Manager for the Office of Diversity Programs & Services. He began graduate school in 2006 and completed his Master of Arts degree in Psychology (Biopsychology concentration) at George Mason University in Spring 2011.